

In planta multi-omic profiling of
pathogenic and commensal bacteria

I n a u g u r a l - D i s s e r t a t i o n

zur

Erlangung des Doktorgrades

der Mathematisch-Naturwissenschaftlichen Fakultät

der Universität zu Köln

vorgelegt von

Tatsuya Nobori

aus Kagoshima, Japan

Köln

2019

Die vorliegende Arbeit wurde am Max-Planck-Institut für Pflanzenzüchtungsforschung in Köln in der Abteilung für Pflanze-Mikroben Interaktionen (Direktor: Prof. Dr. Paul Schulze-Lefert), in der Arbeitsgruppe von Dr. Kenichi Tsuda angefertigt.



MAX-PLANCK-GESELLSCHAFT



Berichterstatter: Prof. Dr. Paul Schulze-Lefert
Prof. Dr. Stanislav Kopriva
Prof. Dr. Corné Pieterse

Prüfungsvorsitzender: Prof. Dr. Gunther Döhlemann

Tag der mündlichen Prüfung: 01.04.2019

Publications

Mine, A., **Nobori, T.**, Salazar-Rondon, M.C., Winkelmüller, T.M., Anver, S., Becker, D. and Tsuda, K., 2017. An incoherent feed-forward loop mediates robustness and tunability in a plant immune network. *EMBO reports*, p.e201643051.

Mine, A., Berens, M.L., **Nobori, T.**, Anver, S., Fukumoto, K., Winkelmüller, T.M., Takeda, A., Becker, D. and Tsuda, K., 2017. Pathogen exploitation of an abscisic acid-and jasmonate-inducible MAPK phosphatase and its interception by Arabidopsis immunity. *PNAS*, 114(28), pp.7456-7461.

Nobori, T., Velásquez, A.C., Wu, J., Kvitko, B.H., Kremer, J.M., Wang, Y., He, S.Y., and Tsuda, K., 2018. Transcriptome Landscape of a Bacterial Pathogen under Plant Immunity. *PNAS*, 201800529.

Nobori, T., Mine, A., and Tsuda, K., 2018, Molecular networks in plant-pathogen holobiont. *FEBS Letters*, doi:10.1002/1873-3468.13071

Nobori, T. and Tsuda, K., 2018, *In planta* transcriptome analysis of *Pseudomonas syringae*. *Bio-protocol* 8(17): e2987. DOI: 10.21769/BioProtoc.2987.

Berens, M.L., Wolinska, K.W, Spaepen, S., Ziegler, J., **Nobori, T.**, Nair, A., Krüler V., Winkelmüller, T.M., Wang, Y., Mine, A., Becker, D., Garrido-Oter, R., Schulze-Lefert, P., and Tsuda, K., 2019, Balancing trade- offs between biotic and abiotic stress responses through leaf age- dependent variation in stress hormone crosstalk. *PNAS*

Nobori, T. and Tsuda, K., 2019, The plant immune system in heterogeneous environments. *Curr. Opin. Plant Biol.* Under review

Nobori, T., Wang, Y., Wu, J., Stolze, S., Harzen, A., Tsuda, Y., Nakagami, H., Tsuda, K., In planta bacterial multi-omics illuminates regulatory logic underlying plant-pathogen interactions. *In preparation*

Table of Contents

Publications	III
Table of Contents	V
List of figures	IX
List of method figures	IX
List of supplementary figures	X
List of tables	X
List of abbreviations	XI
Abstract	XIV
Zusammenfassung	XV
Preamble	XVII
1. Introduction	1
1.1 Plant immune networks	2
1.1.1 Immune receptor networks.....	3
1.1.2 Immune signaling networks.....	4
1.1.3 Resilience and tunability in the plant immune system	5
1.1.4 Mechanisms underlying resilience and tunability.....	6
1.1.5 Balance: harmony between conflicting responses	8
1.2 Bacterial virulence networks	10
1.3 Interactions between plant immune and bacterial virulence networks	14
1.3.1 The plant receptor networks as targets of pathogens	14
1.3.2 Phytohormone networks as targets of pathogens.....	15
1.3.3 Plant-derived compounds affect bacterial virulence-related processes	17
1.3.4 How does plant immunity affect bacterial signaling networks?	18
1.4 Roles of plant immunity in shaping microbiota	19
1.5 Thesis Aims	22
2 Results	24
2.1 In planta transcriptomics of <i>Pto</i> DC3000	24
2.1.1 Method establishment of <i>in planta</i> bacterial transcriptomics	24
2.1.2 <i>Pto</i> transcriptome signatures influenced by plant immune activation	26
2.1.3 <i>In planta</i> bacterial transcriptome patterns at an early time point is tightly linked to later bacterial growth during infection.....	28
2.1.4 The system of bacterial iron acquisition is influenced by plant immunity.....	31
2.1.5 <i>pvdS</i> and its regulatory targets are commonly suppressed by PTI and ETI.....	32
2.1.6 <i>pvdS</i> has a causal impact on bacterial growth <i>in planta</i>	33

2.1.7	Regulation of <i>pvdS</i> in plants is independent of iron concentration	33
2.2	<i>In planta</i> multi-omics of <i>Pto</i>	34
2.2.1	<i>In planta</i> transcriptome and proteome profiling of <i>Pto</i>	34
2.2.2	Bacterial proteins differentially expressed under various conditions	37
2.2.3	Bacterial functions differently expressed in various conditions	38
2.2.4	Comparative analysis of bacterial transcriptomes and proteomes	41
2.2.5	Bacterial iron acquisition process affected <i>in planta</i>	45
2.2.6	The gene co-expression network of <i>Pto</i>	47
2.2.7	The gene co-expression network predicts bacterial gene regulatory logic.....	49
2.2.8	Type III translocator components are selectively affected by plant SA pathways.....	50
2.3	<i>In planta</i> transcriptomics of commensal bacteria	52
2.3.1	Comparative transcriptomics of four <i>Pseudomonas</i> strains.....	52
2.3.2	Selecting and characterizing 12 commensal bacterial strains	53
2.3.3	<i>In vitro</i> and <i>in planta</i> transcriptomics of commensal bacteria from various phyla	54
2.3.4	Transcriptomes responses of <i>A. thaliana</i> against commensal bacteria	58
3	Discussion	60
3.1	<i>In vivo</i> bacterial RNA-seq and Dual RNA-seq as powerful approaches in host-pathogen interaction studies.....	60
3.2	<i>In planta</i> bacterial transcriptomics and proteomics illuminate the mechanisms of pathogen growth suppression by plant immunity.	61
3.2.1	The impact of plant immunity on the transcriptomes of <i>Pto</i>	61
3.2.2	Iron-acquisition pathway of <i>Pto</i> as a major target of plant immunity.....	63
3.2.3	The gene regulatory network of <i>Pto</i>	64
3.2.4	Proteome landscape of <i>Pto in planta</i> and integrative multi-omics	65
3.3	Understanding how plant immunity shapes plant microbiota	67
3.4	How does plant immunity control bacterial growth?.....	69
3.5	Outlook.....	70
3.5.1	Resilience, tunability, and balance at different layers of plant immunity	70
3.5.2	Zooming in: plant immune system at tissue- and cell-specific levels.....	72
3.5.3	Overcoming tradeoffs in agriculture	74
3.5.4	Towards the understanding of molecular super-networks in plant-bacterial interactions.....	74
3.6	Concluding remarks and future perspectives.....	78
4	Materials and Methods	80
4.1	Key resources.....	80
4.2	Plant materials and growth conditions.....	81

4.3	Bacterial strains	81
4.4	Accession numbers.....	82
4.5	<i>In vitro</i> bacterial cultures for bacterial transcriptomics and proteomics.....	82
4.6	Elicitor pretreatment.....	82
4.7	Bacterial infection and sampling for <i>in planta</i> bacterial transcriptomics and proteomics.....	82
4.8	Transcriptome analysis of plants.....	83
4.9	<i>In planta</i> bacterial transcriptomics.....	83
4.9.1	Establishment of a bacterial isolation buffer	83
4.9.2	Bacterial isolation	84
4.9.3	RNA extraction	87
4.9.4	cDNA library generation and RNA-seq.....	87
4.9.5	Statistical analysis of RNA-seq data.....	87
4.9.6	Quality assessment of RNA-seq data	88
4.9.7	Co-expression analysis of <i>Pto</i> genes	89
4.9.8	Analysis of RNA-seq data of commensal strains	89
4.9.9	<i>In planta</i> bacterial transcriptome method based on customized probes.....	89
4.10	<i>In planta</i> bacterial proteomics	90
4.10.1	Bacterial isolation and protein extraction	90
4.10.2	Sample preparation and fractionation.....	90
4.10.3	LC-MS/MS data acquisition	91
4.10.4	Protein identification and quantification	91
4.10.5	Statistical analysis.....	92
4.11	Gene ontology based analyses of transcriptome and proteome data	92
4.12	Software and packages used in this study	93
4.13	Primer information.....	93
4.14	RT-qPCR analysis	97
4.15	Generation of mutant <i>Pto</i> strains	98
4.16	Bacterial growth assay	98
4.17	Apoplasmic and intracellular fluids extraction and iron measurement.....	98
5	References.....	100
6	Supplementary figures	128
	Contributions	142
	Acknowledgements.....	143
	Erklärung	144

List of figures

Figure 1: Possible structures of the plant immune and bacterial virulence networks and their interactions.....	2
Figure 2: Resilience, tunability, and balance in the plant immune system	10
Figure 3: Establishment of <i>in planta</i> <i>Pto</i> transcriptome analysis.....	25
Figure 4: Profiles of <i>Pto</i> transcriptome under various conditions	28
Figure 5: Host genotype effects on bacterial transcriptome.....	30
Figure 6: Iron-related genes of <i>Pto</i> are targeted by plant immunity	31
Figure 7: Iron content in the apoplast does not explain <i>pvdS</i> expression and <i>Pto</i> growth.....	34
Figure 8: <i>In planta</i> transcriptomics and proteomics of <i>Pto</i>	36
Figure 9: Distinct patterns of <i>Pto</i> proteomes in various conditions	38
Figure 10: Bacterial functions differentially expressed in different conditions.	40
Figure 11: Regulation of mRNAs and proteins involved in selected functions.....	41
Figure 12: Integration of bacterial transcriptome and proteome data	43
Figure 13: Conserved and specific regulation of <i>Pto</i> metabolisms at mRNA and protein levels	44
Figure 14: Regulation of bacterial iron acquisition pathway	46
Figure 15: The gene co-expression network of <i>Pto</i>	48
Figure 16: Gene co-expression network predicts the gene regulatory logic of <i>Pto</i>	50
Figure 17: Plant SA pathway selectively affects bacterial T3SS proteins	51
Figure 18: Comparative transcriptomics of four <i>Pseudomonas</i> strains <i>in vitro</i> and <i>in planta</i>	53
Figure 19: Comparative transcriptomics of nine bacterial strains	55
Figure 20: Bacterial functions differently expressed <i>in planta</i>	56
Figure 21: Bacterial strain-dependent plant immune activation	58
Figure 22: The plant immune system at different layers.....	72
Figure 23: Plant immune networks at the single cell/cell-type specific level	73
Figure 24: A conceptual model illustrating the plant–bacterial supernetwork	77

List of method figures

Method figure 1: Crushed leaf sample before incubation in the bacterial isolation buffer.....	84
Method figure 2: Filter and filter holder equipped to a 50 ml Falcon tube.....	85

Method figure 3: A two-layered pellet consists of plants (bottom, green) and bacteria (top, white)	86
--	----

List of supplementary figures

Supplementary figure 1: Bacterial enrichment and quality of RNA extraction in <i>in planta</i> bacterial transcriptome	128
Supplementary figure 2: Normalization and quality control of RNA-seq data	129
Supplementary figure 3: Heatmap of <i>Pto</i> transcriptomes (relative expression; RE) in all samples analyzed in this study	131
Supplementary figure 4: <i>Pto</i> populations did not change at 6 h post infection	132
Supplementary figure 5: Profiles of <i>Pto</i> transcriptome under various conditions	133
Supplementary figure 6: Hierarchical clustering of the relative expression (RE) of <i>Pto</i> sigma factors	134
Supplementary figure 7: Infection assay of <i>pvdS</i> -overexpressing <i>Pto</i>	134
Supplementary figure 8: Colonies of bacterial strains	135
Supplementary figure 9: Expression of genes related to coronatine, alginate, and the type III secretion system	137
Supplementary figure 10: Gene ontologies showing negative correlation in expression	137
Supplementary figure 11: Co-expression patterns of genes in <i>Pto</i>	138

List of tables

Table 1: List of commensal bacteria used in this study	54
Table 2: List of software and packages used in this study	93
Table 3: List of primers used in this study	93
Table 4: qRT-PCR master mix	97

List of abbreviations

ABA	Abscisic acid
AHL	Acyl-homoserine lactone
CDS	coding sequence
cfu	colony forming unit
COR	coronatine
CSI ^{LRR}	LRR-RK interaction network
DAMP	damage associated molecular pattern
<i>de</i>	<i>dde2 ein2</i>
DEG	differentially expressed genes
<i>deps</i>	<i>dde2 ein2 pad4 sid2</i>
ECD	extracellular domain
ECF	extracytoplasmic function
ET	ethylene
ETI	effector triggered immunity
FC	fold change
<i>FLS2</i>	<i>FLAGELLIN-SENSITIVE 2</i>
FW	fresh weight
GO	Gene Ontology
hpi	hours post inoculation
HR	hypersensitive response
IAA	indole- 3-acetic acid
JA	jasmonic acid
JA-Ile	jasmonyl isoleucine

KB	King's B
KO	Kyoto Encyclopedia of Genes and Genomes Ontology
LRR-RK	leucine-rich-repeat receptor-like kinase
MAMP	microbe associated molecular pattern
MAPK	mitogen activated protein kinase
MM	minimal medium
NLR	nucleotide-binding domain leucine rich repeat proteins
OD	optical density
<i>Pph</i>	<i>Pseudomonas syringae</i> pv. <i>phaseolicola</i>
PRR	pattern recognition receptor
<i>ps</i>	<i>pad4 sid2</i>
PTI	pattern-triggered immunity
<i>Psg</i>	<i>Pseudomonas syringae</i> pv. <i>glycinea</i>
<i>Pss</i>	<i>Pseudomonas syringae</i> pv. <i>syringae</i>
<i>Pto</i>	<i>Pseudomonas syringae</i> pv. <i>tomato</i>
QS	quorum sensing
RLK	receptor like kinase
ROS	reactive oxygen species
<i>rr</i>	<i>rps2 rpm1</i>
RT-qPCR	reverse transcriptase quantitative polymerase chain reaction
SD	standard deviation
SE	standard error
<i>spm</i>	<i>sid2 pmr4</i>
T3E	type III effector

T3SS	type III secretion system
TF	transcription factor
wt	wild type

Abstract

Plant pathogens can cause serious diseases that impact global agriculture. Molecular mechanisms of the plant immune system have been intensively studied in the past decades, revealing mechanisms for pathogen recognition and immune signaling in plant cells. However, we still lack a fundamental knowledge of how plant immunity affects pathogen metabolisms to inhibit their growth in plants. In the case of bacterial pathogens, a major bottleneck is the difficulty in profiling bacterial responses *in planta*. Here, I established a method to isolate bacterial cells from *Arabidopsis thaliana* leaves to enrich bacterial information. I profiled the transcriptomes and proteomes of the foliar bacterial pathogen *Pseudomonas syringae* by using various combinations of host and bacterial genotypes and pretreatments. This unveiled that bacterial transcriptome changes affected by plant immunity explain bacterial growth suppression in the plant apoplast and identified that a bacterial iron acquisition pathway is a major plant immune target. Bacterial transcriptomes and proteomes were well correlated in general, but I also found that plant immunity affects the abundance of specific components of the bacterial type III secretion system, an essential component for bacterial virulence, only at the protein level. Together, these analyses provided insights into the long-standing question of how biological processes of bacterial pathogens are influenced by plant immunity. I also applied the *in planta* bacterial transcriptomics method to address an important open question in plant microbiota research: how does plant immunity influence the responses of microbiota members to affect the shape and functions of the plant microbiota? I profiled the co-transcriptomes of plants and bacteria in the monoassociation condition and revealed conserved and specific plant and bacterial responses during interaction events. This approach will help us understand how plants winnow different microbiota members and control the microbiota function, and transform the current plant microbiota research from descriptive studies to mechanistic studies. Taken together, this study sets the foundation for the comprehensive understanding of molecular events on both plant and bacterial sides during their interactions.

Zusammenfassung

Pflanzenpathogene können schwere Krankheiten verursachen, die sich auf die globale Landwirtschaft auswirken. Molekulare Mechanismen des pflanzlichen Immunsystems wurden in den letzten Jahrzehnten intensiv untersucht, wodurch Erkenntnisse über die Pathogenerkennung und die Immunsignaltransduktion in Pflanzenzellen gewonnen werden konnten. Jedoch fehlt grundlegendes Wissen darüber, wie die pflanzliche Immunität Pathogenmetabolismen beeinflusst, um deren Wachstum zu hemmen. Vor allem bei krankheitserregenden Bakterien fehlen experimentelle Methoden, um die bakteriellen Reaktionen auf das pflanzliche Immunsystem *in planta* zu erfassen. Hier habe ich eine Methode zur Isolierung von Bakterienzellen aus *Arabidopsis thaliana*-Blättern etabliert, um Bakterieninformationen anzureichern, ohne deren Stoffwechsel zu beeinflussen. Ich analysierte die Transkriptome und Proteome verschiedener Genotypen des Modell-Bakterienpathogens *Pseudomonas syringae* unter 38 bzw. 15 Bedingungen in Kombination mit verschiedenen Vorbehandlungen und in unterschiedlichen Wirtspflanzen. Diese Experimente zeigten, dass die Aktivität des pflanzlichen Immunsystems bakterielle Transkriptome maßgeblich verändert, was zu einer Unterdrückung des bakteriellen Wachstums innerhalb der Pflanzenzelle führt. Interessanterweise ist dabei ein Stoffwechselweg, über den Bakterien Eisen aufnehmen, ein Hauptziel der pflanzlichen Immunabwehr. Im Allgemeinen konnte ich eine Korrelation zwischen Reaktionen von bakteriellen Transkriptomen und Proteomen auf die pflanzliche Immunabwehr feststellen. Allerdings konnte ich ebenfalls beobachten, dass das Vorkommen spezifischer Komponenten des bakteriellen Typ III-Sekretionssystems, welches für die Virulenz wichtig ist, nur auf der Protein- aber nicht auf der Transkriptionsebene beeinflusst wird. Zusammengefasst liefern diese Analysen Einblicke in die seit langem bestehende Frage, wie Stoffwechselprozesse von bakteriellen Krankheitserregern durch die Immunität von Pflanzen beeinflusst werden. Die hier etablierte Methode für *in planta* Bakterientranskriptome konnte auch angewendet werden, um eine wichtige offene Frage in der Pflanzenmikrobiomforschung zu beantworten: Wie beeinflusst die Immunität von Pflanzen die Metabolismen einzelner bakterieller Mikroben, um ein Pflanzenmikrobiom zu formen und seine Funktionen zu steuern? Ich habe die Transkriptome sowohl von Pflanzen, als auch von Bakterien in Monoassoziationen untersucht und konservierte sowie spezifische Reaktionen von Pflanzen und Bakterien auf

Interaktionsereignisse feststellen können. Dieser Ansatz wird uns helfen zu verstehen, wie Pflanzen aus verschiedenen bakteriellen Mikroben nützliche auswählen und die Mikrobiomfunktion steuern. Dies könnte die derzeitige Pflanzen-Mikroben-Forschung von deskriptiven Studien hin zu mechanistischen Studien führen. Zusammengenommen schafft diese Studie die Grundlage für ein umfassendes Verständnis molekularer Ereignisse während Pflanzen-Bakterien-Interaktionen.

Preamble

Part of this thesis is from manuscripts published, submitted, or in preparation as listed above in the “Publication” section. Figures that have been adopted from these papers were noted in the figure legends. Some paragraphs were adopted from the papers listed above with some modification, but no paragraph in this thesis was entirely quoted from these papers unless otherwise specified. Most of the experiments and analyses described in this thesis were conducted by myself. Those that were conducted by other people were indicated in the “Contribution” section on page 145.

1. Introduction

The ultimate role of plant immunity, from the human point of view, is to stave off all potential pathogens that harm plant survival. One straightforward way to accomplish this might be to devise parallel and constitutively active immune branches that are collectively effective against all pathogens. However, it appears that evolution did not favor this way for several reasons. Firstly, resources that plants can use are limited. Plants need to allocate resources to their growth and responses to abiotic stresses as well as to fight against pathogens; thus constitutively active immunity poses a burden on plant fitness. Secondly, there is no versatile immune response effective against all pathogens and some immune responses lead to conflicting outcomes. For instance, hypersensitive cell death is an immune response effective against some biotrophic pathogens, which rely on living host cells, but it promotes the growth of necrotrophic pathogens, which feed on dead cells (Glazebrook, 2005; Mengiste, 2012). In addition, constitutively active immune responses might be harmful to plant-associated microbial communities (microbiota) that contribute to plant health (Duran et al., 2018). In mammals, it is known that excessive activation of host immunity can lead to abnormal microbiota structure, which negatively affects host health (M. Levy et al., 2017).

An inducible immune system can be a solution plants have adopted to reconcile these problems. Plants have evolved immune systems that are activated upon encountering pathogens by using various types of receptors, such as pattern recognition receptors (PRRs) (Boutrot and Zipfel, 2017) and nucleotide-binding domain and leucine-rich repeat-containing proteins (NLRs) (Kourelis and Van Der Hoorn, 2018). An energy-efficient and flexible immune system would be advantageous for plant survival and therefore be selected. Indeed, plants are able to (i) deploy immune responses that are resilient against perturbations by biotic and abiotic factors, (ii) fine-tune immune responses in context-dependent manners, and (iii) prioritize or balance immune responses in relation to other responses. Such traits can be explained by interwoven plant immune networks comprised of immune receptors, plant hormones, transcription factors, and other components (Nobori et al., 2018a). Here, I introduce our knowledge of the plant immune network system and its resilient, tunable, and balanced properties and discuss roles of the immune system in interactions with pathogens and microbiota. I also introduce molecular networks of bacteria, in particular pathogen virulence networks, and their interactions with plant networks.

1. Introduction

1.1 Plant immune networks

The plant innate immune system relies on an expanded repertoire of immune receptors on the cell surface or inside the cell to detect molecular signatures associated with microbial invasions (Boutrot and Zipfel, 2017; Kourelis and Van Der Hoorn, 2018). Recognition of microbe- and damage-associated molecular patterns (MAMPs and DAMPs) and effector molecules by the plant immune receptors activates pattern-triggered immunity (PTI) and effector-triggered immunity (ETI), respectively (Boutrot and Zipfel, 2017; Kourelis and Van Der Hoorn, 2018). PTI and ETI activate various immune signaling pathways such as phytohormone pathways and restrict microbial invasion and proliferation (Berens et al., 2017; Boutrot and Zipfel, 2017; Cui et al., 2014). Plant immune receptors and immune signaling components have evolved to interact in a complex manner. These immune receptors and signaling networks are collectively defined as plant immune networks in this thesis (Figure 1). The plant immune networks are further connected with components in other physiological processes to optimize plant responses in ever-changing environment. For instance, phytohormone signaling networks coordinate plant immunity with abiotic stress responses and developmental programs (Alcázar et al., 2011; Berens et al., 2017; Heil and Baldwin, 2002; Huot et al., 2014; Smakowska et al., 2016).

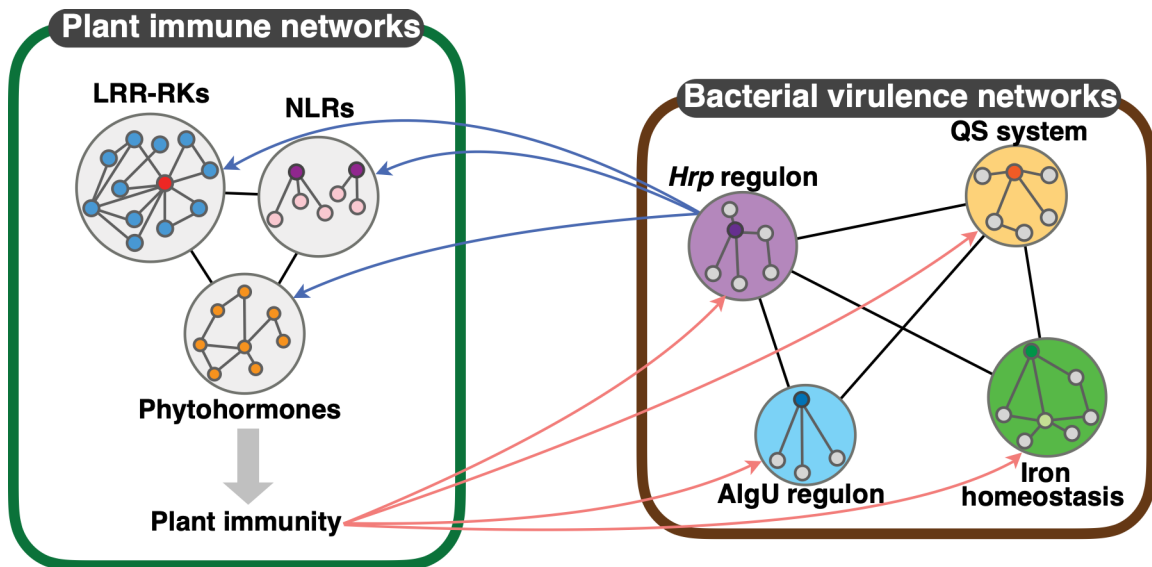


Figure 1: Possible structures of the plant immune and bacterial virulence networks and their interactions

Blue arrows: Bacterial type III effectors and toxins regulated by the *hrp* regulon target the plant immune networks. Red arrows: Plant immunity targets components in the bacterial virulence networks with unknown mechanisms. The plant immune networks include leucine-rich repeat receptor kinases (LRR-RKs) networks, nucleotide-binding domain and leucine-rich repeat-containing

proteins (NLRs) networks, and phytohormone networks. The bacterial virulence networks include *Hrp* regulon, *AlgU* regulon, quorum sensing (QS) system, and iron homeostasis system. The sub-networks in the plant immune or bacterial virulence networks are interconnected (black lines). This figure was adopted from (Nobori et al., 2018a).

1.1.1 Immune receptor networks

PTI is activated through recognition of microbe-derived ligands, called MAMPs, or plant-derived ligands, known as DAMPs, by PRRs, a major class of which are leucine rich-repeat receptor kinases (LRR-RKs) (Boutrot and Zipfel, 2017). For instance, FLS2 senses the MAMP flg22 derived from bacterial flagellin, and PEPR1/PEPR2 recognize Pep peptides, which are DAMPs derived from endogenous PROPEP proteins in *Arabidopsis thaliana* (Boutrot and Zipfel, 2017). Upon ligand binding, these LRR-RKs recruit another LRR-RK, BRASSINOSTEROID INSENSITIVE1-ASSOCIATED KINASE (BAK1), for transducing the signal to the cytosol (Yasuda et al., 2017). Although it has been known that LRR-RKs often interact with each other through their extracellular domains (ECDs) (Belkhadir et al., 2014), a comprehensive analysis on LRR-RK interactions has been difficult due to a massive diversification of this class of receptor proteins in plants (Sun et al., 2017). Recently, a high-throughput *in vitro* interaction assay was conducted to test 40,000 interactions between 200 ECDs in *A. thaliana* to construct an LRR-RK interaction network (CSI^{LRR}) (Smakowska-luzan et al., 2018). The CSI^{LRR} helped to identify previously uncharacterized LRR-RKs that modulate immune responses. For instance, the LRR-RK FIR interacts with both FLS2 and BAK1 and promotes flg22-induced FLS2-BAK1 complex formation and immune responses (Smakowska-luzan et al., 2018). In the CSI^{LRR}, BAK1 and APEX are hub LRR-RKs whose removal could strongly affect network connectivity (Smakowska-luzan et al., 2018). BAK1 interact with multiple PRRs, including FLS2, PEPR1, and PEPR2 (Yasuda et al., 2017). APEX interacts with PEPR1 and PEPR2 and contributes to Pep2-induced immune responses (Smakowska-luzan et al., 2018). Unlike BAK1, the APEX protein does not interact with FLS2. Interestingly, however, genetic removal of APEX enhanced flg22-induced FLS2-BAK1 complex formation and immune responses (Smakowska-luzan et al., 2018), indicating that APEX can affect the FLS2 functions through the CSI^{LRR} even without a direct physical interaction with FLS2. It is possible that the CSI^{LRR} monitors the integrity of APEX and modulates plant immune responses by an unknown mechanism. Similarly, it was shown that perturbations on BAK1 enhance PEPR1/PEPR2-mediated cell death and immune responses

1. Introduction

to compensate for the absence of BAK1-dependent PRR signaling (Yamada et al., 2015). It will be of key future challenge to explore and define such regulatory functions possibly mediated by the CSI^{LRR}.

ETI is mediated by NLRs and is often accompanied by hypersensitive response (HR) cell death (Cui et al., 2014). Typically, NLRs are intracellular immune receptors that can directly recognize pathogen effectors or indirectly sense the activities of effectors (Cui et al., 2014; Kourelis and Van Der Hoorn, 2018). It has been proposed that NLRs form a network structure, in which “sensor” NLRs recognize pathogen effectors and “helper” NLRs transduce signals after the effector recognition (Bonardi et al., 2011; Castel et al., 2018; Qi et al., 2018; Wu et al., 2017, 2016, 2018). In *A. thaliana*, the helper NLRs, ADR1, ADR1-L1, and ADR-L2, contribute redundantly to ETI mediated by three different sensor NLRs that detect the effectors bacteria and oomycetes (Bonardi et al., 2011). Another helper NLR, NRG1, was shown to function downstream of multiple TIR-NLRs in *A. thaliana* and *Nicotiana benthamiana* (Castel et al., 2018; Qi et al., 2018; Wu et al., 2018). *N. benthamiana* NRC2, NRC3, and NRC4 are helper NLRs that redundantly function to elicit HR cell death following recognition of bacterial, oomycete, nematode, or viral effectors by nine different sensor NLRs (Wu et al., 2017). Phylogenetic analysis of plant NLRs revealed that the ADR1 and NRC families are distantly related (Wu et al., 2017). Moreover, the NRC family proteins are present in asterids including *N. benthamiana*, although they are absent in rosids including *A. thaliana* (Andolfo et al., 2014; Collier et al., 2011; Wu et al., 2017). Therefore, it is likely that ADR1 and NRC families have evolved independently as helper NLRs, on which signals from various sensor NLRs converge. This would allow sensor NLRs to gain a new recognition spectrum without losing the inter-relationship with cognate helper NLRs for signal transduction. Thus, the NLR network comprised of pathogen-detecting sensor NLRs and downstream functionally-redundant helper NLRs might drive the evolution of sensor NLRs to cope with a large variety of effectors from fast-evolving pathogens and, at the same time, allow plants to maintain robust NLR signaling mediated by helper NLRs.

1.1.2 Immune signaling networks

Phytohormones are small signal molecules that are produced in plants in response to internal and external stimuli, such as developmental cues and pathogen invasion, and regulate plant responses (Shigenaga et al., 2017). Land plants have expanded the repertoire of

phytohormones, which likely contributed to plant adaptation to more fluctuating terrestrial environments (Berens et al., 2017). An evolutionary and comparative genomic analysis of species representing all the major plant lineages revealed that signaling mediated by the major immunity-related phytohormones jasmonate (JA) and salicylic acid (SA) likely originated in the last common ancestor of land plants (Wang et al., 2015). JA and SA signaling can interact either antagonistically or synergistically, depending on the context, and these interactions are modulated by other phytohormones such as ethylene (ET), abscisic acid (ABA), and auxin, collectively forming a phytohormone signaling network (Berens et al., 2017). The properties of the phytohormone signaling network were difficult to elucidate due to complex interactions among network components. An approach to dissect such a complex network is to remove network components to the level where the network largely loses its functional output and then assign functions to individual network components and their interactions by studying how the network output is recovered during stepwise reconstruction of the network using combinatorial genetic perturbations (Mine et al., 2014). To this end, all possible combinations (from single to quadruple) of *A. thaliana* mutants deficient in signaling mediated by JA, ET, SA, and phytoalexin deficient 4 (PAD4), a major component of plant immunity, were generated, enabling experimental stepwise reconstitution of the four signaling sectors and their interactions in the network (Tsuda et al., 2009).

1.1.3 Resilience and tunability in the plant immune system

In a resilient system, the output is stable even when part of the system is disabled (Katagiri, 2018). Resilience in the immune system is important because pathogens attempt to disrupt plant immune sectors by using effector molecules (Kazan and Lyons, 2014; Toruño et al., 2016); and such pathogen acts are virtually unavoidable because pathogens can evolve much faster than plants (Katagiri, 2018). Environmental stresses also compromise plant immune systems. For instance, high temperature suppresses plant immunity mediated by SA and PAD4, leading to susceptibility against biotrophic pathogens (Alcázar and Parker, 2011; Huot et al., 2017). A system is tunable when the level and spectrum of the outputs can be quantitatively changed depending on the inputs (Katagiri, 2018). Tunability is important because the immune response is costly, making unnecessary activation a burden for plant fitness (Katagiri, 2018). In addition, MAMPs that can be recognized by plant immune receptors are produced by harmless microbes in the plant microbiota as well as by pathogens,

1. Introduction

thus immune activation needs to be carefully regulated according to the hazard levels of individual microbes.

1.1.4 Mechanisms underlying resilience and tunability

Resilient and tunable properties of plant immunity have been uncovered in a four-sector network comprised of SA, JA, ET and PAD4. When one of the sectors is removed, plants still retain a large part of pathogen growth suppression activity induced by flg22 or AvrRpt2, elicitors of PTI or ETI, respectively (Tsuda et al., 2009). However, removal of all four sectors abolished around 80% of inducible immunity in both cases (Tsuda et al., 2009). Similarly, the network reconstitution approach was used to dissect complex regulation of *A. thaliana* transcriptome responses to flg22 by the JA/ET/PAD4/SA signaling network (Hillmer et al., 2017). Statistical modelling of the contributions of the individual signaling sectors and their interactions to expression changes of over 5000 flg22-responsive genes revealed that these genes are not merely dependent on single signaling sectors, but rather on multi-sector interactions (Hillmer et al., 2017). Consequently, the transcriptional responses of most of the flg22-responsive genes are highly buffered (i.e. single mutations do not affect flg22 responsiveness), and thus likely resilient to perturbation of the network components by pathogen effectors and environmental factors. The combination of network reconstitution and statistical modelling also unveiled transcriptional regulatory logic that could not be detected in conventional genetic studies. For instance, the SA-dependent genes defined by a conventional genetic means (genes showing no transcriptional responses in an SA-deficient mutant *sid2*) were not simply regulated by the SA signaling sector alone, but were regulated by the ET, PAD4, and SA signaling sectors and their interactions (Hillmer et al., 2017). The four-sector network also contributes to rapid transcriptional reprogramming during AvrRpt2-triggered immunity, which is critical for suppressing pathogen growth (Mine et al., 2018). Quantitative measurements of expression of marker genes for each signaling sector, as well as the growth of *P. syringae* pv. *tomato* DC3000 (*Pto*) and pv. *maculicola* ES4326 in all possible combinations of plant genotypes treated with three different MAMPs (flg22, elf18, or chitosan) enabled construction of a highly predictive regression model that describes signal flow in the JA/ET/SA/PAD4 signaling network during PTI (Kim et al., 2014). The model showed that the ET sector represses the JA and PAD4 sectors, the latter of which explains a mechanism for ET-mediated SA suppression, as PAD4 is required for SA accumulation in

PTI (Tsuda et al., 2008). Loss of either ET or JA sectors increased network fragility, indicating that the inhibitory effect of the ET sector on the JA sector is important for resilience of the network output (Kim et al., 2014). This model showed that the JA and PAD4 sectors are compensatory in activation of the SA sector, enabling resilient SA-mediated immune responses (Kim et al., 2014). The positive effect of the JA sector on the SA sector was somewhat unexpected. Both JA and SA accumulation increases during PTI and ETI (Doares et al., 1995; Hillmer et al., 2017; Kim et al., 2014; Tsuda et al., 2008), suggesting the importance of JA-SA crosstalk for orchestrating plant immune responses. Nevertheless, our understanding of the biological significance of JA-SA crosstalk was mostly limited to their antagonistic interactions explaining prioritization of JA- or SA-mediated immunity, each of which is effective to suppress the growth of pathogens with different lifestyles over the other (Glazebrook, 2005; Spoel et al., 2007). This is likely because most studies on JA-SA crosstalk have been performed with exogenous application of these hormones or through analysis of single null mutants (Pieterse et al., 2012). Recently, Mine et al. have revealed the molecular mechanisms by which the JA and PAD4 sectors enable resilient and tunable SA responses during flg22-triggered immunity (Mine et al., 2017b) (Figure 2A). Expression of *EDS5*, encoding an SA transporter, is both negatively and positively regulated by JA; JA suppresses the expression of PAD4, a positive regulator of *EDS5*, while JA positively regulates *EDS5* expression via MYC2 (Mine et al., 2017b) (Figure 2A). This network explains the negative role of JA on SA accumulation in the intact network (tunability) and the positive role of JA on SA accumulation when the PAD4 sector is abolished (resilience). Notably, the positive effect of JA on SA is physiologically relevant for the growth suppression of *Pto* under high temperature, which compromises the PAD4 function (Mine et al., 2017b).

Resilience and tunability are also realized by the interactions between PTI and ETI. A recent study revealed a novel immune sector termed EMPIS (ETI-mediating, PTI-inhibited Sector) (Hatsugai et al., 2017). EMPIS regulates ETI responses, including HR cell death, even without the four-sector network and is suppressed by PTI signaling (Figure 2B) (Hatsugai et al., 2017). This system can be interpreted in the context of network resilience and tunability. As long as PTI is effective against pathogens, ETI signaling is suppressed by PTI at EMPIS, but once PTI is compromised by pathogen effectors or other environmental factors, ETI can be activated through EMPIS. The molecular identity of this ETI signaling and its inhibition mechanism by PTI remain elusive, but the latter could be explained by the GYF domain

1. Introduction

protein PSIG1 that is phosphorylated upon MAMP perception and is required for suppressing HR cell death during ETI in an SA- and ROS-independent manner (Matsui et al., 2017). This system avoids unnecessary activation of ETI, which is costly, and is resilient against perturbations of PTI. The study also showed that some avirulent effectors activate EMPIS signaling before EMPIS is suppressed by PTI, suggesting that the strength and dynamics of immune responses can be tuned depending on the repertoire of effectors, which partly determines the potency of pathogens. Thus, this system monitors the pathogen type and activity and protects against pathogens suppressing plant immunity.

1.1.5 Balance: harmony between conflicting responses

Prioritizing responses is considered to be an adapted trait of plants to efficiently use finite energy (Karasov et al., 2017). This is enabled by hormone cross talk such as antagonistic interactions between SA and JA or ABA. During responses against biotrophic pathogens, which activate SA response, plants become more susceptible to attacks by necrotrophic pathogens and insect herbivory, which requires JA responses (Thaler et al., 2012). Also, ABA signal suppresses SA to prioritize abiotic stress responses over biotic stress responses (Yasuda et al., 2008). An apparent paradox is that heterogeneous environments often require plants to accomplish tasks that entail conflicting responses at the same time. It is conceivable that biotrophic and necrotrophic pathogens simultaneously attack plants or that plants experience pathogen attack under abiotic stress conditions such as high salinity (Bai et al., 2018). Recent studies suggested that conflicting stress responses are balanced within the plant body in spatial manners.

Spatial balancing of conflicting responses was observed within a leaf. Real-time monitoring of SA and JA marker gene responses in leaves infected by *Pto* carrying AvrRpt2 revealed that the activation of the SA response was limited to several layers of cells surrounding the pathogen infection site while the JA response was activated widely but exclusively outside of the SA-active region (Betsuyaku et al., 2018). Thus, SA and JA responses are spatially separated within a leaf (Figure 2C). This might suggest that plant leaves fight against biotrophic pathogens by activating SA-mediated immunity at the local infection site and, at the same time, prepare for attacks by other types of pathogen (necrotrophs and herbivores) by activating JA-mediated immunity in the distal area within

the same leaf (Tsuda, 2018) The biological significance of this spatial separation awaits future investigation.

Another balancing effect was seen between leaves when plants experienced biotic and abiotic stresses at the same time. Berens et al., found that ABA antagonized SA responses in old leaves but not in young leaves of four week-old *A. thaliana* plants (Berens et al., 2019). In young leaves, *PBS3*, an SA signaling component, blocks the negative impact of ABA on SA responses and steers young leaves to prioritize for immunity under salt or drought stress. Thus, plants balance SA-ABA crosstalk depending on leaf age (Berens et al., *in press*) (Figure 2D). This balancing crosstalk mediated by *PBS3* appears to contribute to plant growth and reproduction under combined stresses of biotrophic pathogens (bacteria or oomycetes) and salinity (Berens et al., 2019). Moreover, *PBS3* plays a role in shaping leaf age- and salt stress-dependent microbiota assembly (Berens et al., 2019), suggesting that the balancing SA-ABA crosstalk is important to recruit specific microbial communities in old and young leaves under environmental stresses, which may contribute to plant health.

1. Introduction

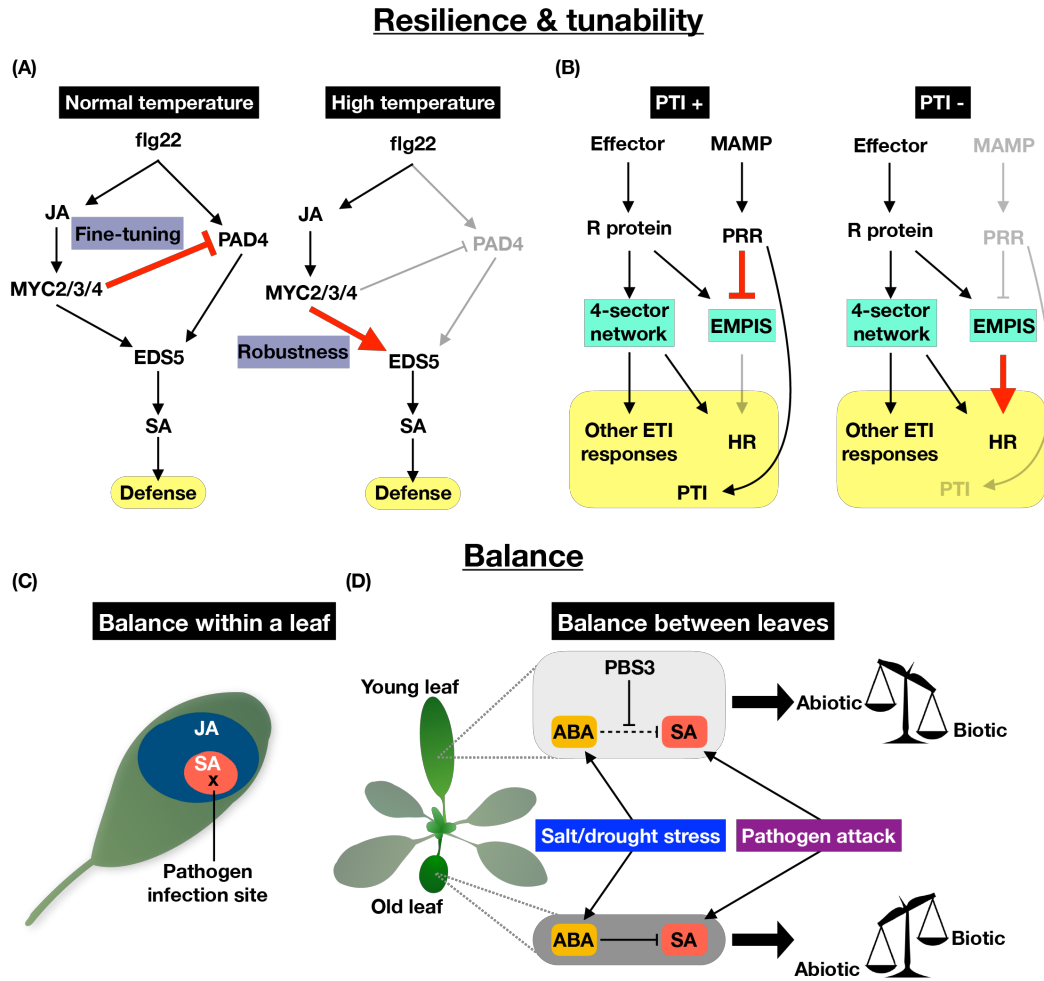


Figure 2: Resilience, tunability, and balance in the plant immune system

(A) The network regulating salicylic acid (SA) accumulation via EDS5. In a normal condition, the jasmonate (JA) pathway negatively regulates PAD4 to fine-tune SA accumulation. At high temperature, where PAD4 function is abolished, the JA pathway positively contributes to SA accumulation by activating EDS5. (B) Interactions between pattern-triggered immunity (PTI) and effector-triggered immunity (ETI) via EMPIS (ETI-mediating, PTI-inhibited Sector). (C) Spatial separation of SA and JA responses upon infection of *Pseudomonas syringae* pv. *tomato* DC3000 (*Pto*) carrying AvrRpt2. (D) Leaf age-dependent prioritization of biotic and abiotic stress responses. Under saline/drought conditions, plant SA responses to biotrophic pathogens are inhibited by the abscisic acid (ABA) pathway in old leaves, while in young leaves, PBS3 protects the SA pathway from suppression by the ABA pathway. This figure was adopted from Nobori et al., 2019 (submitted).

1.2 Bacterial virulence networks

During the course of co-evolution with host plants, pathogens have evolved diverse virulence mechanisms to manipulate the plant immune networks at different levels (Toruño

et al., 2016). A remarkable example is that many pathogens deploy effector proteins or produce phytohormones or their mimics to exploit existing antagonistic interactions in the phytohormone signaling networks, thereby interfering with plant immunity (Kazan and Lyons, 2014; Shen et al., 2018). Thus, the interconnectivity in the plant immune networks provides not only versatile regulation in plants but also vulnerability to pathogen exploitation.

Bacterial pathogens are well-studied with respect to their virulence mechanisms. In addition to proteinaceous type III effectors (T3Es) delivered into the host cell by the type III secretion system (T3SS), many other virulence-related molecules and processes have been characterized, including siderophores, exopolysaccharides, quorum sensing (QS), and production of phytohormones and their mimics (Aslam et al., 2008; Fones and Preston, 2013; Kunkel and Harper, 2017; Quiñones et al., 2005; Ronald and Joe, 2017). Moreover, regulation of these virulence factors are likely coordinated to accomplish diverse tasks in host plants (Mole et al., 2007). These coordinated regulations of virulence factors can be regarded as bacterial virulence networks (Figure 1). Analogous to bacterial virulence molecules that interfere with plant immunity, some plant-derived compounds are known to affect the components of bacterial virulence networks (Yuan et al., 2008).

Bacterial genes and processes that are important for virulence in plants have been characterized in various bacterial species. These include T3SSs, T3Es, QS, and iron homeostasis (Büttner and He, 2009; Fones and Preston, 2013; Quiñones et al., 2005). However, how these processes are regulated *in planta* is poorly understood. In addition, the regulatory mechanisms of pathogen virulence pathways appear to be diverse bacterial species, making it difficult to distil a general concept (Mole et al., 2007). Nevertheless, I highlight relatively well-studied bacterial virulence factors and their regulations *in planta* and discuss the possible feature of the bacterial virulence networks.

T3SSs and T3Es are the best studied bacterial factors in plant pathogens as they are crucial for virulence and for determining host range (Collmer et al., 2000; Fouts et al., 2002; Lindeberg et al., 2009; Tang et al., 2006). Genes related to the T3SS and T3Es are involved in so called the *hrp* regulon and are co-regulated, e.g., they are globally induced upon infection to the host or in growth media mimicking plant environments (Tang et al., 2006). HrpL, an extracytoplasmic function (ECF) sigma factor, is the primary regulator of the T3SS and T3E regulatory pathway in many plant bacterial pathogens (Tang et al., 2006). *P. syringae* lacking *hrpL* showed impaired virulence in tomato and *A. thaliana* (Chen et al., 2009; Sreedharan et

1. Introduction

al., 2006). HrpL also regulates genes that do not encode the T3SS or T3Es. These include *iaaL*, an IAA-amino acid conjugate synthase, *matE*, a putative MATE family transporter, and *corR*, a coronatine regulator, all of which are important for the virulence of *Pto* (Castillo-Lizardo et al., 2015; Mucyn et al., 2014; Sreedharan et al., 2006).

QS is a cell-cell communication process with which bacteria orchestrate their responses as a community and is important for bacterial virulence in the host (Papenfort and Bassler, 2016). QS is mediated by signaling molecules called autoinducers that are produced and secreted into the environment and are perceived by specific receptors. Acyl-homoserine lactones (AHLs) are the most common autoinducer in gram-negative bacteria (Papenfort and Bassler, 2016). In *P. syringae* pv. *syringae* (*Pss*), a mutant lacking both the AHL synthase and AHL receptor showed impaired virulence in bean leaves (Quiñones et al., 2005). The QS system was shown to regulate many downstream genes related to virulence, such as plant cell wall degrading enzymes and the T3SS in *Pectobacterium atrosepticum* during infection in potato (Liu et al., 2008). Bacteria might also employ QS systems to respond to host signals in addition to their own signals. Typically, genes encoding an AHL synthase and AHL receptor are linked on the genome, but some receptor genes lack their paired AHL synthase genes and are called orphan or solo receptors (Patankar and González, 2009). A subgroup of the orphan receptors of plant-associated bacteria responds to plant-derived compounds and regulates bacterial genes related to virulence (González and Venturi, 2013; Venturi and Fuqua, 2013). For instance, an orphan receptor of *Xanthomonas oryzae* pv. *oryzae*, OryR, is important for responding to rice-derived compounds and positively regulating the expression of virulence genes (Ferluga et al., 2007; Ferluga and Venturi, 2009; González et al., 2013).

Iron is an essential element for most organisms including plants and bacteria and iron homeostasis is known to be important for bacterial virulence in plant and animal hosts (Chandrangsu et al., 2017; Fones and Preston, 2013). In many bacterial species, iron responses are primarily regulated by Fur, which typically functions as a transcriptional repressor of its target genes in the presence of Fe²⁺ and this negative regulation is released under an iron deficient condition (Troxell and Hassan, 2013). Among the Fur-regulated genes is *pvdS*, encoding an ECF sigma factor, which regulates genes related to the production of a siderophore, pyoverdine, and other genes (Butcher et al., 2011; Swingle et al., 2008). Siderophores were shown to be important for virulence of *P. syringae* pv. *tabaci* in tobacco

(Taguchi et al., 2010), but are dispensable for virulence of *Pto* in tomato and *A. thaliana* (Jones and Wildermuth, 2011).

Another ECF sigma factor, AlgU, also contributes to the virulence of bacterial pathogens (Markel et al., 2016). AlgU controls alginate biosynthesis and other processes and *algU* mutants of *Pto*, *P. syringae* pv. *glycinea* (*Psg*) PG4180, and *Pss* B728a showed reduced virulence in plants (Markel et al., 2016; Schenk et al., 2008; Yu et al., 2014). Alginate production was shown to be important for the virulence of *P. aeruginosa* and *Pss* (Yorgey et al., 2001; Yu et al., 1999), but be dispensable for the virulence of *Pto* and *Psg* PG4180 (Markel et al., 2016; Schenk et al., 2008), suggesting that other processes controlled by AlgU are important for bacterial virulence. Indeed, RNA-seq analysis of *in vitro* cultured *Pto* showed that, in addition to alginate biosynthesis, AlgU regulates genes related to osmotic and oxidative stress responses and the T3SS, which might explain the role of AlgU in bacterial virulence (Markel et al., 2016). Moreover, a microarray analysis of the *algU* mutant of *Pss* B728 *in planta* showed that AlgU impacts expression of many genes beyond alginate production (Yu et al., 2014).

In some plant bacterial pathogens, the regulation of the T3SS and QS systems are influenced by AlgU and/or iron availability. The *hrp* regulon of *Pto* is positively regulated by AlgU and external iron (Bronstein et al., 2008; Markel et al., 2016). Fur positively regulates *psyI* and *psyR*, which encode an AHL synthase and receptor, respectively, in *P. syringae* pv. *tabaci* (Cha et al., 2008). A PvdS-binding site was found in the upstream region of *psyI* in *Pto* (Swingle et al., 2008), although whether PvdS regulates *psyI* remains elusive. In addition, it has been shown that iron availability affects QS processes in *Pss* (Dulla et al., 2010). Thus, bacterial virulence signaling pathways appear to be interconnected to form bacterial virulence networks. Similar to plant immune networks, this interconnected feature would provide regulatory potential that benefits bacterial pathogens inside and outside the host, but at the same time might be targeted by plant immunity.

1. Introduction

1.3 Interactions between plant immune and bacterial virulence networks

1.3.1 The plant receptor networks as targets of pathogens

Pathogens have evolved effector molecules that target the network of cell surface receptors to dampen PTI. BAK1, a hub of the network, is targeted by multiple effectors: AvrPto, AvrPtoB, HopF1, and HopB1 (Li et al., 2016; Shan et al., 2008; Zhou et al., 2014). Intriguingly, HopB1 protease specifically cleaves immune-activated BAK1, thus conferring virulence without perturbing other BAK1 functions such as those in plant growth (Li et al., 2016). AvrPtoB also targets the MAMP receptors FLS2 and CERK1 (Gimenez-Ibanez et al., 2009; Göhre et al., 2008; Xiang et al., 2008). HopAO1 targets another MAMP receptor, EFR (Macho et al., 2014). Therefore, although the network of cell surface receptors enables plants to finely control PTI responses, it can be exploited by pathogens as the manipulation of a PRR could affect other parts of the network due to its highly interconnected nature.

Although ETI confers potent and resilient immunity against biotrophic pathogens, which feed on living host tissues, ETI is exploited by some necrotrophic pathogens, which actively kill host tissues and feed on the dead cells. In oats, an immune component TRX-h5 is guarded by the NLR LOV1 (Lorang et al., 2012; Wolpert and Lorang, 2016). *Cochliobolus victoriae*, a necrotrophic fungus and the causal agent of Victoria blight, hijacks this immune system by producing an effector molecule, victorin, which binds to TRX-h5 and consequently triggers HR cell death via LOV1, rendering the oat plant susceptible (Lorang et al., 2012; Wolpert and Lorang, 2016). Another necrotrophic fungus, *Parastagonospora nodorum*, produces SnToxA, which indirectly activates the wheat NLR Tsn1 to cause HR cell death and susceptibility (Shi et al., 2016). *P. nodorum* also produces another toxin SnTox1, which directly binds to Snn1, a wall associated kinase class receptor kinase, to trigger cell death for inducing susceptibility (Shi et al., 2016). Thus, plant immune signaling that is associated with cell death is exploited by necrotrophic pathogens for their growth in plants. However, it was shown that prior ETI activation in one half of a leaf has no effect on promoting the growth of the necrotrophic fungus *Alternaria brassicicola* in the other leaf half (Spoel et al., 2007). Furthermore, ETI-associated cell death and immune responses are tightly regulated in a spatiotemporal manner (Betsuyaku et al., 2018; Tsuda, 2018). Therefore, it may be possible

that spatiotemporal regulation of ETI responses including cell death provides certain tolerance against exploitation by necrotrophic pathogens in natural conditions.

1.3.2 Phytohormone networks as targets of pathogens

Bacterial and fungal pathogens have evolved to target the phytohormone network to interfere with plant immunity, often by exploiting the interconnected feature of the phytohormone signaling networks (Kazan and Lyons, 2014; Shen et al., 2018). Hormone crosstalk suppressing SA (e.g., JA-SA, ABA-SA, and auxin-SA) is often exploited by biotrophic bacterial pathogens that are sensitive to SA-mediated immunity. Here, I highlight two types of exploitation/targeting of phytohormone crosstalk in plant-bacteria interactions. The first is the manipulation of phytohormone signaling pathways by using effector proteins. AvrB, HopBB1, HopX1, and HopZ1a employ different mechanisms to inactivate JAZ proteins, the repressors of JA-mediated transcriptional reprogramming, thereby activating JA signaling to suppress SA-mediated immunity (Gimenez-Ibanez et al., 2014; Jiang et al., 2013; Yang et al., 2017; Zhou et al., 2015). Similarly, AvrPtoB and AvrRpt2 enhance the accumulation of ABA and auxin, respectively, and promote virulence (Chen et al., 2007; de Torres-Zabala et al., 2007). The second strategy is the production of phytohormones or their mimics. The phytotoxin coronatine produced by some strains of *P. syringae* functions as an analogue of JA-isoleucine (JA-Ile), an active form of plant endogenous JA, and contributes to suppressing stomatal and apoplastic immunity by reducing SA accumulation and/or by inactivating MAPKs (Mine et al., 2017a; Zheng et al., 2012). Production of coronatine or coronatine-like compounds is known in other bacterial strains, suggesting that producing JA-Ile mimicking compounds may be a wide-spread strategy for bacteria to confer fitness advantages in plant hosts (O'Neill et al., 2018; Zhang et al., 2017). Several plant pathogens produce the auxin indole-3-acetic acid (IAA) and affect host auxin signaling (Kunkel and Harper, 2017). Disruption of bacterial *aldA* and *aldB*, encoding IAA biosynthesis enzymes, leads to reduced bacterial virulence in the plant host in an SA-dependent manner (McClerkin et al., 2018), suggesting that exploiting auxin signaling is a bacterial virulence mechanism that suppresses SA-mediated immunity. Notably, some bacteria are known to produce SA although the physiological significance of this during interaction with plants remains elusive (Bakker et al., 2014; Jones et al., 2007).

1. Introduction

Which of these two strategies (signaling manipulation by proteinaceous effectors or phytohormones) is more advantageous for pathogens? Effector proteins that target phytohormone signaling pathways are risky because effectors can be recognized by plant NLRs and trigger ETI. Indeed, AvrRpt2, AvrB, AvrPtoB, and HopZ1a are known to trigger ETI in certain plant genotypes (Bent et al., 1994; Jiang et al., 2013; Kim et al., 2002; Mackey et al., 2002; Mindrinos et al., 1994). On the other hand, phytohormones or their mimics produced by bacteria would have no or less risk of triggering ETI as they can hardly be recognized as foreign molecules. Thus, it could be argued that the production of phytohormones (mimics) is more advantageous. However, a comparative genome analysis of 287 *P. syringae* strains showed that coronatine is not the dominating JA-activating molecule over other JA-manipulating effectors (Yang et al., 2017). Although more comprehensive analysis including coronatine-like molecules would be helpful, this data implies that there are additional factors that determine the value of these virulence molecules. Since biosynthesis of coronatine requires a series of chemical reactions and enzyme-encoding genes, it is possible that coronatine production may be costly for bacteria compared with T3Es as a single T3E can provide an added value (Bender et al., 1999). Another possible advantage of effectors is that effectors may be able to target specific functions of plants. It was proposed that, while coronatine and HopX1a fully activate JA responses, HopBB1 targets only a subset of the JAZ proteins and activates a subset of JA-mediated responses, potentially minimizing pleiotropic negative effects on the hosts, which could lead to the benefit of the pathogens (Yang et al., 2017).

Plants are not entirely helpless against pathogen virulent effectors. ETI can effectively suppress pathogen growth despite the existence of many virulence T3Es and toxins that interfere with the plant immune networks. An emerging idea for explaining this is that ETI can counteract virulence actions of pathogen effectors. For instance, ETI triggered by AvrRpt2 induces S-nitrosylation and inactivation of the bacterial effector HopAII that suppresses mitogen-activated protein kinases (MAPKs), important components of plant immunity (Meng and Zhang, 2013), thereby restoring plant immunity (Ling et al., 2017). Also, AvrRpt2-triggered ETI cancels coronatine-triggered gene regulation that causes MAPK inactivation (Mine et al., 2017a). Understanding the precise mechanisms of pathogen virulence and its suppression by plant immunity is key to engineer the plant immune networks. For instance, the crystal structure of the receptor-ligand complexes guided the

engineering of the JA receptor COI1 to avoid binding to coronatine while maintaining the binding with JA-Ile (Zhang et al., 2015). Transgenic plants expressing the modified COI1 receptor in *coi1* background showed insensitivity against coronatine while maintaining the functions of endogenous JA (Zhang et al., 2015), supporting its potential benefit in agriculture.

1.3.3 Plant-derived compounds affect bacterial virulence-related processes

The role of plant-derived compounds during plant-bacterial interactions is well studied in the legume-rhizobium symbiosis. Phenolic compounds, especially flavonoids, are secreted by legume plants and recognized by rhizobia in a species-specific manner, which then regulates rhizobial genes important for establishing symbiotic interactions (Cao et al., 2017). However, little is understood about how plant-derived compounds affect bacterial pathogens in plants.

Although we poorly understand about how plants intervene with the bacterial virulence networks, accumulating evidence suggests that plant-derived compounds can affect bacterial physiology. The QS signaling of some bacterial species was shown to be affected by plant-derived compounds *in vitro* (Choo et al., 2006; Degrassi et al., 2007; Gao et al., 2003; Keshavan et al., 2005; Rasmussen and Givskov, 2006; Teplitski et al., 2004, 2000; Vikram et al., 2010; Yuan et al., 2008). For instance, SA and γ -aminobutyric acid activate the quorum-quenching system, *attKLM* operon, in *Agrobacterium tumefaciens* and suppress QS responses (Yuan et al., 2008). Also, flavonoids derived from citrus inhibit the QS system, biofilm formation, and T3SS expression of *Vibrio harveyi* (Vikram et al., 2010). Rosmarinic acid was shown to act as an AHL mimic and directly bind to a QS receptor RhIR of *P. aeruginosa* affecting bacterial physiology (Corral-Lugo et al., 2016). These examples illustrate the possibility that plants modulate bacterial QS processes as a defense strategy.

Phytohormones also can directly affect bacterial physiology. SA was shown to suppress the expression of virulence genes in *A. tumefaciens* and *P. aeruginosa* (Prithiviraj et al., 2005; Yuan et al., 2008). Lebeis et al. showed that SA directly affects *in vitro* growth of some bacterial strains isolated from *A. thaliana* plants grown in a wild soil (Lebeis et al., 2015). Notably, the accumulation of SA in the apoplast, a prevalent growth niche for bacterial pathogens, was shown to increase upon pathogen infection (Carviel et al., 2014). These results imply that plants employ SA to affect metabolisms of bacterial pathogens directly as well as

1. Introduction

through well-described SA-mediated plant immune signaling (Seyfferth and Tsuda, 2014). In addition, a plant-derived auxin, IAA, negatively affects expression of virulence genes in *A. tumefaciens* and the T3SS in *Pseudomonas savastanoi in vitro* (Aragón et al., 2014; Yuan et al., 2008). On the other hand, plant-produced IAA in plants and the exogenous application of IAA *in vitro* positively regulate the expression of virulence genes in *Dickeya dadantii* 3937 (Yang et al., 2007) and genes encoding components of the type VI secretion system of *P. savastanoi* (Aragón et al., 2014), respectively. Although it is evident that phytohormones can affect bacterial metabolism and behaviors, the molecular mechanisms of how bacteria perceive phytohormones and if phytohormone perception is important for bacterial virulence are poorly understood.

The *hrp* regulon is also responsive to plant-derived compounds (Tang et al., 2006). Plant apoplastic extracts can induce the *hrp* genes (Rico and Preston, 2008). Moreover, several organic acids produced by plants were shown to induce the *hrp* genes of *Pto in vitro* as well as *in planta* (Anderson et al., 2014). This may contribute to the induction of the *hrp* genes upon contact with plant cells. Some plant-derived compounds suppress the *hrp* genes. Plant-derived flavonoids suppress the expression of *hrp* genes and flagella (Vargas et al., 2013). Also, the *A. thaliana* mutant of *att1*, a cytochrome P450 monooxygenase catalyzing fatty acid hydroxylation, showed higher expression of T3SS genes of *P. syringae* pv. *phaseolicola* (*Pph*) compared with wild-type plants (Xiao et al., 2004), implying that plant-derived fatty acids may suppress the expression of the T3SS. Collectively, various plant-derived compounds might function as signaling cues for bacterial pathogens to induce the virulence pathways and also function as defense molecules for plants to suppress bacterial virulence.

1.3.4 How does plant immunity affect bacterial signaling networks?

It has been shown that PTI, but not ETI, suppresses the expression of T3SS genes in *Pto* (Crabill et al., 2010a; Nomura et al., 2011) and the translocation of T3Es into plant cells (Crabill et al., 2010a; Nomura et al., 2011; Oh et al., 2010). However, the molecular mechanism of how plant immunity affects bacterial gene expression is mostly enigmatic. It was shown in *A. thaliana* that the MAPK MPK6 suppresses the production of plant organic acids that induce T3SS expression and T3E translocation, thereby inhibiting bacterial growth (Anderson et al., 2014). These organic acids are likely secreted into the plant apoplast and

affect bacterial responses. Changing apoplastic conditions may be a major plant immune strategy to control foliar bacterial pathogens. During ETI triggered by the infection of *Pph*, the leaf apoplast of *Phaseolus vulgaris* showed various changes including increased pH and accumulation of GABA and metal cations, some of which may be responsible for pathogen growth inhibition (O’Leary et al., 2016). Sugar transporters in *A. thaliana* are activated during PTI and sequester apoplastic sugar to inhibit the activity of the T3SS and bacterial growth (Yamada et al., 2016). Plant immunity might also control pathogen virulence by keeping water content in the apoplast low, as *Pto* creates an aqueous apoplast for virulence (Xin et al., 2016). Furthermore, limiting or over-supplying metals is known to be a defense strategy in animals (Chandrangsu et al., 2017). Thus, it is plausible that plants change the content of metals in the apoplast to inhibit bacterial growth (Fones and Preston, 2013). Understanding how these changes in the apoplast caused by plant immunity affect bacterial metabolisms *in planta* is crucial for better understanding the mode of action of plant immunity to inhibit pathogen growth. However, there is no comprehensive study on this topic due to the technical difficulties in profiling global bacterial responses *in planta*.

1.4 Roles of plant immunity in shaping microbiota

Plant immunity not only inhibits the growth of pathogens in the plant body, but it also allows plant microbial communities to assemble and endure (Hacquard et al., 2017). Bacterial communities can promote plant growth and protect plants from pathogenic bacteria or filamentous fungi, suggesting that keeping certain microbes close is crucial for plant survival (Duran et al., 2018; Kwak et al., 2018). Thus, it is likely that plants integrate signals from the microbiota for their decision-making. Microbiota signals can be highly heterogeneous as they contain a variety of microbes that have various MAMPs and other factors that affect plant immune systems. Recently, it has been shown that some plant-associated Rhizobiales species suppress plant immune responses by yet unknown mechanisms (Garrido-Oter et al., 2018). The spatial distribution of microbiota members (niche specificity) can be highly heterogeneous, although no comprehensive study has visualized this. Moreover, a bacterial species can create heterogeneous populations in hosts (Rufián et al., 2016; West and Cooper, 2016). Environmental factors that impact plant immune responses are also heterogeneous in time and space. In soil, nutrients exist in a

1. Introduction

heterogeneous manner and thus nutrient availability varies within a plant body (Farley and Fitter, 1999; Jackson and Caldwell, 1993; Lark et al., 2004). Therefore, plant immunity would need to be resilient, tunable, and balanced to integrate heterogeneous microbial and non-microbial inputs and respond in spatially resolved manners for shaping a healthy microbiota.

To understand the interactions between the plant immune system and plant microbiota, a reductionist approach can be taken. A first step is to understand the potential of plants to respond to a microbial community. Host genetics can then dissect the contribution of plant processes in responding to the microbiota under different environmental conditions. A recent study showed that a bacterial community regulates plant immune responses under phosphate deficiency in a manner dependent on *PHR1*, the master transcriptional regulator of phosphate starvation responses (Castrillo et al., 2017). Studies of plant responses to bacteria and fungi that can trigger induced systemic resistance (ISR) pointed to *MYB72* as a central regulator of ISR (Martínez-Medina et al., 2017; Van der Ent et al., 2008; Verhagen et al., 2004). *MYB72* is known to be induced under iron-deficient conditions and is essential for the excretion of iron-mobilizing compounds, such as coumarins, which also have selective antimicrobial activity (Gnonlonfin et al., 2012; Stringlis et al., 2018; Zamioudis et al., 2014). A recent study showed that *MYB72*-dependent coumarin exudation is important for root microbiota assembly (Stringlis et al., 2018). These examples suggest that the link between plant immunity and plant responses to nutrient conditions is likely an adaptive trait for plants to integrate multiple environmental inputs.

Currently, plant responses to each microbiota member or microbial community are poorly understood except for some microbes beneficial to plants. The roles of plant immune networks in responses to the plant microbiota are important areas of research for the better understanding of plant-microbiota interactions. It is important to understand the plant immune system at multiple layers, i.e., plant cellular responses against microbiota members, immune outputs that directly affect microbiota members, and the impact of plant immunity on microbiota members and microbe-microbe interactions. This would be crucial to address a fundamental question in plant microbiota research: how do plants winnow the surrounding microbial communities to shape the plant microbiota? Transcriptome and proteome studies of each plant microbiota member and metatranscriptome and metaproteome studies of microbial communities are potential strategies to tackle this question (Levy et al., 2018).

1. Introduction

1.5 Thesis Aims

Despite extensive studies on molecular events inside the plant cells during immunity, little is known about how plant immunity influences bacterial cellular processes to inhibit pathogen growth. One approach to gain insights into bacterial cellular changes during plant immunity is *in planta* transcriptome/proteome profiling of bacteria. However, *in planta* bacterial transcriptomics and proteomics of bacteria are challenging due to low abundance of bacterial mRNA/proteins compared to plant RNA/proteins, and it is particularly difficult to obtain sufficient bacterial information at an early stage of infection, where molecular events that critically influence the outcome of the plant-bacterial interaction might occur. Several previous studies profiled *in planta* bacterial transcriptomes by using microarrays and RNA-seq (Chapelle et al., 2015; Chatnaparat et al., 2016; Yu et al., 2014, 2013) and *in planta* proteomes of bacteria on the leaf surface (Müller et al., 2016). However, the impact of plant signaling on the genome-wide bacterial transcriptomes/proteomes remains unknown.

Here, I established methods for profiling transcriptomes and proteomes of *Pto* in naïve and immune-activated plant leaves at early and late infection stages (6 and 48 h post infection, hpi). These methods greatly enriched bacterial information from plant leaves. By profiling *Pto* transcriptomes in various immune activated/compromised conditions, I uncovered specific “immune-responsive” bacterial processes and genes whose expression was altered by PTI and ETI. Also, I showed that expression patterns of *Pto* genes at the early infection stage had a high predictive power for later bacterial growth at 48 hpi. Furthermore, I found that overexpression of *pvdS*, a global iron regulator belonging to the immune-responsive gene sector, could partially counter bacterial growth inhibition during ETI. I also demonstrated that bacterial transcriptomes and proteomes are highly correlated in general, but there are cases where gene and protein expression patterns are discordant. Notably, proteins at the tip part of the bacterial T3SS were suppressed only at the protein level by the plant SA pathway.

Plant immunity not only suppresses pathogen growth, but it also affects the structure of bacterial communities (microbiota) and probably their functions. However, it is not understood how plant immunity affects individual bacterial species surrounding plants and shape the plant microbiota. To address this important question, I developed a pipeline for the co-transcriptome analysis of both *A. thaliana* and various commensal bacteria during

interactions. I found that different bacterial strains trigger plant immunity at different levels and there are common and specific bacterial processes regulated *in planta* among diverse bacterial strains. This approach, combined with bacterial growth assay, has the potential to elucidate the mechanisms by which plants discriminate different bacterial species and control their growth *in planta*. In summary, these approaches would help the research community of plant-microbe interactions to understand the mechanisms of plant immunity to inhibit pathogen growth and to shape the microbiota.

2 Results

2.1 *In planta* transcriptomics of *Pto* DC3000

2.1.1 Method establishment of *in planta* bacterial transcriptomics

To analyze the transcriptome of the model foliar bacterial pathogen *P. syringae* pv. *tomato* DC3000 (*Pto*) in *A. thaliana*, I initially attempted RNA-seq analysis using total RNA extracted from *A. thaliana* leaves infected by *Pto*. This approach failed to capture sufficient bacterial mRNA reads, being masked by overwhelmingly abundant plant RNA reads (Supplementary figure 1 A and B). To solve this problem, I established a method in which bacterial cells are first isolated from infected leaves before RNA extraction (Figure 3A) (Nobori et al., 2018b; Nobori and Tsuda, 2018). Infected leaves were harvested, coarsely crushed, and incubated in “bacterial isolation buffer”, which fixes and stabilizes bacterial RNA (Figure 3C and Supplementary figure 1C; see Materials and Methods for the establishment of a bacterial isolation buffer). After incubation, large plant debris was removed by filtering, and the flow-through was centrifuged to separate bacterial cells from plant tissues. Total RNA was extracted from the isolated bacterial cells, followed by rRNA depletion of both plants and bacteria to enrich mRNA, library preparation, and RNA-seq. This method successfully enriched for bacterial sequences (Figure 3C and Supplementary figure 1 A and B), allowing me to profile high-quality *in planta* bacterial transcriptomes with as few as 10 million total RNA-seq reads using the Illumina HiSeq platform (Supplementary figure 1 C and D and Supplementary figure 2 A-C). RNA-seq results were highly reproducible among independent biological replicates and sensitive enough to capture bacterial transcriptome differences between biologically distinct samples (Supplementary figure 2B). Gene expression data obtained by this RNA-seq strategy strongly correlated with RT-qPCR measurements using total RNA extracted directly from *Pto*-infected leaves (Figure 3D), indicating the accuracy of the RNA-seq data. To further assess the validity of the RNA-seq data, I compared my data with the one from a more costly alternative approach developed by the group of Prof. Dr. Sheng Yang He (Michigan State University), in which bacterial mRNA was isolated directly from infected plants without prior bacterial separation from the plant tissue, but, instead, highly abundant plant mRNA as well as plant and bacterial rRNAs were

removed by customized probes to enrich bacterial mRNA during cDNA library preparation (Figure 3B; See Materials and Methods). Note that these experiments were done completely independently in two laboratories with different growth conditions and pretreatments for plants, different preparations of bacterial inocula, and different kits for RNA extraction and cDNA library preparation (see Materials and Methods). Strikingly, these two methods led to highly similar results (Figure 3E), providing further proof-of-concept for both methods. Collectively, the method I established enabled a reliable profiling of *in planta* bacterial transcriptome with RNA-seq.

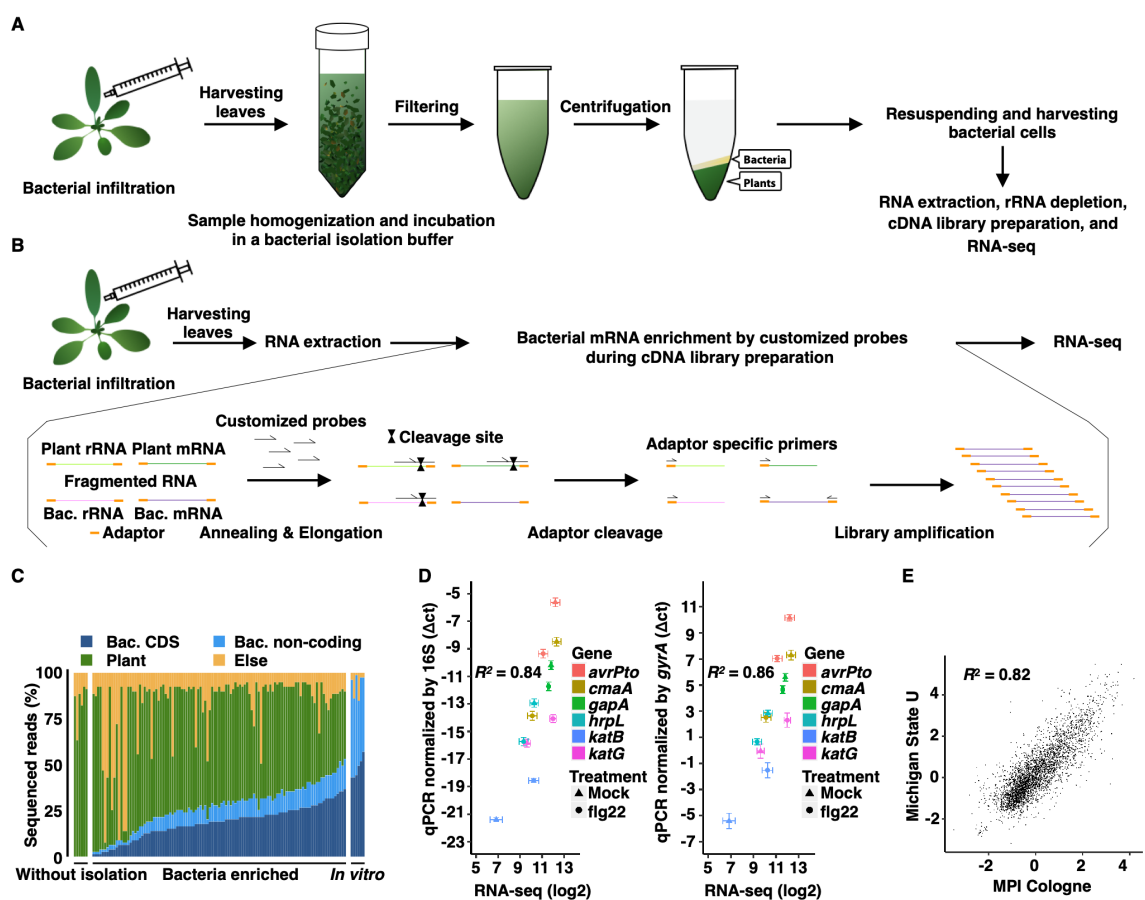


Figure 3: Establishment of *in planta* *Pto* transcriptome analysis

(A) Workflow of *in planta* bacterial transcriptome analysis based on bacterial isolation (See Materials and Methods for further information). (B) Workflow of *in planta* bacterial transcriptome analysis based on selective depletion of plant-derived transcripts (See Materials and Methods for further information). (C) The ratio of sequenced reads mapped on bacterial (“Bac.”) coding sequence (CDS), bacterial non-coding sequence, *A. thaliana* (“Plant”) genome, and else in all samples, including samples without bacterial enrichment as well as *in vitro* samples. (D) Validation of RNA-seq data by RT-qPCR. Four-week-old *A. thaliana* leaves were pretreated with 1 μ M flg22 or water (Mock) one day before infection with *Pto* ($OD_{600} = 0.5$) and harvested at 6 h post infection. The samples were split into two: one was subjected to direct RNA extraction followed by RT-qPCR analysis and the other was

2. Results

subjected to bacterial enrichment followed by RNA-seq. RT-qPCR results were normalized with the *Pto* 16S or *gyrA* expression (mean \pm s.e.m.; n = 4 biological replicates from four independent experiments). RNA-seq data were processed as described in Materials and Methods (mean log₂ count per million \pm s.e.m.; n = 4 biological replicates from four independent experiments). Pearson correlation coefficients (R^2) are shown. (E) *Pto* gene expression fold changes (log₂) in flg22-pretreated plants compared to mock-pretreated plants based on RNA-seq data independently obtained by two different approaches in two different laboratories: the method based on bacterial isolation from infected plants (MPI Cologne; x-axis) and on bacterial mRNA enrichment using customized oligonucleotides to remove abundant plant RNA without bacterial isolation (Michigan State U; y-axis). Pearson correlation coefficient is shown. See Materials and Methods for detailed experimental procedures. This figure was adopted from (Nobori et al., 2018b).

2.1.2 *Pto* transcriptome signatures influenced by plant immune activation

I profiled *Pto* transcriptomes under 27 *in planta* conditions and five *in vitro* conditions using the method shown in Figure 3A (114 samples in total; Figure 4A and Supplementary figure 3; see Supplementary table 1 for the full sample list with the number of replicates). Four *Pto* strains were employed. Wild-type *Pto* strain has T3Es that effectively suppress plant immunity in the *A. thaliana* wild-type Col-0, resulting in effector-triggered susceptibility (ETS). *Pto* strains that ectopically express a T3E, AvrRpt2 or AvrRps4 (hereafter *Pto* AvrRpt2 or *Pto* AvrRps4) trigger ETI dependent on the presence of cognate plant intracellular immune NLR receptor, RPS2 or RPS4, respectively (Bent et al., 1994; Gassmann et al., 1999; Mindrinos et al., 1994). The *Pto* D36E mutant lacks 36 *Pto* T3Es, lacking the ability to suppress plant immunity (Wei et al., 2015). In my conditions, bacterial proliferation was observed at 9 hpi, but not at 6 hpi (Supplementary figure 4) in both ETS and ETI in WT Col-0 plants and highly immune-compromised *dde2 ein2 pad4 sid2* mutant plants (Tsuda et al., 2009). Thus, I decided to profile *in planta* *Pto* transcriptomes at 6 hpi because bacterial population density can affect bacterial gene expression patterns through, for instance, quorum sensing (Papenfert and Bassler, 2016). All four *Pto* strains showed similar transcriptome patterns in nutrient-rich King's B (KB) bacterial growth medium; and these patterns were distinct from that of *Pto* grown in T3E-inducible minimal medium (Huynh et al., 1989) (MM; Figure 4B and Supplementary figure 5A). As expected from the previous studies (Tang et al., 2006), genes related to the T3SS and T3Es were globally induced in MM compared to KB (Figure 4C). Gene ontology (GO) analysis revealed that genes related to the T3SS and coronatine biosynthesis (Mittal and Davis, 1995) were induced in plants as

compared with KB medium (Figure 4C), consistent with the crucial roles of the T3SS and coronatine for *Pto* virulence (Brooks et al., 2004; Hauck et al., 2003).

Pretreatment with a PTI elicitor derived from bacterial flagellin, flg22, triggers strong plant transcriptional reprogramming and resistance against bacterial pathogens (Zipfel et al., 2004). However, the impact of flg22-triggered plant responses on any bacterial transcriptome remains unknown. I found that flg22-pretreated plants affected a substantial number of *Pto* genes and globally suppressed the bacterial processes activated in susceptible plants (Figure 4C). The transcriptome patterns of *Pto* D36E *in planta* resembled that of *Pto* in flg22-pretreated plants (Figure 4 B and C and Supplementary figure 5A). This supports the notion that effector deficient *Pto* D36E lacks the ability to suppress PTI and that pre-activation of PTI with flg22 can overcome effector-mediated immune suppression by wild-type *Pto*. Importantly, these results revealed that PTI suppresses not only bacterial virulence-associated mechanisms such as the T3SS, siderophore and coronatine biosynthesis, but also fundamental housekeeping processes for organisms. For instance, genes related to translation (mostly ribosomal proteins) were induced in *Pto in planta*, but were suppressed by PTI (Figure 4C), implying that the bacterial protein synthesis activity may also be targeted by PTI.

During ETI triggered by AvrRpt2 or AvrRps4, several hundred genes (199 genes for AvrRpt2 and 317 genes for AvrRps4) were differentially expressed when compared with ETS (*Pto* infection; Figure 4C), although the effect was not as dramatic as PTI (Figure 4B). In particular, I found that ETI triggered by AvrRpt2 or AvrRps4 specifically led to down-regulation of genes associated with siderophore and coronatine biosynthesis (Figure 4C). However, T3SS genes were not globally affected during ETI, in contrast to PTI-inducing conditions, suggesting that PTI and ETI differently affect *Pto* transcriptomes despite their overlapping downstream immune signaling components and their common ability to inhibit bacterial growth *in planta*. In addition, within the genes differentially expressed among the different conditions, 658 genes were annotated as “hypothetical proteins” (Supplementary figure 5B), suggesting that a substantial number of *Pto* genes likely playing roles during the interaction with *A. thaliana* have yet to be characterized. Taken together, the data revealed previously unknown transcriptomic responses of *Pto* during the activation of two major forms of plant immunity, PTI and ETI.

2. Results

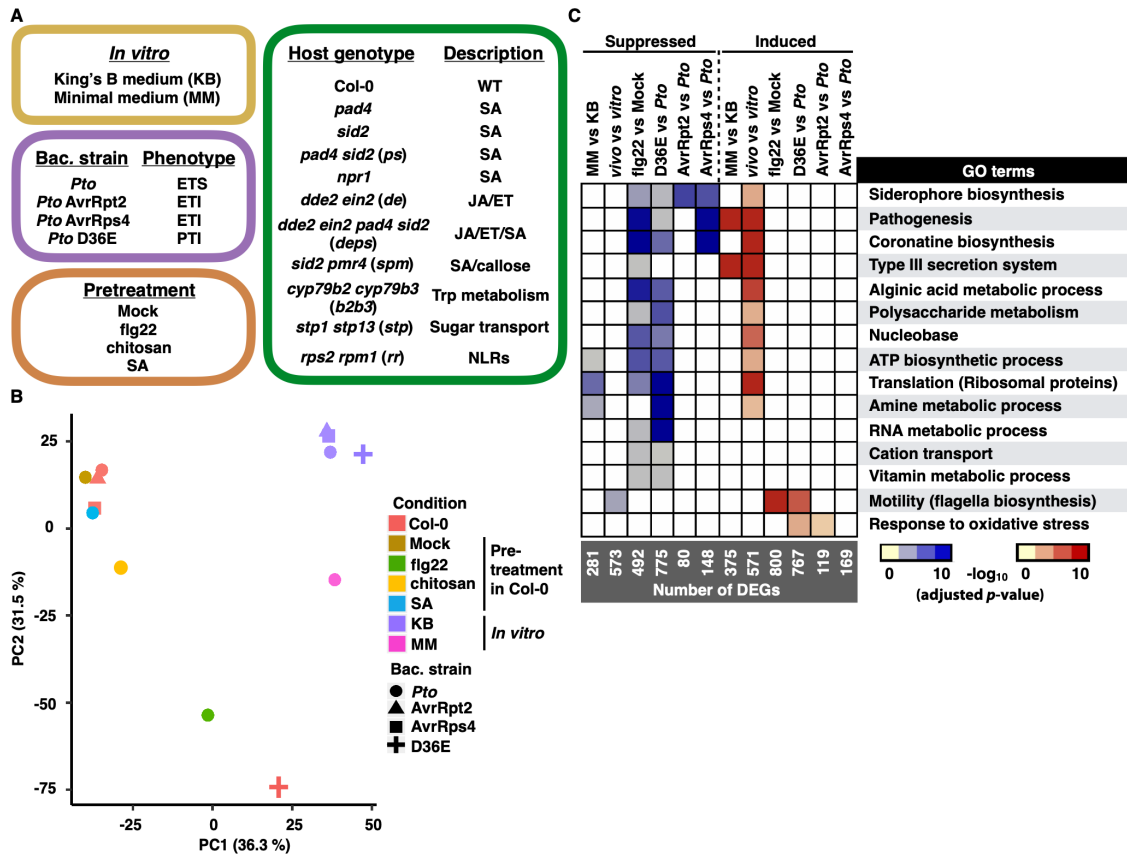


Figure 4: Profiles of *Pto* transcriptome under various conditions

(A) Plant genotypes, bacterial (bac.) strains, and conditions used in this study. For the full sample list, see Supplementary table 1. *Pto*, *Pseudomonas syringae* pv. tomato DC3000; ETS, effector-triggered susceptibility; ETI, effector-triggered immunity; PTI, pattern-triggered immunity; SA, salicylic acid; JA, jasmonic acid; ET, ethylene; Trp, tryptophan; NLRs, nucleotide-binding domain leucine-rich repeat proteins. (B) Principle component analysis of 3344 genes detected in all of the samples. (C) Heatmap of $-\log_{10} p$ -value (adjusted by the Benjamini-Hochberg method) of the gene ontology (GO) terms representing the differentially expressed genes in different comparisons. MM, *Pto* in MM medium; KB, *Pto* in KB medium; *vivo*, *Pto* infection to Col-0; *vitro*, *Pto* in KB medium. This figure was adopted from (Nobori et al., 2018b). For the list of differentially expressed genes and complete enriched GO terms, see (Nobori et al., 2018b).

2.1.3 *In planta* bacterial transcriptome patterns at an early time point is tightly linked to later bacterial growth during infection

Plant signaling pathways mediated by defense hormones, SA, JA, and ET contribute to bacterial growth suppression in a redundant manner (Tsuda et al., 2009). However, it is not known whether these hormone-signaling pathways affect the bacterial transcriptome similarly or differently. To address this question, I investigated transcriptome patterns of *Pto* or *Pto* AvrRpt2 in seven different *A. thaliana* mutants lacking one or more of these hormone

defense pathways (Figure 4A). Host genotype effects were observed more clearly in *Pto* AvrRpt2 infection than in *Pto* infection at 6 hpi; 321 genes of *Pto* AvrRpt2 were differentially expressed between Col-0 plants and at least one of the defense signaling mutants, while only 26 genes of wild type *Pto* were differentially expressed. Thus, I focused on the differentially expressed genes (DEGs) of *Pto* AvrRpt2 (Figure 5A; left panel; blue/yellow heatmap) for further analysis. Comparisons between Col-0 and the immune-compromised mutants revealed that the effects of distinct hormone pathways were qualitatively similar (Figure 5A; middle panel; green/magenta heatmap). For example, the genes suppressed by the SA pathway were also suppressed by the JA/ET pathway. This implies that different immune pathways may converge on a common impact on the global gene expression of *Pto*. Strikingly, the expression patterns of the DEGs at 6 hpi, when bacterial population density remained unchanged compared to that observed at 0 hpi (Supplementary figure 4), strongly correlated with bacterial growth at 48 hpi in different plant genotypes ($R^2=0.94$; Figure 5B), suggesting that bacterial transcriptome patterns at the early phase of infection could explain future bacterial growth.

STP1 and *STP13* encode sugar transporters, which were shown to sequester sugars from the apoplast where foliar bacterial pathogens colonize (Yamada et al., 2016). *CYP79B2* and *CYP79B3* encode enzymes required for tryptophan-derived defense secondary metabolites including camalexin and 4-hydroxyindole-3-carbonyl nitrile (Mikkelsen et al., 2000; Zhao et al., 2002). Previous studies showed that sugar sequestration and tryptophan-derived defense secondary metabolite production contribute to resistance against *Pto* (Rajniak et al., 2015; Yamada et al., 2016). In the present study, *Pto* and *Pto* AvrRpt2 transcriptomes in *stp1 stp13* and *cyp79b2 cyp79b3* mutants were similar to those in Col-0 (Figure 5A), suggesting that these mechanisms do not play a major role in affecting bacterial responses in this experimental setup.

2. Results

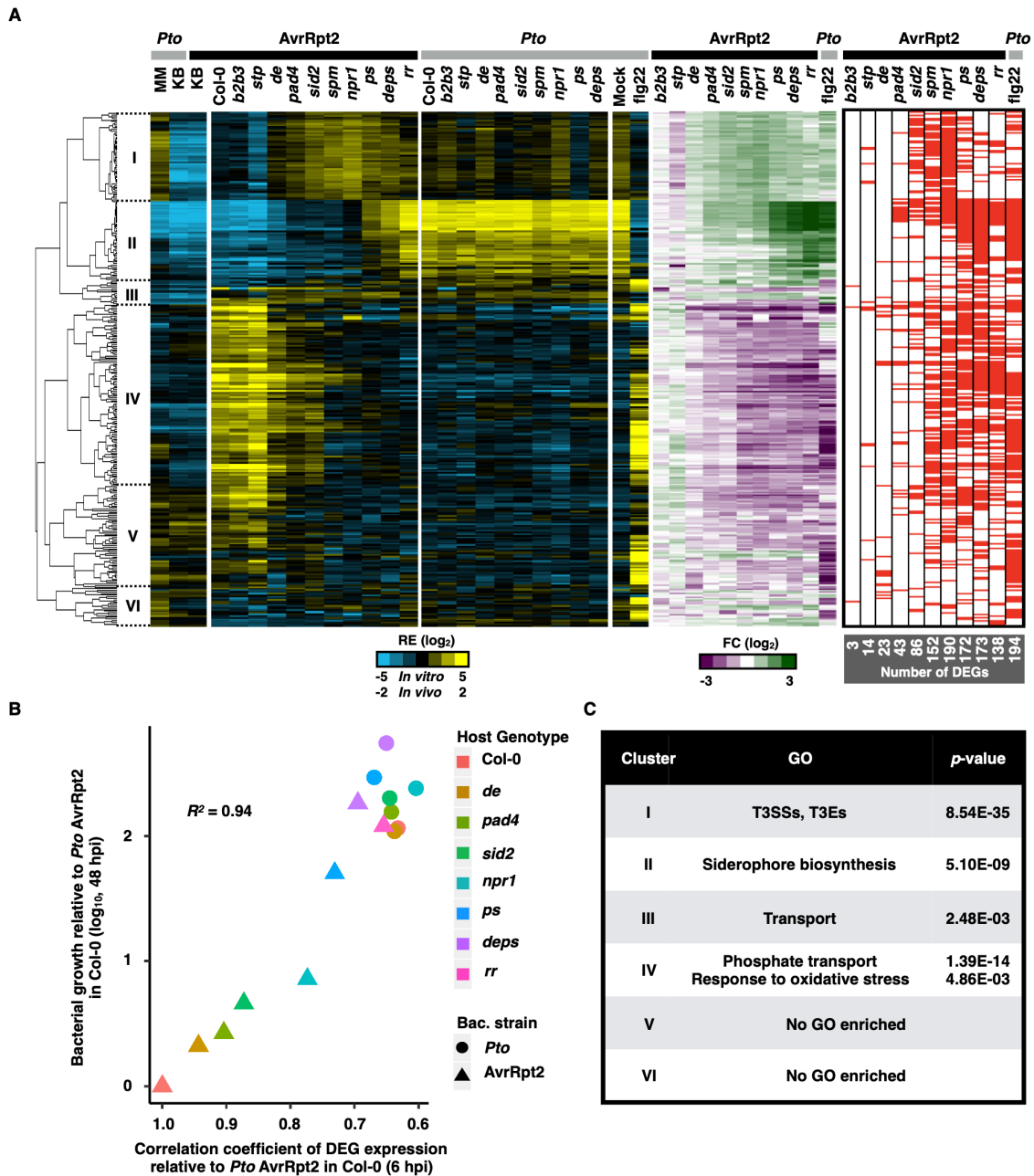


Figure 5: Host genotype effects on bacterial transcriptome

(A) Left panel (blue/yellow heatmap): Hierarchical clustering of the relative expression (RE) of the differentially expressed genes (DEGs) in *Pto* AvrRpt2 based on the pairwise comparisons between Col-0 plants and the mutant plants (FDR < 0.01; $|\log_2FC| > 1$; represented by the red marks in the right panel). Middle panel (green/magenta heatmap): Gene expression fold changes of *Pto* AvrRpt2 in defense mutant plants compared to those in Col-0 or fold changes of *Pto* in flg22-pretreated Col-0 compared to mock-pretreated Col-0. *Pto* and *Pto* AvrRpt2 are represented by gray and black marks, respectively. (B) The relationship between the expression pattern of the bacterial DEGs at 6 h post infection (hpi) and bacterial growth at 48 hpi. The Pearson correlation coefficient is shown ($R^2 = 0.94$). The genes of *Pto* AvrRpt2 identified as DEGs in at least one of the pairwise comparisons between Col-0 and mutant plants (FDR < 0.01; $|\log_2FC| > 2$) were used for the analysis. The x-axis represents Pearson correlation coefficients of DEGs expression patterns between each sample and *Pto* AvrRpt2 in Col-0 plants. The y-axis represents increased bacterial growth levels in each sample as

compared with *Pto* AvrRpt2 in Col-0 plants at 48 hpi (adapted from (Tsuda et al., 2009)). (C) List of gene ontology (GO) terms enriched in the clusters shown in (A) (next to the dendrogram). For the full GO list, see (Nobori et al., 2018b). See Figure 2A for the acronyms. This figure was adopted from (Nobori et al., 2018b).

2.1.4 The system of bacterial iron acquisition is influenced by plant immunity

The host genotype-dependent DEGs in *Pto* AvrRpt2 could be separated into six clusters based on the expression patterns (Figure 5A). I conducted GO term enrichment analysis for each cluster (Figure 5C; For the full GO list, see (Nobori et al., 2018b)). In cluster II, genes related to siderophore biosynthesis, which is known to be induced under iron-deficient conditions and scavenge iron from the environment, were induced in susceptible plants and suppressed by both PTI and ETI (Figure 5C). Because both PTI and ETI impact the expression of iron-related genes, I investigated the link between bacterial responses to iron and plant immunity. Of the 133 previously reported iron-responsive genes in *in vitro* grown *Pto* (Bronstein et al., 2008), a significant number of genes (69 genes) were differentially regulated by plant immunity (4.8-fold over-enriched; $p = 1.89e^{-37}$; hypergeometric test; Figure 6A; overlap between the red and green bars). More strikingly, of the 69 genes co-regulated by iron and plant immunity, iron-repressive genes were almost exclusively suppressed by plant immunity, whereas iron-inducible genes involved both immune-inducible and -repressive genes (Figure 6A). Therefore, plant immunity modulates a part of the bacterial iron responses.

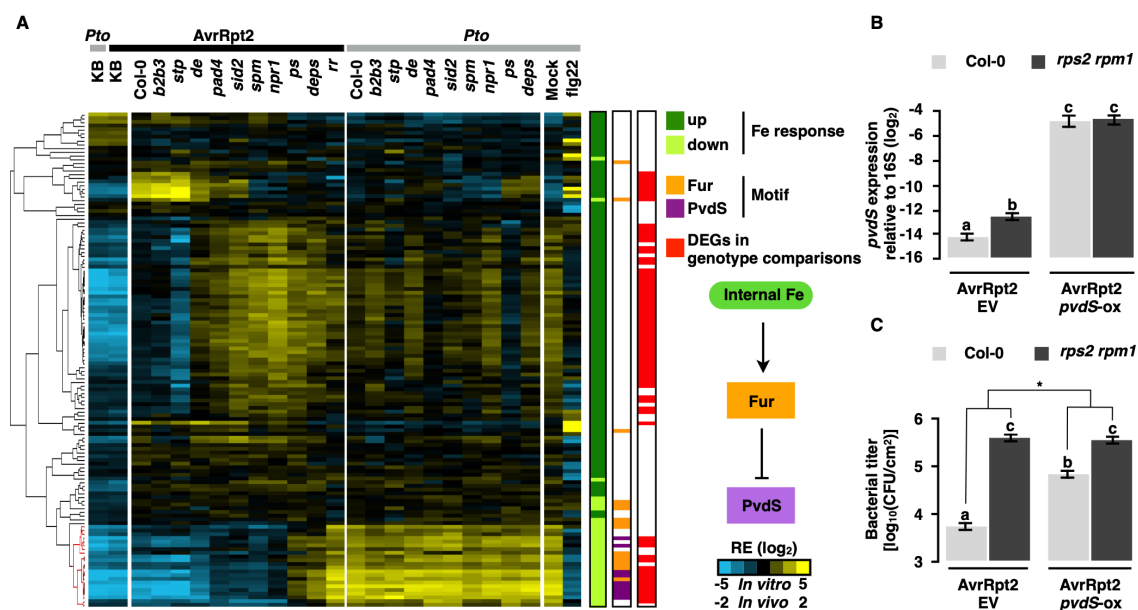


Figure 6: Iron-related genes of *Pto* are targeted by plant immunity

2. Results

(A) Hierarchical clustering of the relative expression (RE) of *Pto* genes previously reported as iron responsive (Bronstein et al., 2008). Iron-inducible and -repressive genes are represented by dark and light green marks, respectively (p -value < 0.05). The red marks represent differentially expressed genes of *Pto* AvrRpt2 in at least one of the pairwise comparisons between Col-0 plants and the defense mutant plants. Binding motifs of Fur, and PvdS are represented by orange and purple marks, respectively. *Pto* and *Pto* AvrRpt2 were represented by gray and black marks, respectively. (B) RT-qPCR analysis of *pvdS* expression of *Pto* AvrRpt2 carrying an empty vector (EV) or *Pto* AvrRpt2 *pvdS*-ox ($OD_{600} = 0.5$) normalized to 16S in Col-0 or *rps2 rpm1* plants at 6 h post infection (hpi). (C) Growth of *Pto* AvrRpt2 EV or *Pto* AvrRpt2 *pvdS*-ox ($OD_{600} = 0.001$) in Col-0 or *rps2 rpm1* plants at 48 hpi. (B and C), Mean \pm s.e.m. was calculated by using a mixed linear model (A: $n = 4$ biological replicates from four independent experiments, B: $n = 72$ and 48 biological replicates from six and four independent experiments for Col-0 and *rps2 rpm1*, respectively). Different letters indicate statistically significant differences (adjusted $P < 0.01$; the Benjamini-Hochberg method). The asterisk indicates statistically significant difference of the host genotype effect between the bacterial strains (p -value = $6.61E-08$; two-tailed Student t -test). This figure was adopted from (Nobori et al., 2018b).

2.1.5 *pvdS* and its regulatory targets are commonly suppressed by PTI and ETI

To understand the molecular mechanisms underlying the impact of plant immunity on bacterial iron responses, I investigated the promoter region of iron-responsive genes for the binding motifs of the transcriptional regulators Fur and PvdS, both of which are known to be involved in iron responses (Llamas et al., 2014) (Figure 6A). Fur is the primary regulator of iron homeostasis and typically functions as a repressor of the downstream iron responses in the presence of iron (Llamas et al., 2014). PvdS, an ECF sigma factor, regulates the biosynthesis of pyoverdine, a siderophore enriched in cluster II (Figure 5A; See (Nobori et al., 2018b) for the list of DEGs.). *pvdS* is negatively regulated by Fur and its expression is derepressed under iron-deficient conditions (Bronstein et al., 2008). The Fur- or PvdS-motif was enriched in the promoter region of the genes suppressed by both plant immunity and iron (Figure 6A; the cluster of genes marked with red in the dendrogram), including the *pvdS* gene itself (Fur: 17.4-fold over enriched, $p = 6.22e^{-9}$; PvdS: 15.2-fold over enriched; $p = 1.85e^{-9}$; hypergeometric test; Figure 6A). RT-qPCR analysis confirmed the RNA-seq data that *pvdS* expression was suppressed by AvrRpt2-triggered ETI (Figure 6B). These results point to the Fur-PvdS pathway as a potential target of plant immunity for impeding bacterial growth. Moreover, three out of five bacterial sigma factors directly regulated by Fur (Markel et al., 2013) were strongly induced *in planta* and suppressed by both flg22-PTI and AvrRpt2-ETI (Supplementary figure 6), suggesting that plant immunity might broadly target iron-related sigma factors to manipulate bacterial iron metabolism.

2.1.6 *pvdS* has a causal impact on bacterial growth *in planta*

The PvdS pathway appeared to be a major target of plant immunity as this pathway was suppressed by both PTI and ETI (Figure 4C and Figure 5 A and C). To examine whether the manipulation of the PvdS regulatory pathway has causal effects on bacterial growth *in planta*, I generated a *Pto* AvrRpt2 strain that constitutively expresses *pvdS* (AvrRpt2 *pvdS*-ox) to counteract the suppression of *pvdS* expression by ETI (Figure 6B). AvrRpt2 *pvdS*-ox grew 12-fold more than *Pto* AvrRpt2 (AvrRpt2 EV) in Col-0 plants at 48 hpi, whereas the growth level of these strains were comparable in *rps2 rpm1* mutant plants, which do not trigger ETI (Figure 6C and Supplementary figure 7 A and B). Thus, high *pvdS* expression confers *Pto* tolerance against AvrRpt2-triggered ETI.

2.1.7 Regulation of *pvdS* in plants is independent of iron concentration

Since *pvdS* suppression occurs under iron-rich conditions *in vitro*, I tested the possibility that ETI suppressed *pvdS* expression by increasing apoplastic iron. Co-inoculating bacteria with Fe-citrate did not influence *pvdS* expression even at an iron concentration detrimental for bacterial growth in plants (Figure 7 A and B). Furthermore, the content of total iron in apoplastic and intracellular fluid did not change upon flg22 treatment or ETI triggered by bacterial infection (Figure 7 C and D). Collectively, these data suggest that altered iron availability is unlikely to be the cause of *pvdS* expression changes by plant immunity and that plant immunity influences *pvdS* expression by means other than directly regulating iron availability.

2. Results

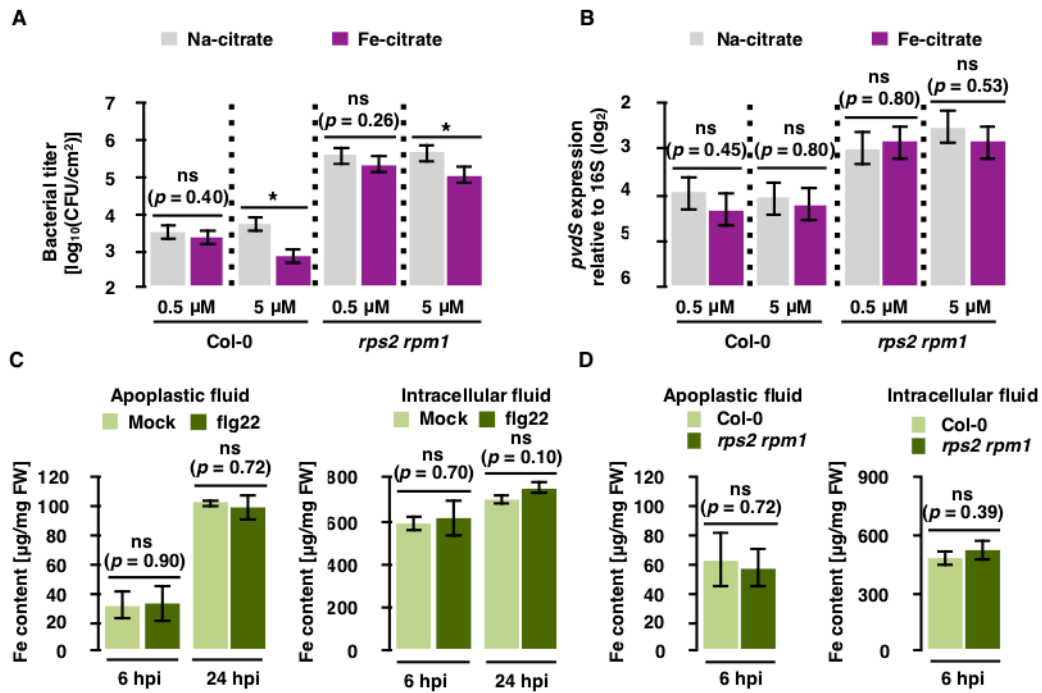


Figure 7: Iron content in the apoplast does not explain *pvdS* expression and *Pto* growth

(A) Growth assay of *Pto* AvrRpt2 infected in Col-0 and *rps2 rpm1* plants at 48 hpi. Bacterial suspension ($OD_{600} = 0.001$) was co-infiltrated with Na-citrate or Fe-citrate. (B) qRT-PCR analysis of *pvdS* expression in *Pto* AvrRpt2 infected to Col-0 or *rps2 rpm1* plants. Bacterial suspension ($OD_{600} = 0.5$) was co-infiltrated with Na-citrate or Fe-citrate. (A and B) Bars represent means and standard errors calculated from independent experiments using a mixed linear model (A: $n = 3$, B: $n = 6$). Different letters or asterisks indicate statistically significant differences (adjusted p -value < 0.01). ns, not significant (adjusted p -values were shown). (C) Iron contents in apoplastic and intracellular fluids extracted from Col-0 plants sprayed with 1 μ M flg22 or water (Mock) at the indicated time points. (D) Iron contents in apoplastic and intracellular fluids extracted from Col-0 or *rps2 rpm1* plants infiltrated with *Pto* AvrRpt2 ($OD_{600} = 0.5$). (C and D) Bars represent means and standard errors calculated from three independent experiments. ns, not significant (p -values were shown; two-tailed Student t -test). This figure was adopted from (Nobori et al., 2018b).

2.2 In planta multi-omics of *Pto*

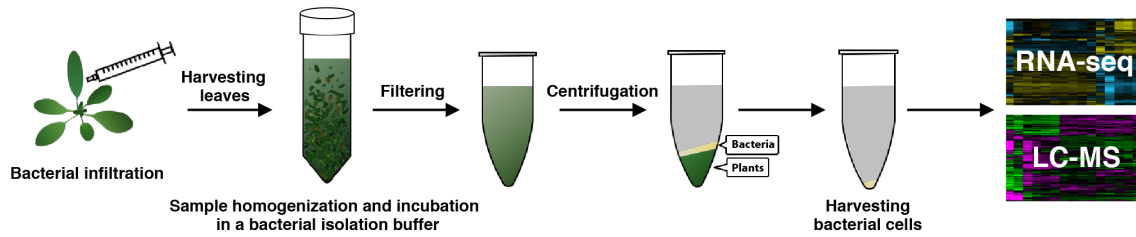
2.2.1 In planta transcriptome and proteome profiling of *Pto*

To enrich bacterial information from plant leaves, I isolated bacterial cells from infected plant leaves using the method established in this thesis (Figure 3A) (Nobori et al., 2018b). RNA and proteins extracted from isolated bacteria were subjected to RNA-seq (transcriptome) and LC-MS (proteome) analysis, respectively (Figure 8A). I profiled the

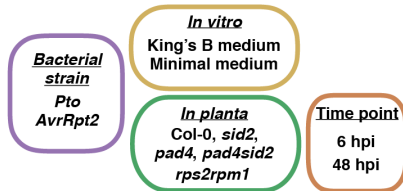
transcriptomes and proteomes of *Pto* under 15 conditions, including *in vitro* (minimal medium (MM) and King' B medium (KB)) conditions and *in planta* conditions using five *A. thaliana* genotypes (Col-0, *sid2*, *pad4*, *pad4 sid2*, and *rps2 rpm1*), two *Pto* genotypes (*Pto* and *Pto AvrRpt2*), and two time points (6 and 48 hpi) (Figure 8B). Note that this is not a time-course study as the doses of starting bacterial inocula are different for the two time points ($OD_{600}=0.5$ for 6 hpi and $OD_{600}=0.005$ for 48 hpi). *Pto AvrRpt2* was not used for the sampling at 48 hpi because this strain caused tissue collapse in the leaves in this condition. RNA-seq analysis detected, on average, 4877, 4659, and 5228 genes of *Pto* in *in vitro*, *in planta* 6 hpi, and *in planta* 48 hpi conditions, respectively (Figure 8C). LC-MS analysis detected, on average, 3617, 1183, and 1889 proteins of *Pto* in *in vitro*, *in planta* 6 hpi, and *in planta* 48 hpi conditions, respectively (Figure 8C). Proportion of the subcellular localization of the detected proteins was comparable among mRNAs/proteins detected in different conditions (Figure 8C), suggesting no obvious bias was introduced to mRNA/proteins detection during bacterial enrichment processes. *Pto* showed distinct responses under different conditions at both transcriptome (Figures 8 D and E) and proteome (Figures 8 F and G) levels. Both transcriptomes and proteomes of *Pto* in *in vitro* conditions were closer to those in *in planta* at 48 hpi compared with 6 hpi (Figures 8 D-G), implying that more drastic transcriptomic and proteomic reprogramming occurs at the early stage of infection than the late stage of infection.

2. Results

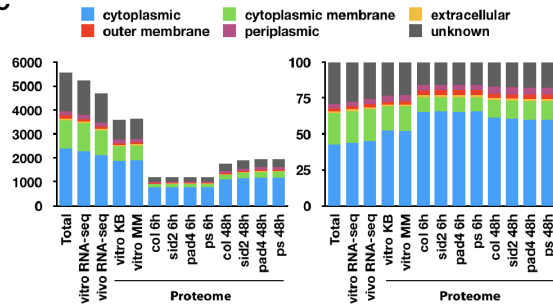
A



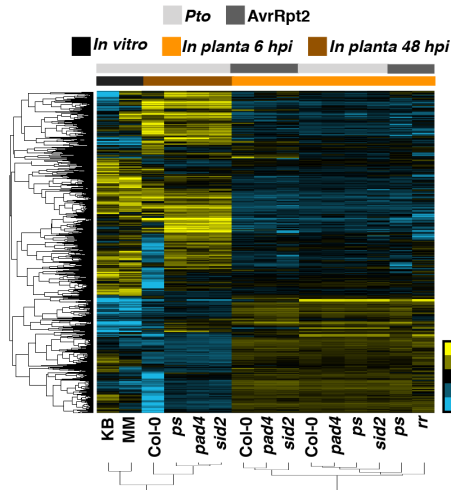
B



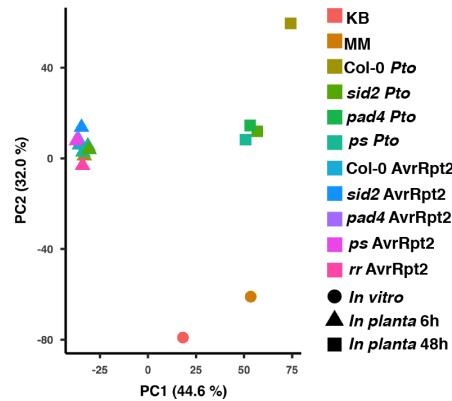
C



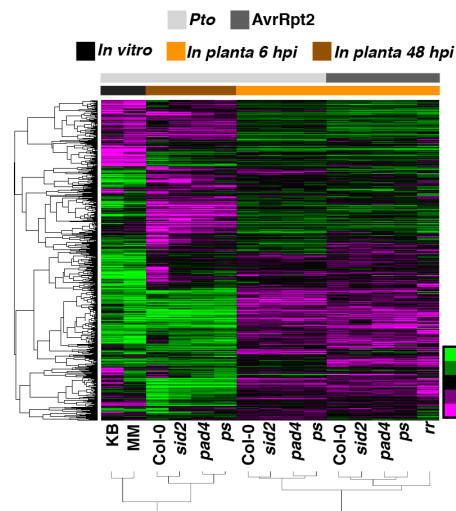
D



E



F



G

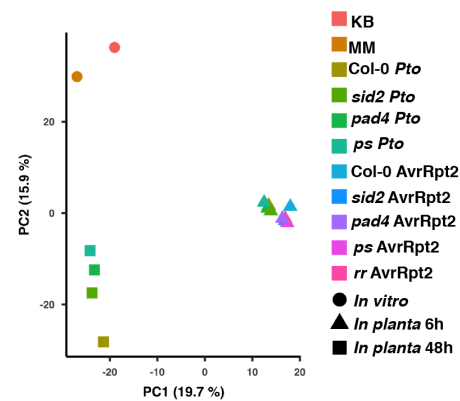


Figure 8: *In planta* transcriptomics and proteomics of *Pto*

(A) Schematic workflow of *in planta* bacterial transcriptome and proteome analysis. (B) Bacterial strains, plant genotypes, and conditions used in this study. (C) Number (left) and proportion (right) of mRNAs/proteins detected in the RNA-seq/LC-MS analysis with the information of protein localization. Total: all annotated genes of *Pto*. (D) Hierarchical clustering of relative expression (RE)

of the genes of *Pto* and *Pto* AvrRpt2 detected in RNA-seq analysis. (E) Principle component analysis of the genes of *Pto* and *Pto* AvrRpt2 detected in RNA-seq analysis. (F) Hierarchical clustering of relative expression (RE) of the proteins of *Pto* and *Pto* AvrRpt2 detected in LC-MS analysis. (G) Principle component analysis of the proteins of *Pto* and *Pto* AvrRpt2 detected in LC-MS analysis. This figure was adopted from Nobori et al., (*in preparation*).

2.2.2 Bacterial proteins differentially expressed under various conditions

I analyzed proteins whose expression was significantly changed between the *in vitro* (KB) and *in planta* (Col-0) conditions at 6 hpi or 48 hpi. GO enrichment analysis showed that bacterial proteins related to “pathogenesis” were induced both at 6 and 48 hpi (Cluster III in Figure 9A). Interestingly, tRNA synthases and ribosomal proteins, both of which are related to protein translation, showed the opposite expression patterns, i.e., tRNA synthases were suppressed at 48 hpi, while ribosomal proteins were induced (Figure 9A). Whether bacterial translation efficiency is reduced or enhanced at 48 hpi compared with the other conditions remains to be elucidated. Proteins annotated as “response to oxidative stress” were induced at 48 hpi, implying that *Pto* experienced oxidative stress at the later time of infection or that a longer exposure to oxidative stress caused such induction. A substantial number of proteins (559 proteins) of *Pto* were differentially expressed among different host genotypes at 48 hpi (Figure 9B), whereas host genotype effects were small at 6 hpi (only one protein was differentially expressed). *Pto* AvrRpt2, which was strongly affected by host SA pathways at 6 hpi at the transcriptome level (Figure 5A), showed similar proteome patterns among SA mutant plants (only one protein was differentially expressed). This might be because transcriptional changes were not reflected to the protein accumulation yet at 6 hpi. Therefore, I focused on analyzing host genotype effects on protein expression in *Pto* at 48 hpi. There were 196 proteins whose expression was significantly affected in at least one of the SA mutants (Figure 9B). I found that pathogenesis-related proteins (“Interaction with host”) were highly expressed in the SA mutants (Figure 9B), suggesting that the SA immune pathway suppresses the expression of pathogenesis-related proteins. On the other hand, expression of “translation” related proteins (ribosomal proteins) was suppressed in the SA mutants (Figure 9B). Taken together, the SA pathway affects expression of bacterial proteins related to bacterial virulence and basic metabolisms *in planta*. It remains to be investigated whether the SA pathway directly affects expression of these proteins or the effect is the indirect consequence of different bacterial population density *in planta* at this time point.

2. Results

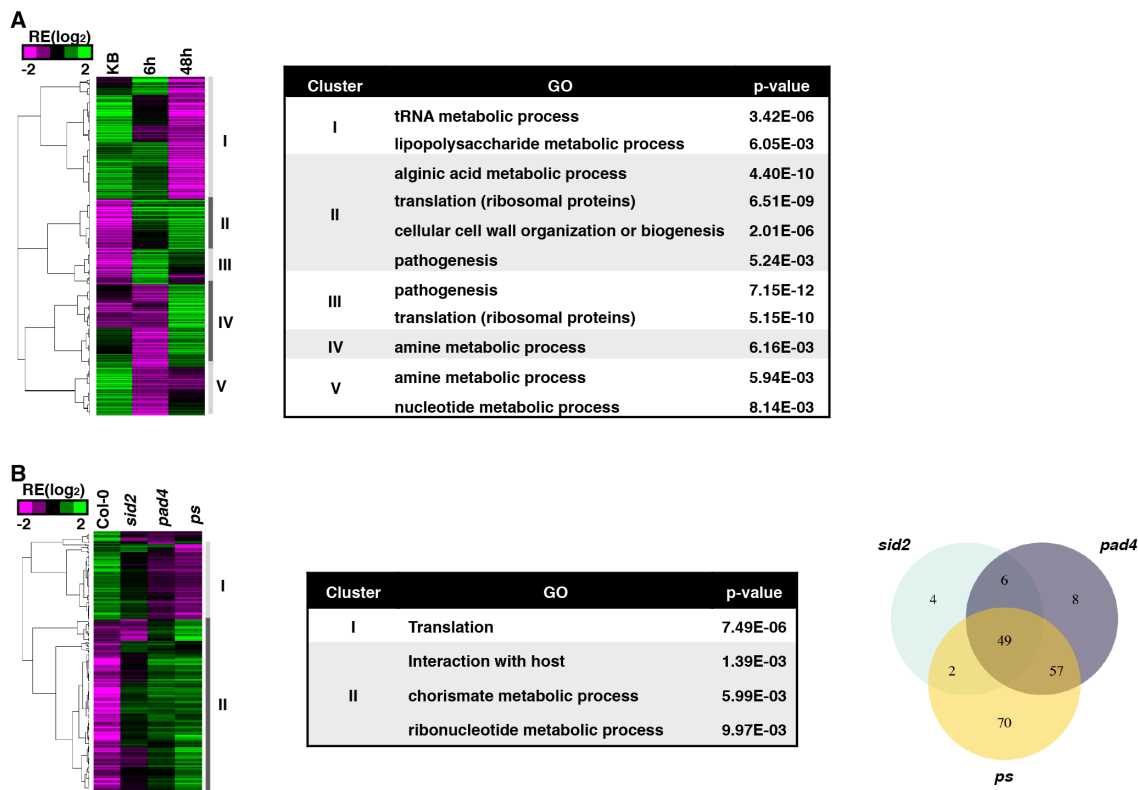


Figure 9: Distinct patterns of *Pto* proteomes in various conditions

(A) Hierarchical clustering of the relative expression (RE) of *Pto* proteins differentially expressed in at least one condition among *in vitro* (KB) and *in planta* (Col-0) at 6 hpi and 48 hpi (FDR < 0.01; $|\log_2FC| > 1$). List of GO terms enriched in the clusters shown in the sidebar of the heatmap. (B) Hierarchical clustering of the relative expression of *Pto* proteins differentially expressed in at least one plant mutant compared with the wild-type Col-0 at 48 hpi (FDR < 0.01; $|\log_2FC| > 1$). List of GO terms enriched in the clusters shown in the sidebar of the heatmap. Venn diagram of *Pto* proteins differentially expressed in each plant mutant compared with Col-0. This figure was adopted from Nobori et al., (*in preparation*).

2.2.3 Bacterial functions differently expressed in various conditions

Bacterial functions differentially expressed in different conditions could be studied by GO enrichment analysis following to statistical tests (Figure 9 A and B). However, this analysis is highly dependent on thresholds to be applied for selecting differentially expressed genes or proteins, and thus some important information can be lost before GO enrichment analysis. Moreover, it is difficult to compare the global expression pattern of GO terms across many conditions in this approach. To gain more insights into biological functions that are

differentially regulated in various conditions, I first annotated the *Pto* genome with GO terms before statistical tests. Gene/protein expression data was standardized using z-score and GO expression matrix was generated by taking the mean z-score for each GO term. To select GO terms that show distinct expression pattern among different conditions, I performed statistical tests in all pairwise comparisons among 15 conditions for each GO term and manually curated GO terms with high number of significant pairs (redundant GO terms were avoided). This allowed me to select 24 and 18 highly condition-dependent GO terms in transcriptome and proteome data, respectively, and to analyze expression changes across 15 conditions (Figure 10 A and B). I also analyzed expression of individual genes/proteins in selected GO terms (Figure 11). A GO term “pathogenesis” was one of top hits in both transcriptome and proteome data (Figure 10 A and B and Figure 11). These genes/proteins were strongly induced *in planta* at 6 hpi; their expression remained high at 48 hpi and clear host genotype effect was observed at this time point, i.e., expression was higher in the SA mutants compared with Col-0 (Figure 10 A and B and Figure 11), suggesting that SA-mediated immunity suppresses the “pathogenesis” related function at 48 hpi. This is consistent with the GO enrichment analysis following the gene/protein-based statistical tests (Figure 9B), supporting the reliability of both approaches. “Coronatine”-related genes/proteins (not involved in the GO term “pathogenesis”) showed similar expression patterns as “pathogenesis”-related genes/proteins *in planta* (Figure 10 A and B and Figure 11). Genes/proteins annotated as “catalase activity” were strongly induced only under ETI condition at 6 hpi, but their expression was even higher at 48 hpi without ETI (Figure 10 A and B and Figure 11). Host genotype effect on expression of the “catalase activity”-related function was seen only at the protein level: highly expressed in Col-0 compared with the SA mutants (Figure 10 A and B and Figure 11), implying that SA-mediated immunity affected this function at the protein level. “Cell division”-related genes/proteins were highly expressed at 6 hpi, but not at 48 hpi (Figure 10 A and B and Figure 11). This might suggest that bacterial growth approached a plateau at 48 hpi.

2. Results

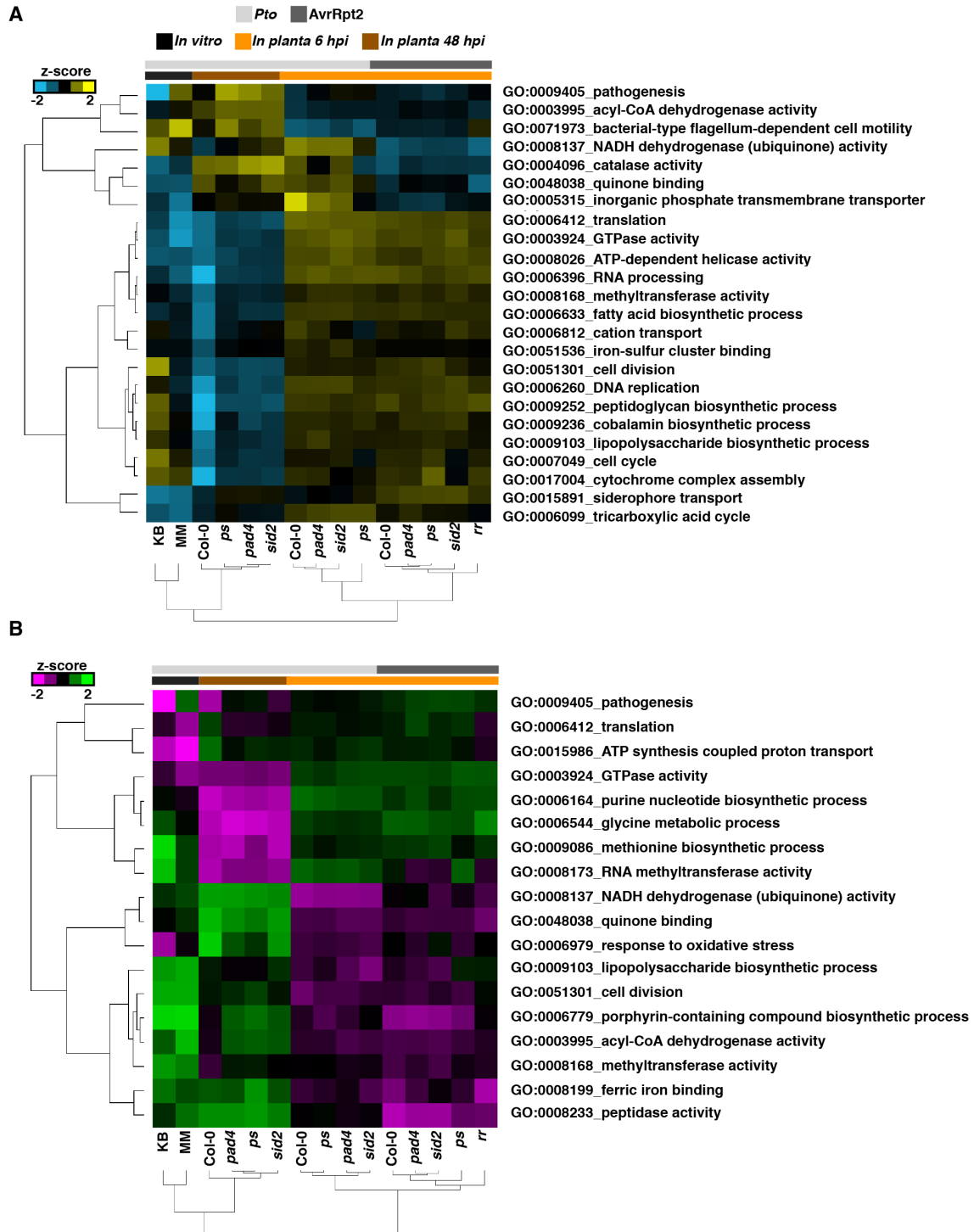


Figure 10: Bacterial functions differentially expressed in different conditions.

(A and B) Hierarchical clustering of selected GO terms in transcriptome (A) and proteome (B) data. Transcriptome and proteome data were standardized by using z-scores and mean z-scores of genes/proteins involved in individual GO terms were shown. This figure was adopted from Nobori et al., (*in preparation*).

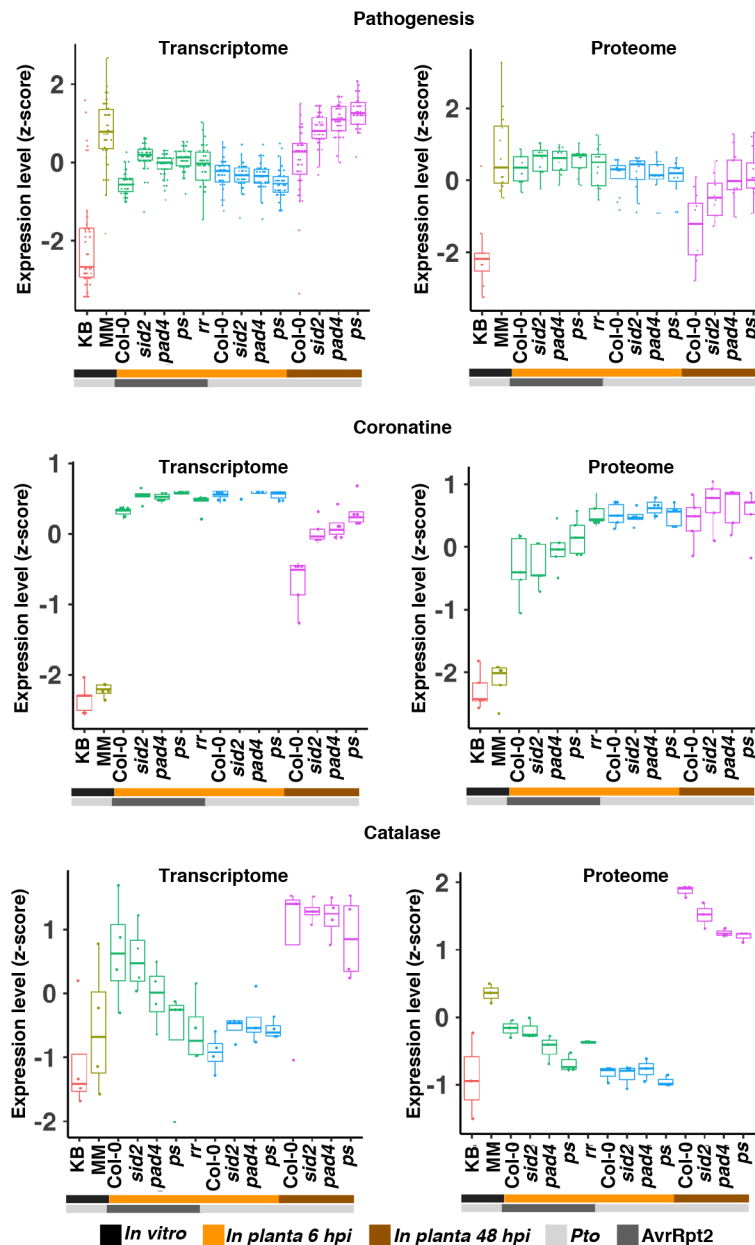


Figure 11: Regulation of mRNAs and proteins involved in selected functions

Box plots show expression (z-score) of mRNAs (left) and proteins (right) related to “pathogenesis”, “coronatine biosynthesis”, and “catalase” under various conditions. Light and dark green sidebars represent transcriptome and proteome data, respectively. Black, orange, and brown sidebars represent *in vitro* (KB), *in planta* (Col-0) 6 hpi, and *in planta* 48 hpi, respectively. This figure was adopted from Nobori et al., (*in preparation*).

2.2.4 Comparative analysis of bacterial transcriptomes and proteomes

To compare global expression patterns of genes and proteins, I combined the transcriptome and proteome data of all 15 conditions. For this, expression of genes/proteins

2. Results

detected in all conditions was standardized by using z-scores and hierarchical clustering was performed (Figure 12). Intriguingly, transcriptome and proteome data were clustered together by three major conditions (*in vitro*, *in planta* 6 hpi, and *in planta* 48 hpi) (Figure 12), suggesting that the global pattern of bacterial gene expression and protein expression is similar in both *in vitro* and *in planta*.

I compared the RNA-seq and proteome data in the fold changes between *Pto in vitro* (KB) and each of the other conditions (Figure 13A). Overall, transcriptome and proteome data correlated well ($R^2 = 0.52 - 0.69$), suggesting that bacterial mRNA abundance explains part of protein abundance, but posttranscriptional regulation might also play roles during interaction with plants. Of 1129 genes/proteins detected in both RNA-seq and proteome analyses, 144 genes/proteins (12.8%) were differentially regulated at both transcriptome and proteome levels *in planta* 6 hpi compared with in KB (Figure 13B). GO analysis showed that “pathogenesis”-related process was induced at both transcriptome and proteome levels (Figure 13C), consistent with previous analyses (Figure 10 A and B and Figure 11). Interestingly, more proteins were down-regulated (151 proteins) than up-regulated (44 proteins) in a protein-specific manner (Figure 13B). This may be explained by a prominent role of protein degradation *in planta* or by that plant immunity affect bacterial metabolisms via protein degradation (Figure 13B). GO analysis showed that “Cell wall biogenesis”-related proteins were enriched in this group of proteins (Figure 13C). Biological relevance of this remains to be elucidated.

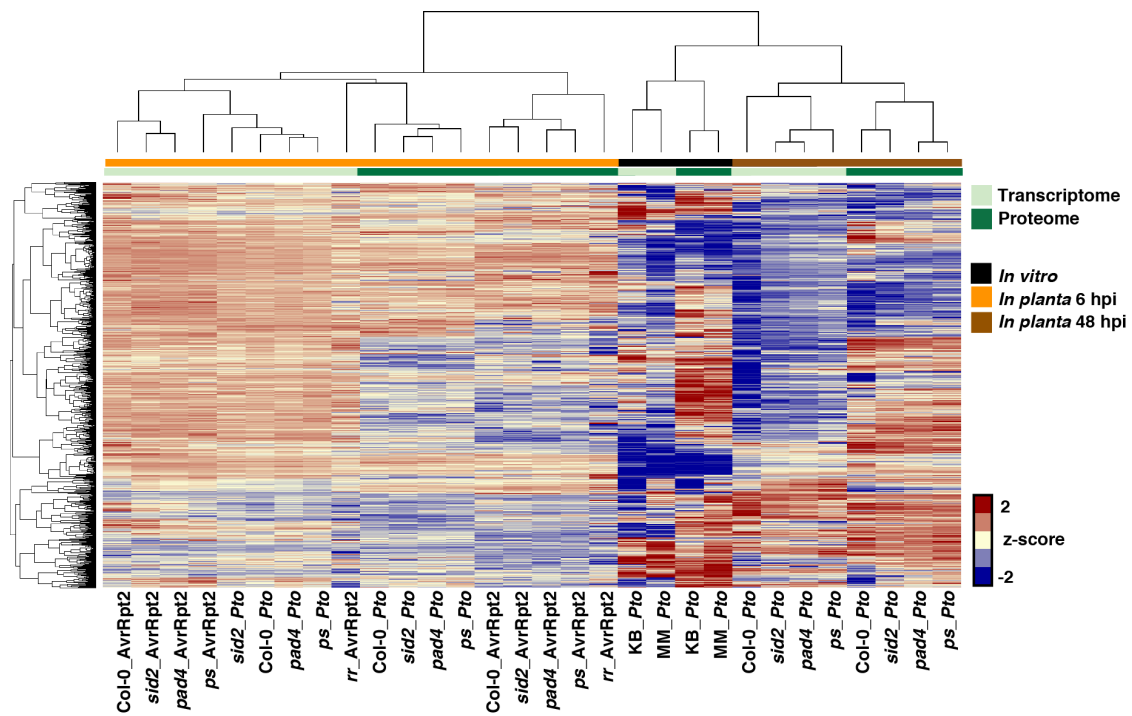


Figure 12: Integration of bacterial transcriptome and proteome data

Transcriptome and proteome data were standardized by using z-score and combined, followed by hierarchical clustering. Genes/proteins detected in all conditions were subjected to the analysis. Light and dark green sidebars represent transcriptome and proteome data, respectively. Black, orange, and brown sidebars represent *in vitro* (KB), *in planta* (Col-0) 6 hpi, and *in planta* 48 hpi, respectively. This figure was adopted from Nobori et al., (*in preparation*).

2. Results

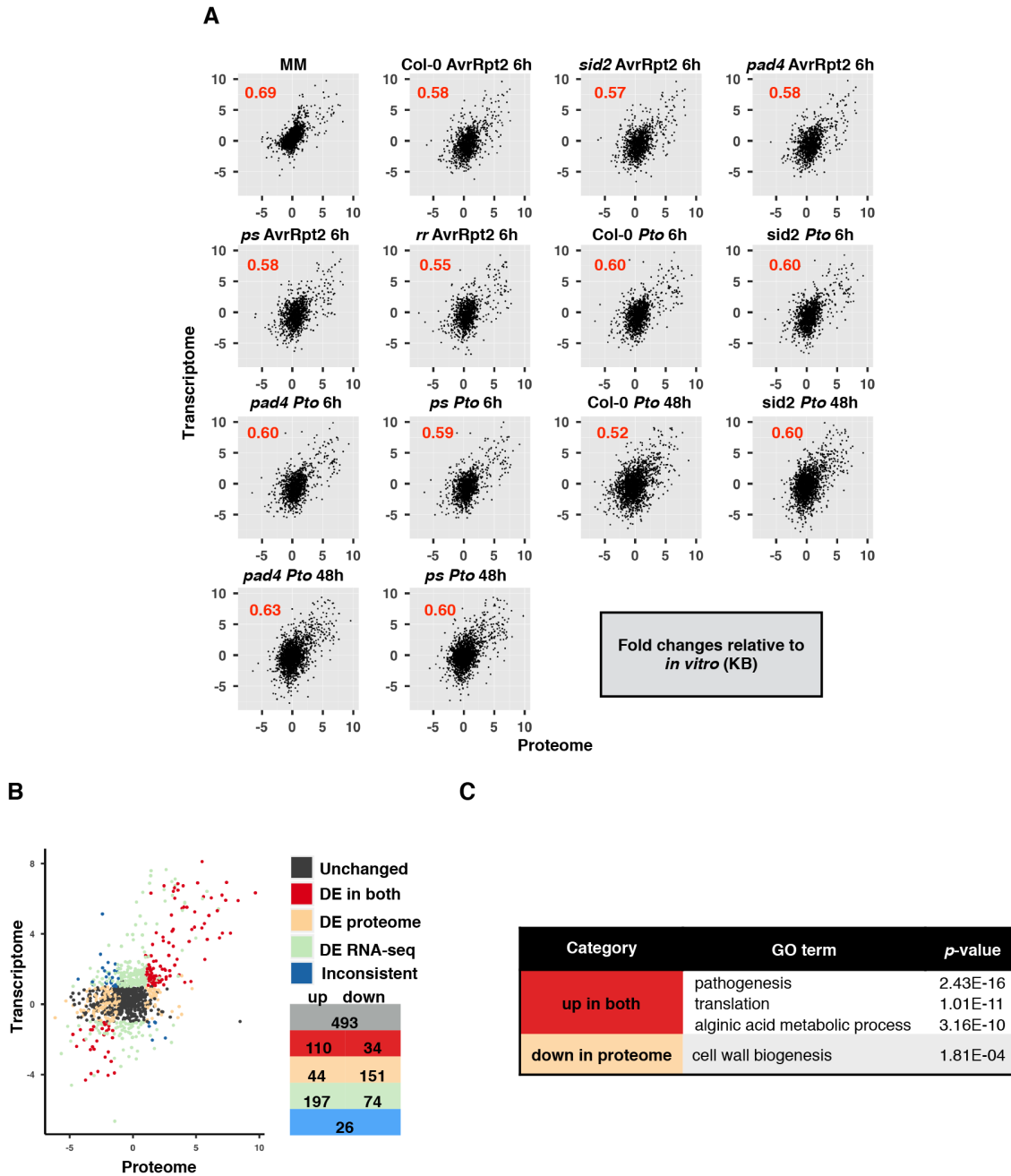


Figure 13: Conserved and specific regulation of *Pto* metabolisms at mRNA and protein levels

(A) Comparisons between transcriptome and proteome data in each condition. Fold changes relative to *in vitro* (KB) condition were subjected to the analysis. Pearson's correlation coefficients were shown. (B) For RNA-seq and proteome data, gene/protein expression fold changes between *in planta* (Col-0) at 6 hpi and *in vitro* (KB) were compared. Genes/proteins differentially expressed (DE; FDR < 0.01; $|\log_2 \text{fold change}| > 2$) in both, either, and none ("Unchanged") of transcriptome and proteome studies were grouped and colored. Genes/proteins differentially expressed to the opposite direction were colored in blue ("Inconsistent"). The numbers of genes/proteins are shown for each category. (C) List of gene ontology (GO) terms enriched in the group of proteins that are significantly induced *in planta* at both mRNA and protein levels or proteins that are significantly suppressed *in planta* only at the protein level. This figure was adopted from Nobori et al., (*in preparation*).

2.2.5 Bacterial iron acquisition process affected *in planta*

I have shown above that gene expression of bacterial iron acquisition pathway is strongly affected by plant immunity at 6 hpi (Figure 6). I investigated expression of bacterial genes responsive to iron availability using the dataset shown in Figure 8D. Genes suppressed by iron supplementation (iron starvation genes) were globally induced at 6 hpi, but their expression was lower at 48 hpi, although the level was still higher than *in vitro* conditions (Figure 14 A and B). Interestingly, the accumulation of Fur protein was negatively correlated with expression of iron starvation genes among three major conditions (*in vitro*, *in planta* 6 hpi, and *in planta* 48 hpi) (Figure 14C), implying that *Pto* controls the protein accumulation of Fur to regulate iron starvation genes *in planta* or that plants affect iron starvation genes via Fur expression.

2. Results

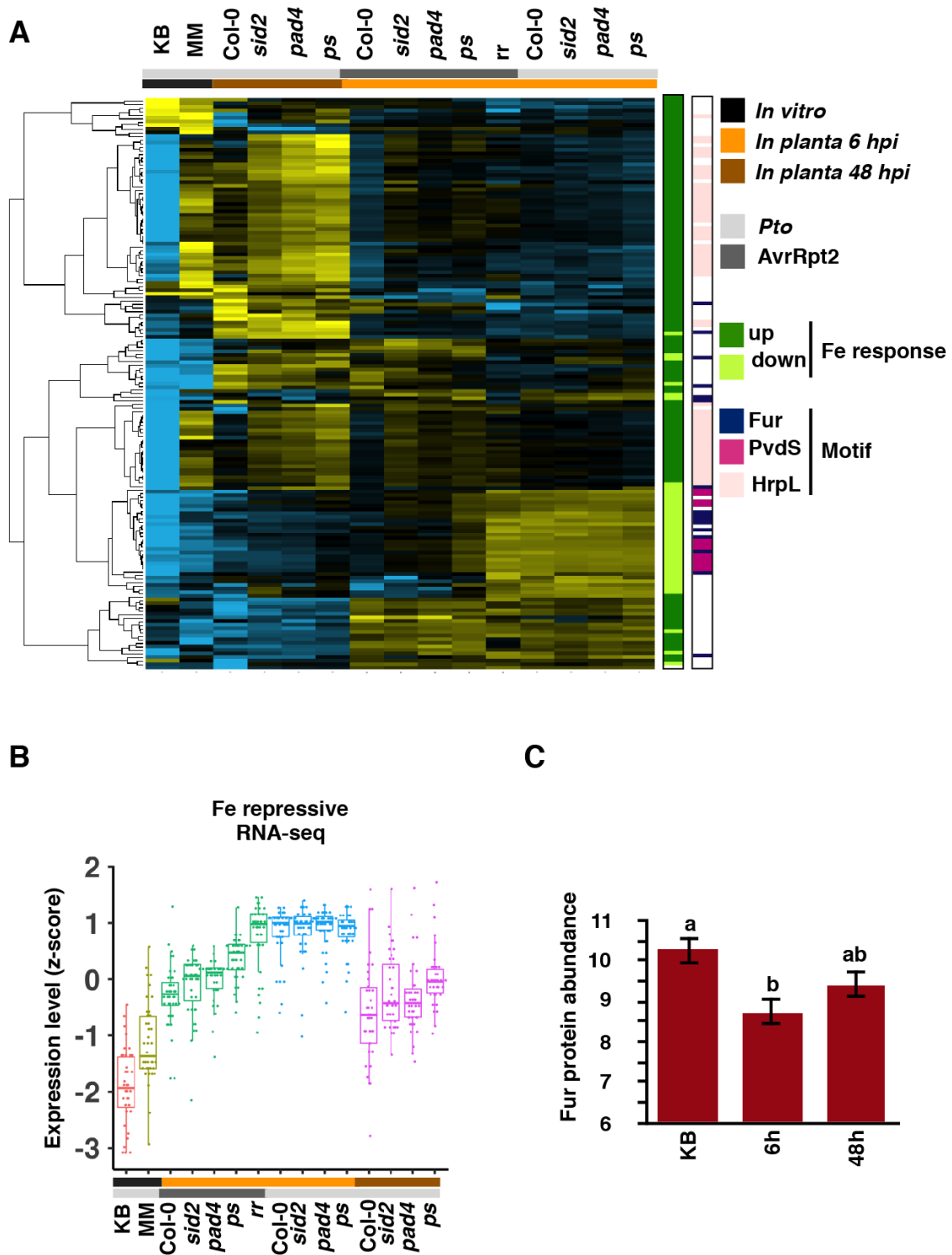


Figure 14: Regulation of bacterial iron acquisition pathway

(A) Hierarchical clustering of the relative expression (RE) of *Pto* genes previously reported as iron responsive (Bronstein et al., 2008). Iron-inducible and iron-repressive genes are represented by dark and light green marks, respectively (p -value < 0.05). Binding motifs of Fur, PvdS, and HrpL are represented by color bars. (B) Expression (z-score) of *Pto* genes previously reported as iron repressive (Bronstein et al., 2008). (C) Expression of Fur protein in the proteome data (\log_2 normalized). This figure was adopted from Nobori et al., (*in preparation*).

2.2.6 The gene co-expression network of *Pto*

Motivated by highly diverse bacterial transcriptome patterns among different conditions, I sought to investigate the gene regulatory network of *Pto*. I used 132 transcriptome data of *Pto* in 38 conditions. Correlation matrix of 4765 genes revealed highly correlated gene clusters, some of which contain genes that are known to be co-regulated (Figure 15A). I built a gene co-expression network based on the correlation matrix and annotated some genes with known functions and found that genes with the same function tend to be co-expressed (Figure 15B). For instance, genes related to pathogenesis (mostly T3SS and T3E genes), coronatine biosynthesis, alginate biosynthesis, and iron starvation responses were found in highly co-expressed gene clusters (Figure 15B). Intriguingly, genes involved in coronatine biosynthesis and alginate biosynthesis were clustered very closely, suggesting that these processes might share the same regulatory mechanism (Supplementary figure 9A). On the other hand, genes related to coronatine biosynthesis and the T3SS were only mildly correlated (Supplementary figure 9A), although it has been known that the expression of CorR, the master regulator of coronatine biosynthesis genes, is dependent on HrpL, the master regulator of the T3SS (Sreedharan et al., 2006). This suggests that there might be additional regulators that differentiate the expression patterns of genes related to coronatine biosynthesis and the T3SS. I also found that some genes annotated as T3Es were not co-expressed with the majority of T3Es (Supplementary figure 9), suggesting that they are not functioning as effectors or they function as effectors in different contexts.

Strong negative correlation was found between some genes. To understand negatively correlated functions of bacteria, I created a correlation matrix based on GO expression (Supplementary figure 10). Strong anti-correlation was observed between “siderophore transport” genes, which are iron-repressive, and “ferric iron binding” genes, which involve iron-inducible bacterioferritin (Supplementary figure 10), indicating that this analysis could capture known expression patterns of GOs. I found that genes related to chemotaxis were negatively correlated with genes involved in translation. Whether this negative correlation is explained by a direct molecular link between these processes needs further study.

2. Results

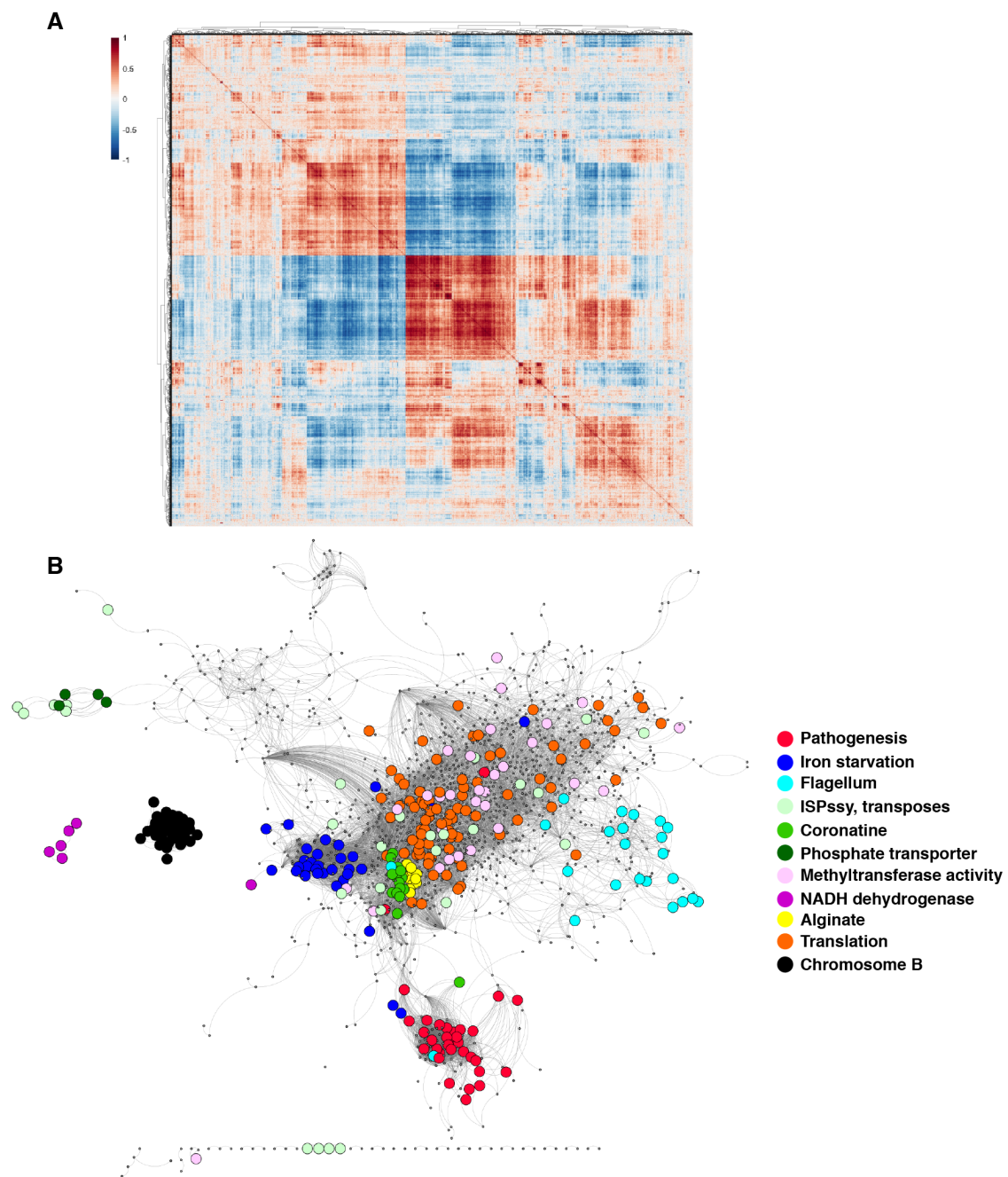


Figure 15: The gene co-expression network of *Pto*

(A) Correlation matrix of bacterial gene expression generated from 132 bacterial transcriptome data (38 conditions). (B) Gene co-expression network of *Pto*. Each node represents a gene. Highly correlated ($R^2 > 0.8$) genes are connected with edges. Functions are annotated with colors. This figure was adopted from Nobori et al., (*in preparation*).

2.2.7 The gene co-expression network predicts bacterial gene regulatory logic

Under the premise that transcriptional regulators and their targets are often co-expressed, I assumed that the highly correlated gene clusters infer transcriptional regulators in individual clusters. Indeed, *hrpL* was found in the cluster of T3SS genes; and the cluster of iron starvation genes includes iron starvation related sigma factors, PSPTO_1203, PSPTO_1209, and PSPTO_2133 (*pvdS*). I selected three co-expressed gene clusters that involve putative transcriptional regulators (TRs), PSPTO_0384 (ArsR family transcriptional regulator), PSPTO_3050 (AraC family transcriptional regulator), and PSPTO_4908 (TetR family transcriptional regulator) (Figure 16). To test if these TRs have the ability to regulate expression of genes in the same cluster, *Pto* strains that overexpress each of TRs were generated (Figure 16). Expression of PSPTO_7653 (iron(III) dicitrate transport system, periplasmic iron-binding protein FecB), PSPTO_4540 (proline iminopeptidase), and PSPTO_2681 (penicillin-binding protein 7) was highly correlated with each of TRs and these genes were selected as candidate target genes (Figure 16). Remarkably, expression of all of three candidate target genes were highly enhanced in bacterial strains overexpressing respective candidate TRs compared with wild type *Pto in vitro* (Figure 16). This indicates that the gene co-expression analysis of *Pto* has the potential to predict transcriptional regulators and their targets, thereby revealing the gene regulatory logic of bacteria. Further analyses will be conducted to test this in plants.

2. Results

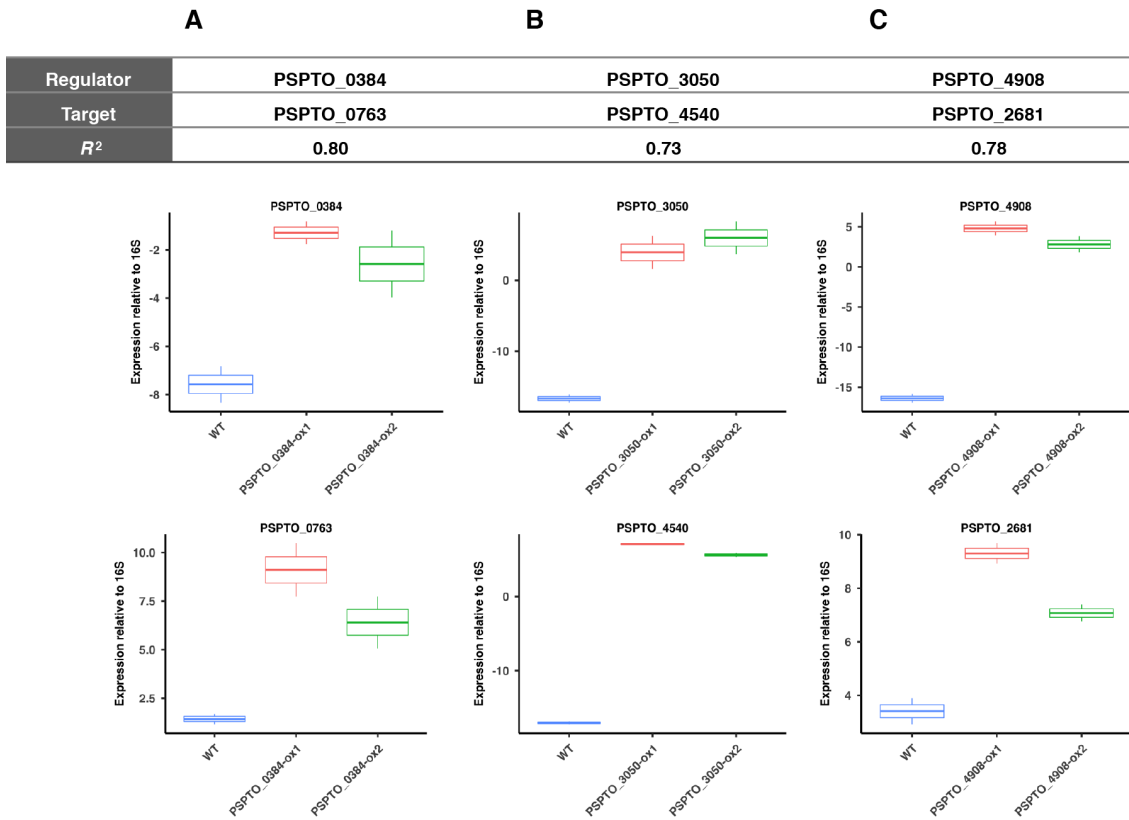


Figure 16: Gene co-expression network predicts the gene regulatory logic of *Pto*

Two independent *Pto* strains overexpressing putative transcriptional regulators (TRs) were generated. Expression of the TRs and the predicted target genes of them was measured by RT-qPCR. For each pair of a TR and its predicted target, pearson correlation coefficient (R^2) is shown based on the result in Figure 15A. $n = 2$. This figure was adopted from Nobori et al., (*in preparation*).

2.2.8 Type III translocator components are selectively affected by plant SA pathways

Many of pathogenesis-related proteins that were negatively affected by the SA pathway at 48 hpi were proteins comprising the T3SS. Integrative analysis of bacterial transcriptomes and proteomes revealed that some of the T3SS components were affected by the SA pathway particularly at the protein accumulation level (Figure 17A). I further investigated the effect of plant SA pathways on each component of bacterial T3SS and found that proteins comprising the tip part of the T3SS, namely HrpZ, HrpK, and HrpW, were affected by the SA pathways, while most of the other T3SS proteins showed similar expression level among the host genotypes (Figures 16 B and C). This implies that the SA pathways selectively target the tip part of bacterial T3SS. This observation was confirmed by immunoblotting using proteins extracted directly from *Pto* infected leaves and a HrpZ antibody (Figure 17D), exemplifying that the bacterial isolation process did not introduce

artefacts in the proteome data. There was no significant effect of the SA pathway on the gene expression of *hrpZ* and *hrcC* based on the RNA-seq data (Figure 17C), and this was confirmed by RT-qPCR (Figure 17E), suggesting the selective effect of the SA pathways is likely at the protein level. The mechanisms by which the SA pathways selectively affect the proteins of some T3SS components remain to be elucidated.

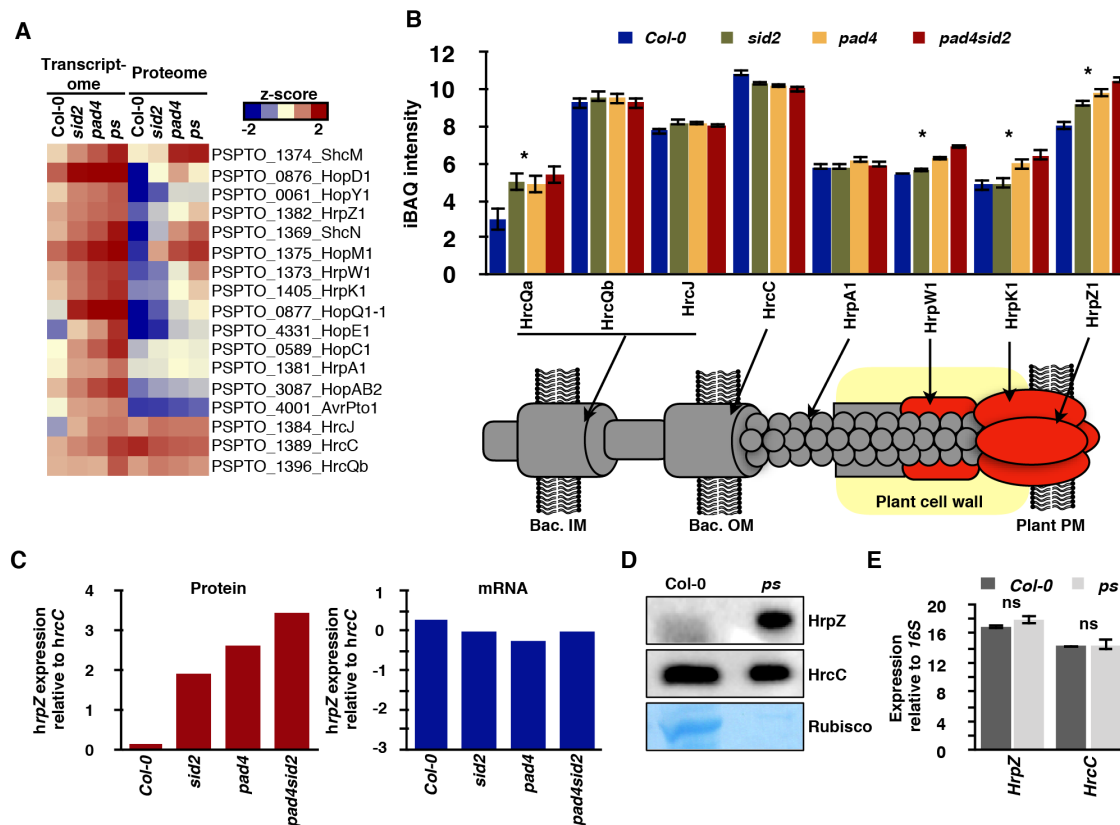


Figure 17: Plant SA pathway selectively affects bacterial T3SS proteins

(A) Hierarchical clustering of expression (z-score) of genes and proteins related to the T3SS. (B) Expression of T3SS-related proteins based on the proteome data (normalized iBAQ intensity). Approximate localization of each protein was shown in the diagram. (C) Expression of HrpZ protein and gene relative to HrcC in the proteome and transcriptome data, respectively. (D) HrpZ and HrcC proteins detected by western blotting using specific antibodies provided by Prof. Dr. Sheng Yang He. Protein loading amount was adjusted by the expression of HrcC protein. Similar results were obtained in three independent experiments. (E) RT-qPCR analysis of *hrpZ* and *hrcC* relative to 16S. n = 2. (A-E) Plants were infiltrated with *Pto* at OD₆₀₀ = 0.05 and harvested at 48 hpi. This figure was adopted from Nobori et al., (*in preparation*).

2. Results

2.3 *In planta* transcriptomics of commensal bacteria

2.3.1 Comparative transcriptomics of four *Pseudomonas* strains

I applied the bacterial enrichment method described in 2.1 to study the transcriptomes of commensal bacteria. As a proof of principle experiment, I used two bacterial strains (EK10 and EK47; both are *Pseudomonas* spp.) that were isolated from the leaf endosphere of wild *A. thaliana* plants by the group of Prof. Dr. Eric Kemen (University of Tübingen, Germany). Bacterial enrichment successfully worked for both strains in Col-0 plants and I also profiled an *in vitro* condition (KB). Gene expression fold changes between *in planta* and *in vitro* were used for comparative analysis among different strains. For comparative transcriptome analysis, I annotated the genome of each strain with KEGG ontologies (KOs) and combined the RNA-seq data of both strains and that of *Pto* and D36E. This analysis could capture distinct transcriptome patterns of different strains in different conditions (Figure 18A). Interestingly, the commensal *Pseudomonas* EK10 and EK47 showed relatively similar transcriptome patterns and they were clustered closer with D36E rather than *Pto* (Figure 18A). This suggests that there is a correlation between bacterial transcriptome patterns and bacterial virulence. Since these *in planta* bacterial transcriptomes were profiled at 6 hpi, when even the population density of virulent *Pto* remains unchanged (Supplementary figure 4), bacterial population density does not explain the different transcriptome patterns. Thus, there might be a transcriptional signature that only virulent bacteria can achieve at an early stage of infection to aggressively proliferate in plants. I investigated expression of genes with functions related to the interaction with plants. Genes related to flagellar tended to be induced in the avirulent strains (D36E, EK10, and EK47), but not in virulent *Pto* (Figure 18B). Similarly, genes annotated as “catalase” were strongly induced only in the avirulent strains (Figure 18C). Genes related to iron-starvation tended to be strongly induced only in *Pto* (Figure 18D), which is in line with the finding in 2.1 that the expression level of iron-starvation genes correlated with the virulence of *Pto in planta* (Figure 6A). Notably, I also found genes that are differently regulated between non-virulent bacteria. Genes involved in alginate biosynthesis were strongly induced in *Pto* and EK10 *in planta*, but the induction level was substantially lower in D36E and EK47 (Figure 18E). In summary, the

comparative transcriptome analysis among four *Pseudomonas* strains could capture shared and distinct features, some of which are associated with bacterial virulence.

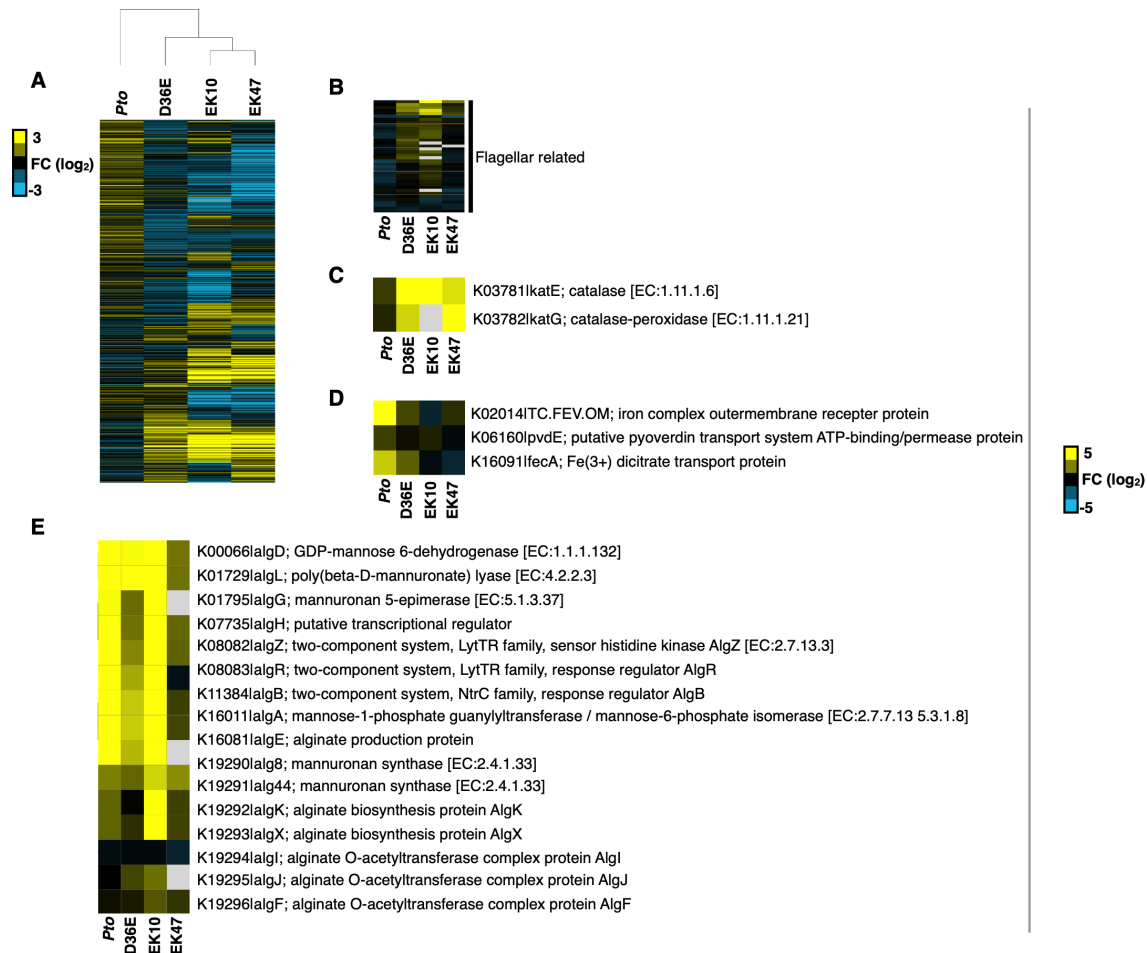


Figure 18: Comparative transcriptomics of four *Pseudomonas* strains *in vitro* and *in planta*

(A) Hierarchical clustering of KEGG ontology (KO) expression fold changes (FC) between *in vitro* and *in planta*. (B-E) Hierarchical clustering of expression FC of KO related to (B) flagellar, (C) catalase, (D) iron-starvation, and (E) alginate biosynthesis.

2.3.2 Selecting and characterizing 12 commensal bacterial strains

Motivated by the results in 2.3.1, I extended the comparative transcriptome approach to more bacterial strains. I selected 12 commensal bacterial strains from the culture collection of bacteria isolated from *A. thaliana* plants grown in natural soils (Bai et al., 2015) (Table 1). The strains represent major phyla of plant-associated bacteria, which include Actinobacteria,

2. Results

Bacteroidetes, Firmicutes, and Proteobacteria; and they are morphologically different with each other (Supplementary figure 8).

Table 1: List of commensal bacteria used in this study

ID	Phylum	Class	Order	Family
Leaf1	Actinobacteria	Actinobacteria	Actinomycetales	Microbacteriaceae
Leaf130	Proteobacteria	Gammaproteobacteria	Pseudomonadales	Moraxellaceae
Leaf155	Proteobacteria	Alphaproteobacteria	Rhizobiales	Rhizobiaceae
Leaf176	Bacteroidetes	Sphingobacteriia	Sphingobacteriales	Sphingobacteriaceae
Leaf177	Proteobacteria	Betaproteobacteria	Burkholderiales	Burkholderiaceae
Leaf187	Firmicutes	Bacilli	Bacillales	Exiguobacterium
Leaf404	Bacteroidetes	Flavobacteriia	Flavobacteriales	Flavobacteriaceae
Root147	Firmicutes	Bacilli	Bacillales	Bacillaceae
Root563	Actinobacteria	Actinobacteria	Actinomycetales	Intrasporangiaceae
Root604	Proteobacteria	Gammaproteobacteria	Xanthomonadales	Xanthomonadaceae
Root935	Bacteroidetes	Flavobacteriia	Flavobacteriales	Flavobacteriaceae
Soil763	Actinobacteria	Actinobacteria	Actinomycetales	Micrococcaceae
EK10	Proteobacteria	Gammaproteobacteria	Pseudomonadales	
EK47	Proteobacteria	Gammaproteobacteria	Pseudomonadales	

2.3.3 *In vitro* and *in planta* transcriptomics of commensal bacteria from various phyla

In this experiment, 50% Tryptic Soy Broth (TSB) medium was used instead of KB medium for *in vitro* transcriptome analysis. To find an optimal sampling time point in the liquid medium, the growth curve of each commensal strain was determined and bacteria were harvested at the late exponential phase before the plateau. For *in planta* transcriptome analysis, the leaves of Col-0 plants were infiltrated by each commensal strain and harvested at 6 hpi. As described in Figure 3A, bacterial cells were isolated from the harvested leaves and RNA was extracted, followed by rRNA depletion, cDNA library generation, and RNA-seq. Here, I present preliminary results based on 1-2 biological replicates; more replicate will be analyzed in the future. Principle component analysis was conducted using the expression fold changes (*in planta* – *in vitro*) of KOs shared among five commensal strains in Table 1 and four *Pseudomonas* strains used in 2.3.1 (Figure 19). The preliminary result showed that bacterial transcriptome responses *in planta* show a phylogenetic pattern, i.e., four Gammaproteobacteria (*Pseudomonas*) strains were clustered together and two Bacteroidetes strains were clustered together (Figure 19). I compared expression of genes annotated with known functions among the nine strains. Genes related to catalase tended to be highly expressed *in planta* compared with *in vitro* (Figure 20A); and avirulent *Pseudomonas* strains showed strong induction of these genes compared with the other strains (Figure 20A). If this

gene expression pattern reflects the activation of plant immunity remains to be investigated. Flagellar related genes, which were induced in avirulent *Pseudomonas*, were not induced in two commensals L155 and L187; and they were not annotated in the other three commensal strains (Figure 20D). Thus, induction of flagellar related genes in avirulent bacteria is not a general phenomenon, but may be specific to *Pseudomonas* spp. Genes encoding ribosomal proteins were globally induced in *Pto* and mildly induced in avirulent *Pseudomonas* strains, but suppressed in non-*Pseudomonas* commensals (Figure 20B). Expression of ribosomal proteins may reflect the metabolic and reproductive activity of bacteria, i.e., *Pseudomonas* strains are more actively proliferating compared with the other strains *in planta*. *In planta* bacterial growth assay is one way to test this hypothesis. I also observed that genes encoding the components of the type VI secretion system (T6SS) were strongly induced in L155 *in planta* compared with other strains (Figure 20C). As the T6SS is known to be involved in microbe-microbe interactions (Russell et al., 2014), this result implies that L155 may actively interact with other microbes using T6SS *in planta*. More bacterial strains and replicates will be analyzed in the near future.

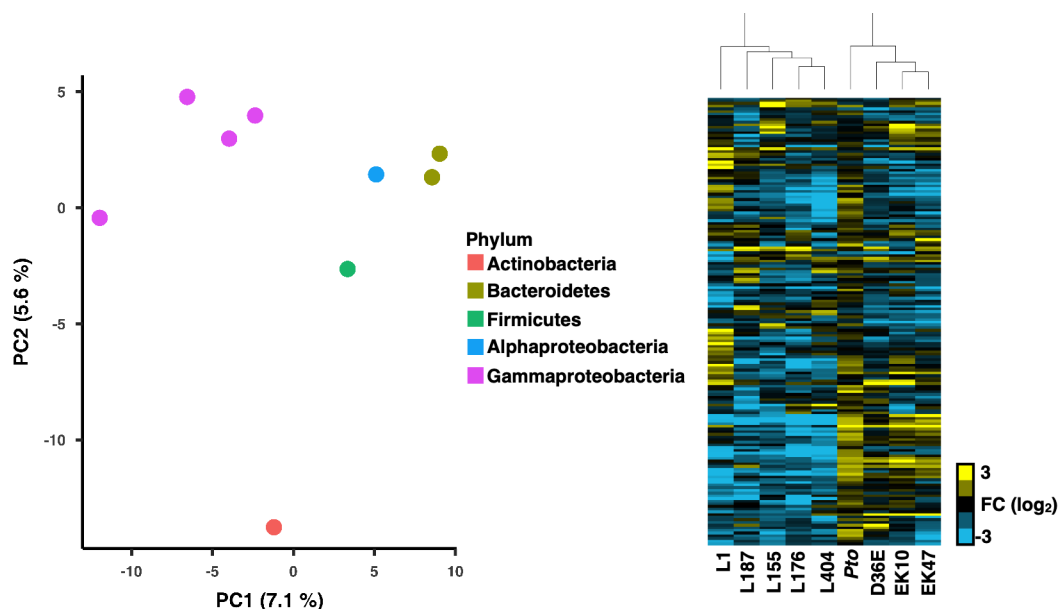


Figure 19: Comparative transcriptomics of nine bacterial strains

Principle component analysis (left) and hierarchical clustering (right) based on KEGG ontology (KO) expression fold changes (FC) between *in vitro* (TSB) and *in planta* (Col-0, 6 hpi). KOs shared among the all strains are used for the analysis.

2. Results

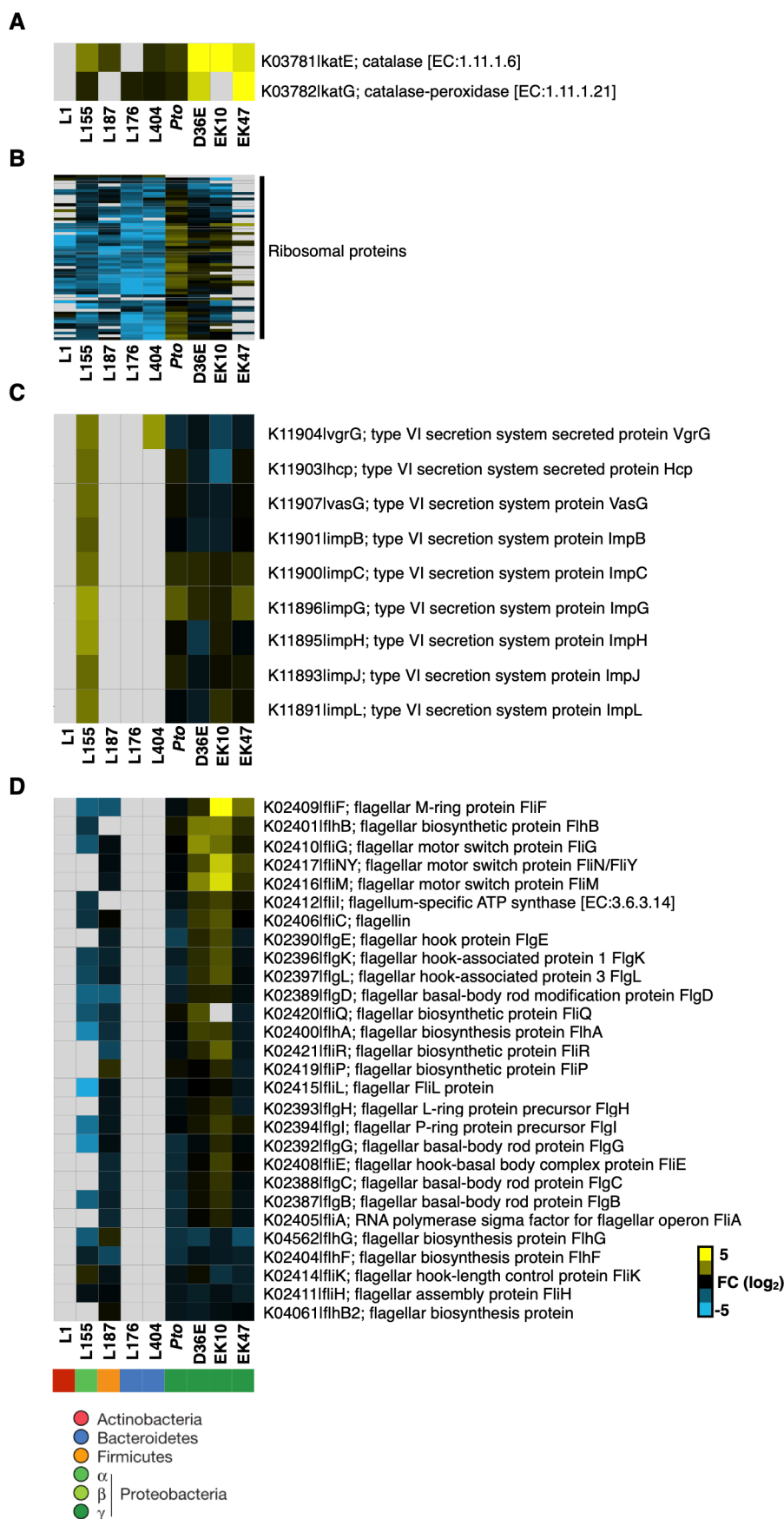


Figure 20: Bacterial functions differently expressed *in planta*

2. Results

Hierarchical clustering of KEGG ontology (KO) expression fold changes (FC) between *in vitro* and *in planta* in nine bacterial strains. (A) catalase, (B) ribosomal proteins, (C) type VI secretion system, (D) flagellar. The taxonomic affiliation (phylum level) of the strains is depicted using various colors.

2. Results

2.3.4 Transcriptomes responses of *A. thaliana* against commensal bacteria

Bacterial responses *in planta* varied depending on strains (Figure 20). To investigate whether the strain-specific responses reflect different plant immune responses triggered by different bacterial strains, I profiled plant transcriptome responses upon bacterial infiltration in the same experimental condition used for *in planta* bacterial transcriptome analysis. Plant genes related to immunity showed bacterial strain-specific expression patterns (Figure 21). Interestingly, *Pto* D36E appeared to trigger the strongest plant immune responses. As bacterial population is similar among all the strains tested at 6 hpi, it is plausible that *A. thaliana* recognized certain molecular feature of D36E, such as the flg22 peptide, to trigger relatively strong immunity. There was no clear phylogenetic pattern in plant immune activation, but Actinobacteria tended to trigger stronger immunity compared with commensal bacteria from other phyla. At this point, it is difficult to link *in planta* bacterial responses and plant responses due to the limited data points, but comprehensive profiling of the co-transcriptomes of plants and bacteria can address the question of whether bacterial strain-specific immune activation explains different bacterial responses in plants.

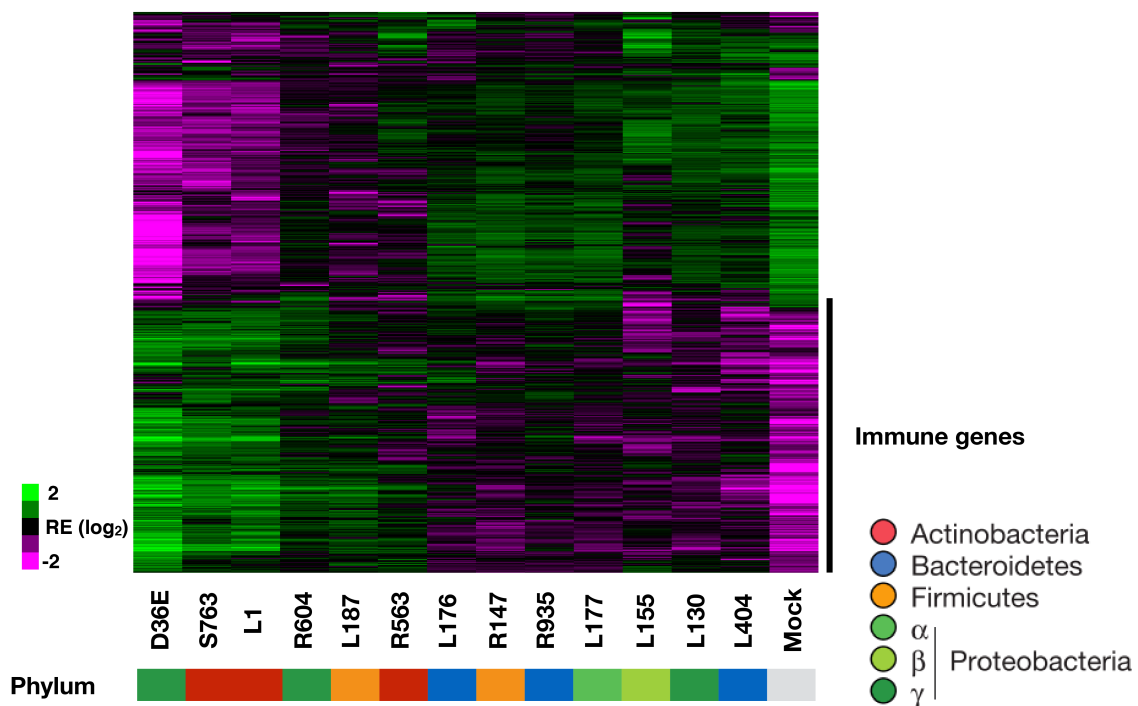


Figure 21: Bacterial strain-dependent plant immune activation

Plant genes that showed significant changes ($FDR < 0.01$; $|\log_2FC| > 1$) upon the infiltration of at least one of the bacterial strains compared with mock (water) treatment. The leaves of Col-0 were

2. Results

infiltrated with each bacterial strain at $OD_{600} = 0.5$ or mock. The leaves were sampled at 6 hpi. The color code below the strain names indicates the taxonomic affiliation (phylum level) of each strain.

3 Discussion

3.1 *In vivo* bacterial RNA-seq and Dual RNA-seq as powerful approaches in host-pathogen interaction studies

Bacterial transcriptomics within hosts has been a popular and powerful strategy in animal infection biology. In the 2000s, a number of studies profiled the transcriptomes of various bacterial pathogens in various hosts by using microarrays (La et al., 2008). RNA-seq technologies enabled the unbiased profiling of bacterial transcriptomes at higher resolution initially *in vitro* and, in 2010s, *in vivo* (Westermann et al., 2012). For instance, RNA-seq analysis of *Vibrio cholerae* isolated from the caecum of infected rabbits or the intestine of infected mice identified a set of bacterial genes induced upon infection, including known virulence factors and genes previously not linked to virulence (Mandlik et al., 2011). Rapid advancement of DNA sequencing technologies allowed the field to quickly move to the next level: simultaneous RNA-seq profiling of hosts and pathogens (Dual RNA-seq) (Westermann et al., 2017, 2012). Dual RNA-seq study of *Salmonella typhimurium* and infected HeLa cells identified a pathogen small RNA that is induced upon infection and suppresses host immune responses (Westermann et al., 2016). A number of other Dual RNA-seq studies revealed novel virulence mechanisms of pathogens or genes associated with virulence (Avraham et al., 2015; Nuss et al., 2017; Stapels et al., 2018). However, since many studies focus on the virulence of pathogens they gained relatively limited insights into the mechanisms of host resistance, i.e., how resistant hosts respond to pathogens and affect pathogen responses. A recent study conducted Dual RNA-seq analysis using *Staphylococcus aureus* and two mouse strains, susceptible or resistant to the pathogen, as well as immunocompromised mutants of the resistant mouse strain (Goldmann et al., 2017). This experimental design allowed the authors to evaluate the impact of host immunity on pathogen transcriptomes and to show that pathogen virulence factors are affected by host immunity (Goldmann et al., 2017). Therefore, testing various conditions that differ in host immune activation and pathogen virulence for *in vivo* bacterial transcriptomics or Dual RNA-seq analysis is important to elucidate the impact of host immunity on pathogens.

3.2 *In planta* bacterial transcriptomics and proteomics illuminate the mechanisms of pathogen growth suppression by plant immunity.

Study of plant disease resistance in the past decades have revealed two major forms of plant innate immunity (PTI and ETI). PTI and ETI are highly effective in restricting pathogen growth. However, how PTI and ETI halt pathogen growth remains an outstanding question that has been difficult to elucidate. In this thesis, using *in planta* bacterial transcriptome and proteome analyses, I was able to link activation of various immune signaling pathways to specific changes of global bacterial metabolic changes. Moreover, comparative analyses of bacterial transcriptomes and proteomes illuminated the potential regulatory mechanisms of bacterial genes *in planta*.

3.2.1 The impact of plant immunity on the transcriptomes of *Pto*

In this thesis, I profiled *in planta* transcriptomes of *Pto* with RNA-seq in various plant-bacterial strain combinations that show a wide spectrum of PTI/ETI activation (Figure 4A). Dual RNA-seq approach was not taken because this approach is still costly to get high-resolution data, and thus not suitable for testing a large number of conditions. By comparing bacterial transcriptomes under 27 conditions, I defined the “immune-responsive sector” of the *Pto* transcriptome at an early stage of infection (Figure 4 and Figure 5). I found that the expression pattern of the immune-responsive sector genes at an early time point of infection is tightly linked to bacterial growth at a later time point (Figure 5B). Importantly, among the immune-responsive sector genes is *pvdS* (Figure 6), a transcriptional regulator previously known for its role in regulating iron responses (Llamas et al., 2014). I found that overexpression of *pvdS* is sufficient to partially counter AvrRpt2-triggered ETI (Figure 6C), exemplifying a causal role of the immune-responsive sector genes in mediating bacterial growth inhibition by plant immunity.

The T3SS and T3Es have long been known as essential virulence factors of bacterial pathogens (Büttner and He, 2009). Suppression of T3E translocation and T3SS expression by PTI has been proposed to be a mechanism to attenuate pathogen virulence capacity during plant immunity (Crabill et al., 2010a) (Figure 4C). Remarkably, however, the *in planta* transcriptome analysis revealed that PTI has a much broader impact on bacterial metabolism

3. Discussion

beyond the T3SS, including fundamental processes of life, such as protein translation (Figure 4C). This suggests that bacterial growth inhibition during PTI may be caused by alteration of multiple bacterial processes other than or in addition to T3SS suppression. Because the bacterial transcriptome profiling was conducted at an early time point before bacterial population densities diverged in different samples (Supplementary figure 4), these broad effects are not a consequence of differential bacterial population densities *per se*. Furthermore, although ETI can also effectively halt bacterial growth, the data suggested that ETI has a narrower impact on the bacterial transcriptome. Most notably, ETI did not markedly affect the expression of the T3SS genes (Figure 4C and Figure 5A, see *Pto* vs *Pto* AvrRpt2 in Col-0 plants or Col-0 vs *rps2 rpm1* plants in *Pto* AvrRpt2), which is in agreement with a previous study (Nomura et al., 2011). This is consistent with the notion that PTI, but not ETI, invariably blocks T3Es translocation into host plant cells (Crabill et al., 2010b; Nomura et al., 2011). I cannot exclude the possibility that the different effects observed between PTI and ETI could be partially due to different kinetics of immune activation during PTI and ETI. Time-course analyses of bacterial transcriptomes would be an important future direction to understand the dynamic transcriptome responses of bacteria in plants.

In this thesis, I profiled the transcriptomes of *Pto* at another time point, 48 hpi. Although this is not a time-course experiment (the doses of bacterial inocula were different between experiments for the two time points), comparison of bacterial transcriptomes at 6 hpi and 48 hpi provided insights into time-dependent responses of *Pto* in plants. I found that *Pto* showed distinct transcriptome patterns at 48 hpi compared with 6 hpi (Figure 8 D and E). For instance, genes related to pathogenesis were further induced at 48 hpi compared with 6 hpi; and the expression was the highest in *pad4 sid2* (Figures 10A and 11), in which bacterial population is the highest. This result seems counterintuitive since it is known that expression of the T3SS is negatively regulated by QS signaling (Henke and Bassler, 2004), which is activated when bacterial population density is high (Papenfort and Bassler, 2016). It is possible that there are host factors that can induce the T3SS even when bacterial population is high. Importantly, *Pto* likely creates heterogeneous populations within a leaf and/or colony (Rufián et al., 2016; West and Cooper, 2016); thus, spatially-resolved analysis of bacterial gene expression is crucial to fully understand the impact of plant immunity on bacterial functions especially at a later stage of infection, where bacteria have established niches. Genes encoding catalase were highly expressed at 48 hpi (Figure 11). Since catalase is important for protecting

the cell from oxidative damage by reactive oxygen species (ROS), it is plausible that expression of catalase genes reflects the level of the ROS stress. Indeed, expression of these genes clearly correlated with the level of plant immune activation at 6 hpi (Figure 11), which is likely associated with ROS burst. However, whether high expression of catalase genes at 48 hpi reflects the strong ROS burst remains elusive.

3.2.2 Iron-acquisition pathway of *Pto* as a major target of plant immunity

As discussed above, the bacterial transcriptome data can provide some clues for the changes of apoplastic environments during immune activation. I found that both PTI and ETI commonly suppress the expression of bacterial iron starvation-related genes and this was associated with bacterial growth inhibition (Figure 6C). This finding enabled me to uncover that the bacterial sigma factor gene *pvdS* plays a causal role in mediating part of bacterial growth inhibition during ETI (Figure 6B). PvdS is a widely conserved global iron response regulator in plant/animal pathogenic and commensal bacteria (Swingle et al., 2008), implying that the suppression of bacterial iron starvation responses may be a general strategy for plant immunity to control bacterial growth *in planta*. Future research should examine whether PvdS and related sigma factors are also required for basic *Pto* virulence in plants. *Pto* has four other sigma factor genes that are responsive to iron starvation (Markel et al., 2013), at least two of which, PSPTO_1203 and PSPTO_1209, were suppressed by plant immunity (Supplementary figure 6). Understanding the roles of these sigma factors in basic bacterial virulence is an important future issue.

Iron is a two-faced element for bacterial growth; it is essential for biological processes, yet excess amount of iron can be toxic (Verbon et al., 2017). Animal hosts regulate iron availability in both directions, iron sequestration and intoxication, to inhibit pathogen growth (Chandrangsu et al., 2017). It is also known that some bacterial pathogens have evolved mechanisms to avoid host-mediated iron regulation (Chandrangsu et al., 2017). Thus, regulation of iron homeostasis seems to be an important factor in host-bacteria interactions. However, this study could not establish whether and how plant immunity affects *Pto* iron homeostasis during infection. Since PvdS-target genes may function in cellular processes beyond iron homeostasis (Swingle et al., 2008), it is possible that bacterial processes regulated by PvdS other than iron homeostasis may also be critical for *Pto* growth in plants. A previous study suggested that, in *A. thaliana*, the iron concentration in the apoplast was not a limiting

3. Discussion

factor for bacterial growth (O’Leary et al., 2016). It has also been shown that a PvdS-regulated siderophore, pyoverdine, and other high-affinity iron-scavenging systems are dispensable for the virulence of *Pto* in plants (Jones and Wildermuth, 2011). Together with my observation that iron co-infiltration did not promote *in planta* *Pto* growth (Figure 7A), I infer that iron limitation in the apoplast unlikely explains poor *Pto* growth under ETI. However, PTI and ETI clearly suppressed *Pto* genes that are known to be suppressed by iron supplementation *in vitro* (Figure 6A), suggesting that plant immunity causes an iron-rich-like response in bacteria. As I showed that PTI and ETI do not change the iron content in the plant apoplast (Figure 7), plant immunity likely influences bacterial iron responsive genes independent of iron content. In this regard, it is tempting to speculate that plants may secrete an iron-mimicking compound that manipulate the Fur-PvdS regulon to force bacteria into an iron-starved state without drastically changing the apoplastic iron content, which otherwise may cause collateral damages on plant growth and reproduction. Future research is needed to test the hypothesis that production of iron-mimicking compounds to perturb bacterial iron response might be an antibacterial strategy in plant immunity.

3.2.3 The gene regulatory network of *Pto*

Correlation analysis of bacterial gene expression under various conditions revealed bacterial genes/processes that are co-regulated, some of which are not explained by our current knowledge. For example, expression of genes related to coronatine biosynthesis and alginate biosynthesis correlated very strongly (Figure 15B and Supplementary figure 9A), suggesting that these processes might share the upstream regulator(s). AlgU, a transcriptional sigma factor, is known to be a master regulator of alginate related genes, but a ChIP-seq study of AlgU in *Pto* did not detect coronatine-related genes as targets (Markel et al., 2016). Coronatine-related genes are known to be regulated by CorR (Sreedharan et al., 2006). It may be possible that CorR also regulates alginate related genes. Further studies are required to understand the molecular link between these two processes. I also found that genes related to coronatine and the T3SS were only mildly co-expressed (Supplementary figure 9A), which was counterintuitive because CorR is known to be regulated by HrpL (Sreedharan et al., 2006), the master regulator of the T3SS. A major difference in expression of genes related to coronatine and the T3SS was that coronatine related genes are not induced in minimal medium, while T3SS genes are strongly induced (Supplementary figure 9B). The results

suggest that there might be additional regulators that differentiate expression of genes in these processes. Collectively, the analysis of the gene co-expression network has illuminated novel gene regulatory mechanisms of bacterial functions that are well studied for pathogenesis.

Gene co-expression networks also have the potential to identify clusters of highly co-expressed genes with unknown functions. In addition, as transcriptional regulators (TRs) and their targets are often co-expressed, a cluster of co-expressed genes can involve the TR(s) of other genes in the cluster. In this study, I selected three putative TRs from three gene clusters, none of which showed obvious functional enrichment. Strikingly, overexpression of each of these three TRs all led to enhanced expression of genes predicted to be downstream of the TRs based on my co-expression data (Figure 16), indicating that gene co-expression analysis can predict gene regulatory logic. The knowledge of functional TRs allows to globally manipulate genes involved in the same cluster by manipulating expression of the TRs, which is particularly useful to study the functions of the gene cluster. Since expression of genes in the three clusters is highly affected in the plant apoplast or immune activation (Supplementary Figure 11), it is possible that these genes may play roles in bacterial growth and/or virulence *in planta*. The role of the selected TRs will be further investigated by generating the knockout *Pto* strains of these TRs and the overexpressing/knockout strains will be tested for their growth in plants.

3.2.4 Proteome landscape of *Pto in planta* and integrative multi-omics

Unlike transcriptome responses, proteome responses of bacterial pathogens in hosts are mostly unexplored in any interaction systems including animals. In the present study, the proteomes of *Pto* were profiled under 15 conditions, both *in vitro* and *in planta*. This is, to my knowledge, the first study profiling the proteomes of bacteria in the plant apoplast. *In planta* proteome analysis of *Pto* detected up to 2000 proteins (Figure 8C). As about 3500 proteins could be detected *in vitro* (Figure 8C), it is likely that the sensitivity of the *in planta* proteome analysis has not reached the completeness yet. Especially, the number of proteins detected at an early time point of infection was low probably due to the low abundance of bacteria in the plant (Figure 8C). Improving the sensitivity of *in planta* bacterial proteomics is a future challenge. Nevertheless, *in planta* proteome analysis of *Pto* could capture distinct protein

3. Discussion

expression patterns among various conditions (Figure 8 *F* and *G*), providing novel insights into the proteome landscape of the bacterial pathogen in plants.

The abundance of transcripts does not necessarily correlate with the abundance of proteins because of various factors such as translation efficiency and protein stability. Studies comparing genome-wide abundance of transcripts and proteins in plants, yeasts, and mammals showed that transcriptomes and proteomes modestly correlate with each other in most cases (Foss et al., 2007; Ghazalpour et al., 2011; Gygi et al., 1999; Lan et al., 2012), whereas Marguerat et al. observed relatively high correlation between mRNA and protein levels of yeasts (Marguerat et al., 2012). In the present study, I found that the correlation between transcript and protein fold changes *in planta* is high (R^2 values are around 0.6) in general in *Pto* (Figure 13A), providing evidence that bacterial transcriptomes can explain large part of bacterial proteomes *in planta* at different stages of infection. Transcriptomes and proteomes are highly correlated in all conditions tested in this study (Figure 13A), thus there was no signal that plant immunity globally affects the relationship between mRNA and protein expression of bacteria. In addition to this, it is notable that, since the profiling of transcriptomes and proteomes was conducted completely independently, the relatively high correlation between transcriptome and proteome data supports that the quality of both omics data is high.

Integrative analysis of transcriptome and proteome data illuminated the regulatory mechanisms of bacterial iron responses *in planta*. Transcription suppression activity of Fur on iron-starvation genes has been known to be dependent on the binding of Fe(II) to Fur protein (Llamas et al., 2014). However, whether the regulation of the abundance of Fur protein is also important for iron-starvation responses is unknown. The proteome data showed that the abundance of Fur protein partially anti-correlates with expression of Fe responsive genes (Figure 14 *B* and *C*), suggesting that the regulation of the accumulation of Fur protein might contribute to iron-starvation responses. Whether the protein abundance of Fur has a causal impact on bacterial iron-starvation responses and how plants affect the accumulation of Fur proteins will be a future issue.

There were cases in which mRNA regulation and protein regulation do not correlate with each other (Figure 13). Expression of the T3SS was one of such cases (Figure 17A). The T3SS of *Pto* must cross the plant cell wall and plasma membrane as well as inner/outer membranes of bacteria to successfully translocate T3Es into plant cells. Harpins, HrpZ1,

HrpW1, and HopAK1 and HrpK comprise the tip part of the T3SS and were shown to function redundantly on T3E translocation (Kvitko et al., 2007). Also, lack of HrpK alone compromised growth of *Pto* in *A. thaliana* (Petnicki-ocwieja and Alfano, 2005), indicating the importance of harpin proteins for pathogen virulence. In the present study, I showed that the SA pathway of *A. thaliana* globally suppresses expression of HrpZ1, HrpW1, and HrpK at the protein level but not at the mRNA level (HopAK1 was not detected in the proteome analysis) (Figure 17 B-E). This suggests that plant immunity mediated by the SA pathway might degrade harpin proteins and/or affect translation of harpin proteins; and this might be a plant's strategy to suppress effector translocation into plant cells and to inhibit pathogen growth. This is, to my knowledge, the first study suggesting that T3SS components are targeted by host immunity at the protein level. Since most of the non-harpin proteins in the T3SS were not affected by the SA pathway, it is tempting to speculate that plant immunity selectively and directly target the harpin proteins, which have direct contact with the plant cell wall. The mechanism by which plant SA pathway suppresses expression of these proteins is an exciting research topic.

3.3 Understanding how plant immunity shapes plant microbiota

Beyond uncovering enigmatic transcriptome responses of *Pto* to plant immunity, the *in planta* bacterial RNA-seq pipeline opens up an exciting possibility to study the *in planta* transcriptomes of a variety of bacterial species and bacterial communities naturally associated with plants.

A preliminary analysis comparing the transcriptomes of four *Pseudomonas* strains, including pathogens and non-pathogens, revealed that there is a correlation between bacterial gene expression patterns *in planta* and their virulence (Figure 18A). For instance, avirulent strains (D36E, EK10, and EK47) strongly induced catalase genes, while the virulent strain (*Pto*) did not (Figure 18C). As catalase is important for detoxifying ROS, the induction of catalase genes in avirulent strains could be explained by ROS burst associated with plant immune activation, which is suppressed by effectors in the case of *Pto* infection. There were some genes differently responded even between commensals. Commensal *Pseudomonas*, EK10 and EK47, showed similar response as *Pto* and D36E, respectively, regarding expression of genes related to alginate biosynthesis (Figure 18E). The differential responses between

3. Discussion

commensal strains can be explained by two non-mutually exclusive possibilities: (i) different bacterial strains triggered different plant responses and (ii) the same plant environment affected differently on different bacteria strains. Indeed, transcriptome analysis of plants infiltrated with various commensal bacteria showed a variety of immune responses (Figure 21). The preliminary result of the comparative transcriptomics using nine bacterial strains from wide range of phyla showed a phylogenetic pattern in transcriptome responses *in planta* (Figure 19). A major challenge in this analysis is the sparsity of the dataset. Only a small number of KOs were shared among different strains, making comparison of KO expression difficult. Improving the quality of KO annotation and gene prediction in individual genomes would help to extract more information. Alternatively, using the orthologous gene list could increase the number of genes that can be compared among strains. Extensive co-transcriptomics of plants and bacteria will deepen our understanding of the interactions between plants and the microbiota.

It is important to note that, the co-transcriptome analysis in this thesis was not done in the gnotobiotic condition, i.e., plants might already be colonized by microbes before the infiltration of the bacterial strain of interest. Therefore, caution is required when interpreting the results; the potential effect of the already established microbiota on plant and bacterial responses needs to be taken into account. Nevertheless, as I used a single plant genotype (Col-0) and the plants were grown in the same condition, the background microbiota structure should be comparable among all samples, and thus comparisons between different plant-commensal strain combinations are still highly informative. Implementing the co-transcriptome analysis in the gnotobiotic condition would be an important future challenge.

The primary focus of plant microbiota studies has been, in most cases, the relative abundance of microbiota members, but the absolute abundance of them are less understood. It is of great importance to investigate the growth potential of individual commensal bacteria in the plant body and how plants affect bacterial growth to shape the microbiota. Therefore, *in planta* growth assay of commensal bacteria in the monoassociation condition is an important next step. Combined with the co-transcriptome data, this can reveal the bacterial strain-specific mechanisms by which plants respond to microbiota members and affect bacterial metabolisms to control bacterial growth *in planta*.

Microbe-microbe interactions are widespread among plant-associated microbes and can affect the outcome of plant-microbe interactions (Duran et al., 2018; Helfrich et al.,

2018). Thus, it is possible that plants have evolved mechanisms to direct microbe-microbe interactions for the benefit of plants. However, whether and how plant immunity affects interactions between microbes is not understood. Accumulation of knowledge regarding plant and bacterial responses during the monoassociation allows a reductionist approach to understand microbe-microbe interactions in the context of microbial communities. For instance, by inoculating the mixture of bacterial strains that show different responses *in planta* in the monoassociation condition, one can ask whether the presence of other bacterial species affect responses of plants and bacteria and investigate molecular bases underlying microbe-microbe or microbe-plant-microbe interactions.

3.4 How does plant immunity control bacterial growth?

Unlike animal immune cells, such as macrophages, plant cells do not appear to actively kill bacteria. Bacterial population in plants is not significantly reduced when infiltrated into plant leaves even under strong activation of PTI or ETI (compare bacterial growth in Figure 6C and Supplementary figure 7A) (Narusaka et al., 2009; Tsuda et al., 2009). Thus, the central role of plant immunity might be to suppress the excessive growth of bacteria without killing them. Successful activation of plant immunity is prerequisite for plants to inhibit pathogen growth, the mechanisms of which have been shown (or suggested) in this study and previous studies: (i) Pre-activated PTI can suppress expression of genes encoding the T3SS/T3Es (Figure 4B) and the translocation of the T3Es into plant cells (Crabill et al., 2010a; Oh et al., 2010), thereby avoiding immune suppression by pathogens, (ii) the SA pathway can suppress the protein accumulation of specific components of the T3SS, which might abolish its function (Figure 17), and (iii) ETI can overcome the suppression of immune responses by the T3Es (Ling et al., 2017; Mine et al., 2017a). How successfully activated plant immunity inhibits pathogen growth is a long-standing question in the plant-microbe interactions research, yet we have limited knowledge on this thus far. Asking a question on the flip side of the coin might be helpful: what makes bacteria virulent? The T3SSs and T3Es are essential for the virulence of various bacterial pathogens, but many other processes are likely involved in bacterial growth *in planta* as the present study and previous studies showed that a number of bacterial functions are activated upon infection (Figure 4B) (Yu et al., 2013). Intriguingly, GO enrichment analysis showed that most of GO terms significantly changed in

3. Discussion

expression upon infection were induced rather than reduced (Figure 4B), implying that the induction rather than the suppression of a set of functional processes is necessary for bacterial virulence in plants. Thus, blocking the induction of such processes might be key for plant immunity to inhibit pathogen growth. Indeed, I found that PTI suppresses various processes that are activated in *Pto* upon infection, including “iron acquisition”, “coronatine biosynthesis”, “alginate biosynthesis”, and “translation”, whereas ETI suppressed a specific process, “iron acquisition“ (Figure 4B). As both PTI and ETI are effectively inhibit pathogen growth, there are probably multiple ways for plant immunity to inhibit pathogen growth. It remains elusive what is the minimum set of bacterial processes whose suppression is sufficient for inhibiting *Pto* growth. Intriguingly, I observed, in a preliminary study, that plants do not allow commensal bacteria to induce genes related to translation and iron acquisition (Figure 18D and Figure 20B), implying that these processes might be important targets for plant immunity to control the growth of plant-associated bacteria in general. Recent advancement of DNA sequence technologies empowered scientists to identify bacterial genes required for colonization and growth in plants by comparative genomics of large number of bacterial species or saturation mutagenesis of specific bacterial species by using transposon insertion site sequencing (Tn-seq) (Cole et al., 2017; Levy et al., 2017; Levy et al., 2018). Understanding bacterial processes important for virulence or successful colonization in plants and their regulation by plant immunity is crucial for elucidating the molecular basis of how plant immunity acts on bacteria to control their growth.

3.5 Outlook

3.5.1 Resilience, tunability, and balance at different layers of plant immunity

As described in the introduction, plant immune networks provide plants with a resilient, tunable, and balanced ability to suppress pathogen growth. The resilient pathogen growth suppression could partly be explained by highly buffered transcriptome responses of plants mediated by the immune hormone network (Hillmer et al., 2017). In this thesis, bacterial transcriptome analysis at an early point of infection in a panel of *A. thaliana* immune-compromised mutants (single and multiple mutants) suggested that the SA, JA, ET, and PAD4 sectors affect bacterial transcriptomes in a qualitatively similar manner (Figure

5A). Bacterial T3SS and iron acquisition systems were shown to be major targets of plant immunity that were commonly suppressed by these hormone pathways (Figure 5A), suggesting the resilient targeting of pathogenesis-related functions by plant immunity. Importantly, abiotic factors can directly affect microbial responses as well as plant responses (Velasquez et al., 2018). For instance, elevated temperature enhances effector secretion of a bacterial pathogen and promotes disease susceptibility of plants (Huot et al., 2017). Combined with plant genetics and environmental perturbations, *in planta* microbial ‘omics’ profiling is a powerful strategy to elucidate molecular mechanisms underlying host-microbe-environment interactions. Another bottleneck is that we have scant knowledge about immune outputs that directly execute pathogen growth suppression and how such immune outputs are regulated. Quantitative analyses of immune outputs such as metabolites, peptides, nutrients, pH, ROS, redox state, and plant hormones would help to understand how immune outputs are regulated by the plant immune network. The temperature of the apoplastic space in relation to plant immunity is one of the unexplored research topics. The activation of plant immunity causes stomatal closure (Melotto et al., 2017) and stomatal closure is known to lead to higher leaf temperature (Mustilli, 2002). Thus, it may be possible that apoplastic temperature rises during plant immune activation and affects bacterial virulence as analogous to the fever response of vertebrates, a hallmark of infection and inflammatory response (Evans et al., 2015). The past decade has produced a rich and growing toolbox for the imaging analysis of those factors (Hilleary et al., 2018; Martinière et al., 2018; Nietzel et al., 2018). Phytoalexins and glucosinolates are known metabolites that suppress fungal growth (Piasecka and Jedrzejczak-rey, 2015). Imaging mass spectrometry analyses showed that the accumulation of a phytoalexin, camalexin, is limited to pathogen infection sites (Ryffel et al., 2015), implying that camalexin production is tuned/balanced in plant leaves.

In summary, there are a number of open questions regarding resilience, tunability, and balance of plant immunity at different layers such as plant responses, substances that directly act on microbes, impacts on microbial metabolism, and microbe-microbe interactions (Fig. 22).

3. Discussion

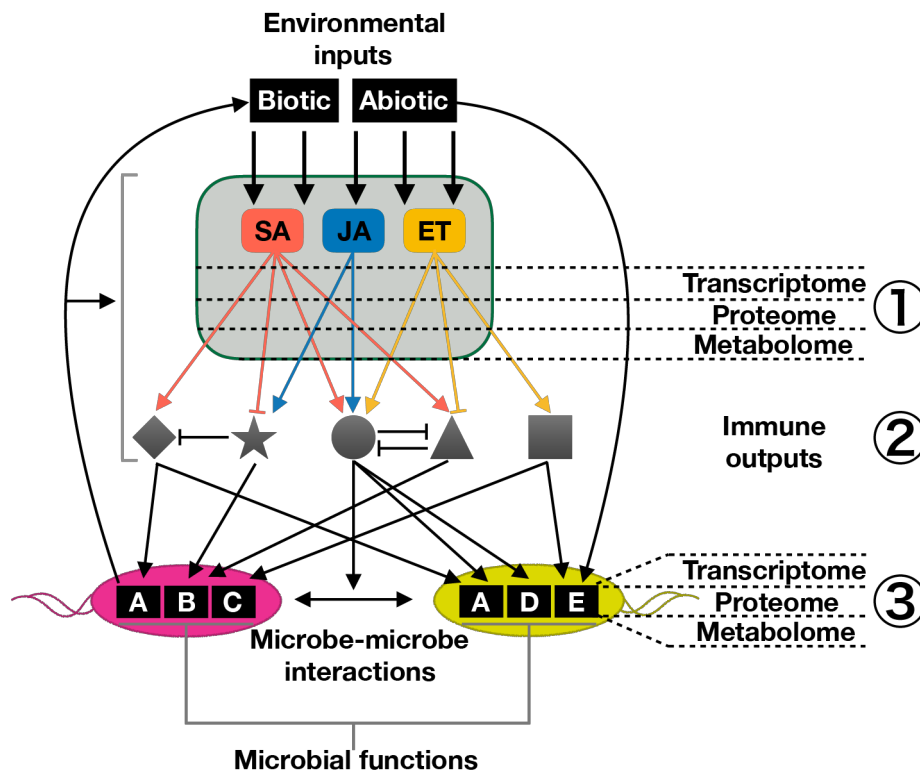


Figure 22: The plant immune system at different layers

Biotic and abiotic inputs trigger and modulate plant immune responses through plant immune networks (e.g., hormone networks). (1) Immune responses inside plant cells occur at the level of transcriptome, proteome, and metabolome. (2) Immune outputs that directly affect microbial responses can interact with each other to fine-tune the outcomes. (3) Impact of plant immunity on microbial functions at different layers, i.e., transcriptome, proteome, and metabolome of the microbe. This figure was adopted from Nobori et al., 2019 (*submitted*).

3.5.2 Zooming in: plant immune system at tissue- and cell-specific levels

The initial encounter of plants with microbes mainly occurs at the level of single or few cells. Unlike animals, plants do not have mobile immune cells, thus it is considered that all plant cells have the potential to defend themselves in addition to other functions. Since different cell types have different functions, the properties of immune networks and their connections with other processes are likely cell type-specific. Indeed, mesophyll cells and guard cells show opposite properties regarding the roles of SA and ABA. SA and ABA positively regulate guard cell immunity, i.e., stomatal closure, while ABA adversely affects SA-mediated immune responses in mesophyll cells (Melotto et al., 2017; Pieterse et al., 2012). However, our current understanding of the plant immune system is mostly limited to the bulk tissue level. Defining cell types that play distinct roles in plant-microbe interactions and

studying cell type-specific plant immune networks has the potential to elucidate systems that are masked when studied in bulk tissues.

As discussed in the previous section, plant microbiota can be a source of heterogeneous inputs. How plants integrate the heterogeneous microbial inputs and fine-tune their responses is still enigmatic. Cell type-specific expression of receptors might be a way. FLS2, a receptor for a well-conserved peptide derived from bacterial flagellin, expresses in stele but not in root epidermis (Beck et al., 2014), implying that root epidermal cells are not highly responsive to bacteria on the root surface, but once bacteria reach the endodermis (a sign for potential pathogens), endodermal cells trigger immune responses. This may be a plant strategy to avoid unnecessary immune activation by commensal bacteria harmlessly existing on the root surface, allowing allocation of resources in the cells to other tasks such as nutrient acquisition.

‘Omics’ profiling of cell-type specific responses helps understand the immune regulatory networks in different cell types. Cell type specific responses to MAMPs, flg22 and Pep1, were shown in *A. thaliana* roots by RNA-seq analysis of FACS-sorted cell types based on fluorescent markers (Rich et al., 2018). Recent advances in single cell analysis technologies hold promise for the studies of plant immune systems at the single cell level (Efroni and Birnbaum, 2016). Understanding plant immune receptor/signaling networks at single cell/cell type-specific levels is an important future challenge (Figure 23).

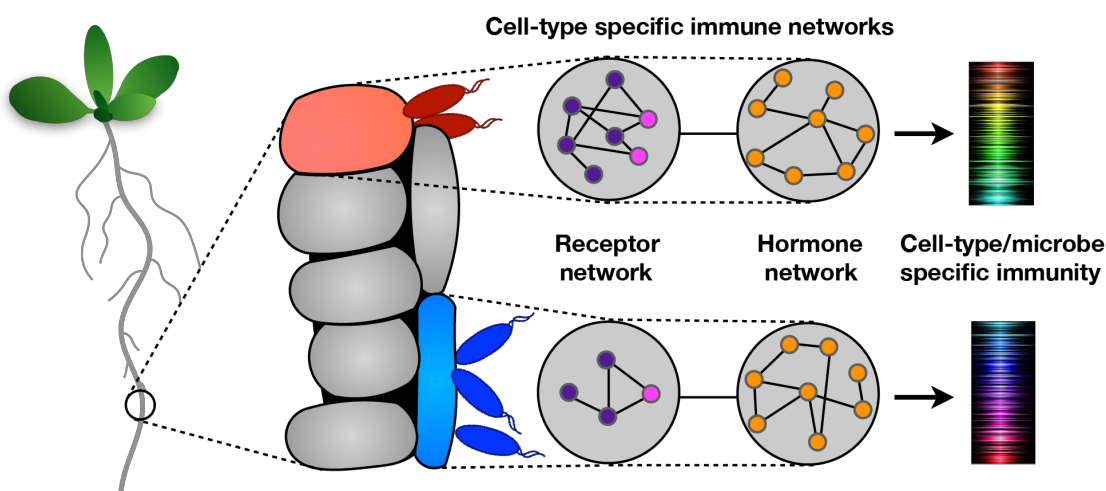


Figure 23: Plant immune networks at the single cell/cell-type specific level

3. Discussion

Different cells/cell types have different immune network structures (e.g., receptor networks and hormone networks) and encounter different sets of microbes, resulting in different spectra of immune outputs. This figure was adopted from Nobori et al., 2019 (*submitted*).

3.5.3 Overcoming tradeoffs in agriculture

Plants have evolved complex molecular systems to adapt to rapidly evolving microbes and changing climates. Although these systems would benefit the survival of the species in nature, they can pose a burden in agriculture, where yields are more appreciated than the survival of species and growth conditions are relatively less heterogeneous than the natural environment. Such phenomena are pervasively called as “tradeoffs”. A classical example is that crops with enhanced disease resistance often have reduced yield (“growth-defense trade-off”) (Karasov et al., 2017). A recent study showed that the genetic link mediating a tradeoff between JA-mediated defense against insects and plant growth can be unlinked by rewiring JA and phytochrome B signaling (Campos et al., 2016), suggesting that resource limitation is not the sole reason for this growth-defense tradeoff in laboratory conditions. Such mutant plants may show reduced fitness in the natural environment, but if we could artificially control plant growth conditions and remove the environmental factors that require the tradeoff, the tradeoff could truly be overcome in an agricultural setup. Therefore, better understanding of plant immune systems and their connections with plant responses to heterogeneous and complex environmental factors paves the way to unlocking the potential of crop engineering combined with tailor-made agricultural management.

3.5.4 Towards the understanding of molecular super-networks in plant-bacterial interactions.

Plants and bacteria both have evolved their own molecular signaling networks. The molecular networks of plants and bacterial pathogens appear to be interconnected to form supernetworks, as bacterial pathogens interfere with plant immune networks by multiple means and plant immunity also affects components of the bacterial virulence networks as described in this thesis (Figure 1). Here, I discuss small molecules produced by plants and bacteria that potentially play a role in assembling the supernetworks between the two organisms.

Bacteria produce a variety of phytohormones (mimics), such as IAA, SA, ET, ABA, cytokinin, gibberellin, and coronatine (Bakker et al., 2014; Fahad et al., 2015; Kunkel and Harper, 2017; Nagel and Peters, 2017; Zhang et al., 2017); some of these phytohormones (mimics) produced by bacteria can affect plant physiology including plant immunity (Kunkel and Harper, 2017; Zhang et al., 2017). On the other hand, bacteria also use phytohormones to regulate their own responses. For instance, IAA is used as a QS signal in some bacteria (Yue et al., 2014), suggesting that plant-derived IAA has the potential to affect bacterial physiology including virulence via the QS system. The ability of both plants and bacteria to produce and perceive phytohormones raises the possibility that phytohormones are key molecules that connect the plant immune and bacterial virulence networks. Moreover, plants can perceive siderophores (Aznar and Dellagi, 2015) and AHLs (Mathesius et al., 2003; Miao et al., 2012; Schenk et al., 2014) produced by bacteria to trigger defense responses, suggesting that the role of these small molecules is not restricted within or between bacterial species but that they might be used for direct interactions between plants and bacteria. Intriguingly, a number of bacterial strains produce pipercolic acid and likely release a large amount of this chemical into the soil (Vranova et al., 2013). Pipercolic acid is also produced by plants and plays an important role in mediating systemic acquired resistance, which is effective against a broad range of pathogens (Návarová et al., 2012). Therefore, bacteria-derived pipercolic acid may have a significant effect on inducing systemic acquired resistance, thereby protecting plants from potential pathogens. Reciprocally, plant-derived pipercolic acid may affect bacterial networks. Indeed, it is known that a number of bacterial strains assimilate pipercolic acid (Vranova et al., 2013). Collectively, small molecules that play important roles in the signaling networks within plants and/or bacteria can potentially connect these two networks, assembling supernetworks and potentially driving the evolution of the plant-bacterial pathogen interactions (Figure 24).

The concept of supernetwork is not specific to the interaction between plants and pathogenic bacteria. For instance, in legume-rhizobium symbiosis, regulation of symbiosis-related genes of the hosts and bacteria are tightly connected by the exchange of small molecules produced by both sides (Cao et al., 2017). It is plausible that plants form molecular supernetworks also with various commensal bacteria in the plant microbiota, in which inter- and intra-kingdom communications occur via diverse signals (Leach et al., 2017).

3. Discussion

Transcriptome and proteome analyses of bacteria and plants will open a new avenue for better understanding the molecular supernetworks of diverse interactions.

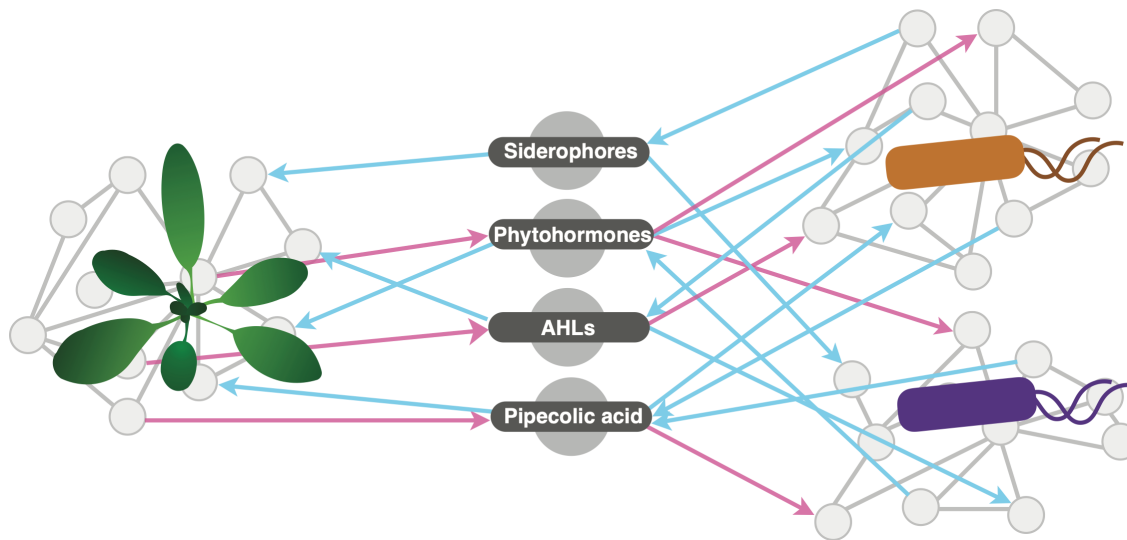


Figure 24: A conceptual model illustrating the plant–bacterial supernetwork

In the supernetwork, the molecular networks of plant immunity and bacterial virulence are connected by small molecules shared between plants and bacteria. Red and blue arrows indicate signals derived from plants and bacteria, respectively. AHLs, Acyl-homoserine lactones. This figure was adopted from (Nobori et al., 2018a).

3. Discussion

3.6 Concluding remarks and future perspectives

Plant-microbe interactions are processes in which responses of plants and microbes are tightly connected to determine the outcomes of interactions. Interactions between plants and pathogens have been intensively studied in the past decades and we gained an enormous amount of knowledge about plant immune responses against pathogens and how pathogens affect the plant immune systems. However, we have relatively limited knowledge about pathogen responses necessary for their virulence and how plant immunity influences pathogen responses to fight against them. In this thesis, I established methods to profile transcriptomic and proteomic responses of bacterial pathogens in plant leaves. This approach allowed me to gain unprecedented insights into the mechanisms by which plant immunity affects bacterial metabolisms to inhibit pathogen growth and into bacterial gene regulatory mechanisms in plants.

I further extended this approach to investigate plant-microbiota interactions, an emerging field in plant-microbe interactions research. Many studies have investigated the structure of plant-associated microbial communities under various conditions, revealing microbial species adapted to plant environments and factors that affect microbiota assembly (Bulgarelli et al., 2013; Hacquard et al., 2015; Vorholt, 2012). However, it remains largely enigmatic how individual interactions between plants and each microbiota member influence the shape and functions of the microbiota. To tackle this issue, accumulation of knowledge in the individual interactions is crucial. Here, I established a pipeline for the RNA-seq analysis of plants and bacteria in monoassociation conditions, which revealed that different combinations of plants and bacterial species have both common and specific transcriptomic signatures in plant and bacterial responses. This approach can be applied, in the future, to simplified bacterial communities to investigate the transcriptome landscape of plant-microbiota holobiont and its role in affecting microbiota structure and functions.

Further research using the approaches established in this thesis has the potential to (i) identify previously unknown virulence-related processes in bacterial pathogens and molecular mechanisms by which resistant plants target these processes and (ii) understand the commonalities and differences of molecular supernetworks in diverse plant-bacterial interactions. Such knowledge will help us unlock the complex molecular interactions between

plants and pathogens/microbiota, which will provide untapped engineering potential in plant breeding.

4. Materials and Methods

4 Materials and Methods

4.1 Key resources

REAGENT or RESOURCE	SOURCE
Chemicals and Peptides	
Tryptic Soy Broth	Sigma-Aldrich
Rifampicin	Duchefa
Tetracycline	Sigma
Kanamycin	Duchefa
Gentamycin	Duchefa
Salicylic acid	Duchefa
flg22	EZBiolab Inc.
Chitosan	Sigma
pegGOLD TriFast™	Peqlab
EvaGreen DNA Dye	Biotium
Phenol solution pH 8.0	Sigma
100% ethanol	VWR international
NaOH	Carl Roth
Chloroform	Carl Roth
Sodium citrate	Sigma
Iron(III) citrate	Sigma
Tris(2-carboxyethyl)phosphine (TCEP)	Sigma
Nuclease-Free Water (not DEPC-Treated)	Ambion
Kits	
TURBO DNA-free Kit	Ambion
RNAqueous-Micro Total RNA isolation Kit	Ambion
RNeasy Mini Kit	Qiagen
RNapro™ Solution	MP Biomedicals
Lysing Matrix E	MP Biomedicals
FastRNA PRO™ BLUE KIT	MP Biomedicals
Ovation® Complete Prokaryotic RNA-Seq Library	NuGEN
Ribo-Zero rRNA Removal Kit (Plant)	Illumina
SuperScript™ III Platinum™ One-Step qRT-PCR	Invitrogen

REAGENT or RESOURCE	SOURCE
Plant materials	
see 4.2	
Bacterial strains	
see 4.3	
Software and algorithms	
see 4.11	
Primers	
see 4.12	

4.2 Plant materials and growth conditions

The *Arabidopsis thaliana* accession Col-0 was the background of all *A. thaliana* mutants used in this study. The *A. thaliana* mutants *cyp79b2 cyp79b3* (Zhao et al., 2002), *npr1-1* (Cao et al., 1997), *rpm1-3 rps2-101C* (Mackey et al., 2003), *stp1 stp13* (Yamada et al., 2011), and combinatorial mutants (Tsuda et al., 2009) of the *A. thaliana* mutants *dde2-2* (Malek et al., 2002), *ein2-1* (Alonso et al., 1999), *pad4-1* (Jirage et al., 1999), and *sid2-2* (Wildermuth et al., 2001) were described previously. The double mutant *sid2-2 pmr4-1* was generated by standard genetic crosses (Nishimura et al., 2003). Plants were grown in a chamber at 22°C with a 10-h light period and 60% relative humidity for 24 days and then in another chamber at 22°C with a 12-h light period and 60% relative humidity. For all experiments, 31 to 34 day-old plants were used.

4.3 Bacterial strains

Pto DC3000 carrying empty vector (pLAFR), *avrRpt2* (pLAFR), and *avrRps4* (pVSP61) (Tsuda et al., 2013) and effector-deficient mutant *Pto* D36E (Wei et al., 2015) were described previously. Commensal Pseudomonas strains, EK10 and EK47, were kindly provided by the group of Prof. Dr. Eric Kemen. The other commensal strains shown Table 1 were described previously (Bai et al., 2015).

4. Materials and Methods

4.4 Accession numbers

The accession numbers for the genes discussed in this article are as follows: *AtACTIN2* (At2g18780), *AtPR1* (AT2G14610), *AtDDE2* (AT5G42650), *AtEIN2* (AT5G03280), *AtPAD4* (AT3G52430), *AtSID2* (AT1G74710), *AtNPR1* (AT1G64280), *AtPMR4* (AT4G03550), *AtSTP1* (AT1G11260), *AtSTP13* (AT5G26340), *AtCYP79B2* (AT4G39950), *AtCYP79B3* (AT2G22330), *AtRPS2* (AT3G03600), *AtRPM1* (AT3G07040), *pvdS* (PSPTO_2133), *hrpL* (PSPTO_1404), *avrPto* (PSPTO_4001), *cmaA* (PSPTO_4709), *gapA* (PSPTO_1287), *katB* (PSPTO_3582), *katG* (PSPTO_4530), *gyrA* (PSPTO_1745), *hrcC* (PSPTO_1389), *hrpZ* (PSPTO_1382).

4.5 *In vitro* bacterial cultures for bacterial transcriptomics and proteomics

P. syringae strains were grown in either King's B medium or type III-inducible medium (Huynh et al., 1989) (50 mM KH₂PO₄; 7.6 mM (NH₄)₂SO₄; 1.7 mM NaCl; 1.7 mM MgCl₂·6H₂O; 10 mM fructose) to OD₆₀₀ = 0.65 (late log phase) at 28°C. In the experiments using commensal bacteria, bacterial strains were grown in 50% Tryptic Soy Broth (TSB; Sigma) to the late log phase at 23°C. Upon harvesting bacterial cells, 0.1 volumes of 5% phenol and 95% ethanol were added to the culture which was then resuspended and centrifuged, followed by total RNA extraction for RNA-seq of the bacterial pellet.

4.6 Elicitor pretreatment

One day before bacterial infection, leaves were sprayed with H₂O (Mock), 1 μM flg22 (EZBiolab), 100 μg/ml chitosan (Sigma), or 50 μM SA (Duchefa Biochemie).

4.7 Bacterial infection and sampling for *in planta* bacterial transcriptomics and proteomics

Pto stains were cultured in King's B medium at 28°C. Commensal strains were cultured in 50% TSB medium at 23°C. Bacteria were harvested by centrifugation and resuspended in sterile water to an OD₆₀₀ of 0.5 and 0.005 for the sampling at 6 and 48 h post

infection, respectively. In total, 80 to 100 *A. thaliana* leaves (four leaves per plant) were syringe-inoculated with bacterial suspensions using a needleless syringe. The infected leaves were harvested at 6 h post infection, immediately frozen in liquid nitrogen, and stored at -80°C.

4.8 Transcriptome analysis of plants

Bacterial suspensions were prepared and syringe infiltrated as described in 4.6. Water was used for mock treatment. Six infected leaves were harvested at 6 h post infection, immediately frozen in liquid nitrogen, and stored at -80°C. RNA was extracted by using RNApro™ Solution and Lysing Matrix E (MP Biomedicals) followed by DNase treatment with TURBO DNA-free kit (Ambion). Illumina TrueSeq cDNA libraries were subjected to RNA-seq at the Max Planck Genome Centre Cologne using Illumina HiSeq3000 with 150 bp strand-specific single-end read, resulting in approximately 30 million reads per sample.

4.9 *In planta* bacterial transcriptomics

*Sections 4.9.1 – 4.9.4 were adopted from my previous publication (Nobori and Tsuda, 2018).

4.9.1 Establishment of a bacterial isolation buffer

The bacterial isolation buffer needs to be able to fix bacterial metabolism, protect bacterial RNA from degradation, and separate bacterial cells from plant cells. I first tested a commonly used solution containing 9.5% ethanol and 0.5% phenol. This could protect bacterial RNA when bacteria were incubated alone, but not when mixed with crushed plant leaves (Supplementary figure 1C). Adding the reducing agent Tris(2-carboxyethyl)phosphine (TCEP; Sigma) to a final concentration of 25 mM protected bacterial RNA in the mixed condition in a pH-dependent manner: buffers with lower pH protected bacterial RNA better (Supplementary figure 1C). I determined pH 4.5 as an optimal condition, where both RNA protection and bacterial enrichment could be sufficiently accomplished. Incubating bacterial cells in this buffer did not affect bacterial transcriptome patterns, suggesting that this buffer fixed bacterial metabolism (Supplementary figure 1D).

4. Materials and Methods

4.9.2 Bacterial isolation

Bacterial isolation Day1

1. Infiltrate bacterial suspension ($OD_{600} = 0.5$) to 80 leaves (approximately 3 g) of *A. thaliana* leaves from the abaxial side to the entire leaf area with a 1 ml needle-less syringe. 4 leaves/plant x 20 plants.
2. Six hours after infiltration, collect 80 leaves with forceps in a 50 ml Falcon tube containing 8-10 stainless steel balls (4 mm; sterilized by washing with ethanol and air dried). Flash-freeze with liquid nitrogen. Samples can be stored at $-80\text{ }^{\circ}\text{C}$.
3. Shake thoroughly by hand and crush the leaves into small pieces (Method figure 1). Ensure that the samples do not thaw during crushing.



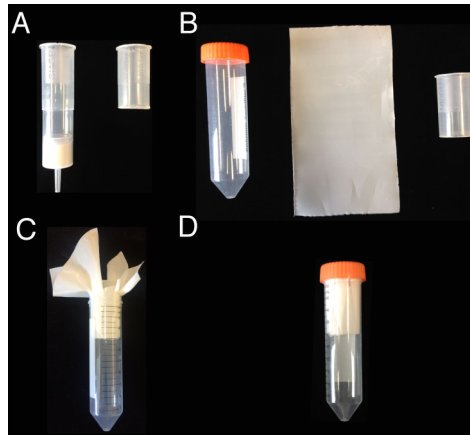
Method figure 1: Crushed leaf sample before incubation in the bacterial isolation buffer

4. Add 30 ml ice-cold **bacterial isolation buffer** (Nuclease-Free Water, 25 mM TCEP (tris(2-carboxyethyl)phosphine), pH 4.5 adjusted with 10 N NaOH 9.5% ethanol 0.5% Phenol solution; prepare it fresh every time) in a fume hood and vortex immediately for 10 sec followed by shaking vigorously by hand for 10 sec. Incubate the tubes for 20 h with shaking at 33 rpm using Roller mixer SRT1 at $4\text{ }^{\circ}\text{C}$.

Bacterial isolation Day2

4. Materials and Methods

1. Equip a 50 ml Falcon tube with a filter holder (handmade from a QIAGEN-tip 500 column; the upper half was cut by a plastic cutter; autoclaved before using) and a single layer of 6 μm filter mesh (cut into 12 cm x 15 cm size, and then autoclaved) (Method figure 2). Trim away the excess filter mesh with scissors so that the cap can fit the tube.



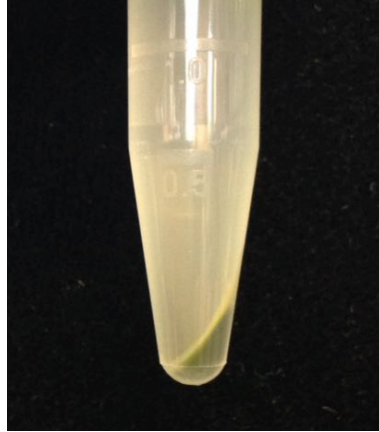
Method figure 2: Filter and filter holder equipped to a 50 ml Falcon tube

(A) A QIAGEN-tip 500 column is cut to make a filter holder. (B) A 50 ml Falcon tube, a 6 μm filter mesh (12 cm x 15 cm), and the filter holder. (C) Equip the 50 ml Falcon tube with the filter holder and the filter mesh. (D) Trim away the excess filter mesh so that the cap can fit the tube.

2. Apply the sample (15 ml; without stainless steel balls) to the column and filter it by centrifuging at 1,300 $\times g$ for 10 sec (or until all the liquid goes through) at 4 $^{\circ}\text{C}$. While keeping the flow-through in the tube, apply the rest of the sample (15 ml) to the column and repeat the filtering.
3. Remove the filter and the filter holder. Centrifuge the flow-through for 20 min at 3,200 $\times g$ at 4 $^{\circ}\text{C}$. Discard the supernatant with an electronic pipette equipped with a 25 ml serological pipette. You may leave some liquid (100 μl) to avoid the sample loss.
4. Add 900 μl of ice-cold bacterial isolation buffer and resuspend the pellet by vortexing, then transfer it to a new 1.5 ml tube on ice by pipetting. Make sure that the pellet is completely resuspended.
5. Centrifuge for 20 min at 2,300 $\times g$ at 4 $^{\circ}\text{C}$. You will see two-layered pellet: white on the top and green at the bottom (Method figure 3).

4. Materials and Methods

Note: Sometimes the upper part of the tube gets pale green. In this case, you may remove the green part by pipetting with a small amount of the liquid phase and discard it to avoid a potential plant contamination.



Method figure 3: A two-layered pellet consists of plants (bottom, green) and bacteria (top, white)

- Equip 20 μl Gilson pipette with 10 μl filter tip (with 20 μl capacity) and set the volume to 18 μl . Carefully resuspend only the top white layer by pipetting up and down close to the surface of the pellet. When the buffer gets cloudy by the bacterial cells, transfer the buffer (approximately 1,000 μl) to a new 1.5 ml tube on ice using 1,000 μl pipette. Then, carefully add 1 ml of new ice-cold bacterial isolation buffer without disrupting the pellet by tiling the tube. Repeat resuspending and collecting bacterial cell suspensions in new 1.5 ml tubes (total three times or until the white layer is completely removed).

Note-1: You may use larger tips that fit the pipette, but smaller tips make it easier to resuspend the bacterial layer without breaking the plant layer.

Note-2: If the layer of plant tissues is collapsed and mixed with the layer of bacterial cells, you can recover the bacterial layer by completely resuspending the entire pellet by vortexing and then repeating the centrifugation step (step C-5).

- Centrifuge the bacterial suspensions for 2 min at 10,000 $\times g$ to harvest bacterial cells. Discard the supernatant by pipetting.

4.9.3 RNA extraction

For *Pto* strains, the TriFast solution was mixed with 200 μ l of chloroform and the aqueous phase was isolated by centrifugation (typically 400 μ l). The aqueous phase was mixed with 200 μ l (half volume) of ethanol and then applied to the column of RNAqueous kit (Ambion). RNA was eluted in 30 μ l of RNase free water following the manufacturer's protocol. For commensal bacteria, RNA was extracted by using FastRNA PRO™ BLUE KIT (MP Biomedicals) following the manufacturer's protocol. Extracted RNA was treated with 2 U of TURBO DNase (Ambion) for 30 min at 37°C. Then, plant rRNA was removed using RiboZero plant kit (Epicentre) following the manufacturer's protocol. Input RNA amount ranged from 2.5 to 5 μ g depending on the yield of RNA after DNase treatment. Plant rRNA-depleted RNA was purified and concentrated with RNeasy MiniElute kit (Qiagen).

4.9.4 cDNA library generation and RNA-seq

cDNA libraries were generated with Ovation Complete Prokaryotic RNA-seq kit 1-8 (NuGEN), following the manufacturer's protocol with some modifications. Ten ng of plant rRNA-depleted RNA was used as input. DNA fragmentation was conducted with a Covaris S-Series instrument. cDNA libraries were subjected to RNA-seq at the Max Planck Genome Centre Cologne using Illumina HiSeq3000 with 150 bp strand-specific single-end read, resulting in approximately 10 million reads per sample. Illumina CASAVA pipeline (version 1.8.2) was used for base calling and cutadapt (Martin, 2011) was used for discarding reads containing the Illumina adaptor sequences. The resulting reads were mapped onto the *Pto* DC3000 genome/CDS (*Pseudomonas* Genome Database) and the *A. thaliana* genome (TAIR10) using Bowtie2 (Langmead and Salzberg, 2012) and TopHat2 (Kim et al., 2013), respectively. Mapped reads were counted with the Python package HTSeq (Anders et al., 2014).

4.9.5 Statistical analysis of RNA-seq data

The statistical analysis of the RNA-seq data was performed in the R environment. Genes with zero counts in at least one of the samples were excluded. The count data of the remaining genes was normalized and log-transformed by the function calcNormFactors

4. Materials and Methods

(TMM normalization) in the package edgeR (Robinson et al., 2010) and the function voomWithQualityWeights in the package limma (Smyth, 2005), respectively. Density plot analysis, carried out with the function plotDensities in the package limma, showed that TMM normalization successfully normalized the read-count distribution of each sample (Supplementary figure 2C). To each gene, a linear model was fit by using the function lmFit in the limma package with the following terms: $S_{gtr} = GT_{gt} + R_{r+} + \epsilon_{gtr}$, where S is the \log_2 count per million, GT is the host genotype: *Pto* strain interaction and the random factors, R is the biological replicate, and ϵ is the residual. The eBayes function in the limma package was used for variance shrinkage in the calculation of the p -values, which was then used to calculate the false discovery rate (FDR; the Storey's q -values) using the qvalue function in the qvalue package (Storey and Tibshirani, 2003). All normalized mean expression values (\log_2 counts per million) of bacterial genes are available in a previous paper (Nobori et al., 2018b). To extract genes with significant expression changes, the cutoff of q -value < 0.01 and $|\log_2FC| > 2$ was applied. The prcomp function was used for principal component analysis. MDS plot was created with the plotMDS function in the package edgeR. Hierarchical clustering was done using the dist and hclust functions in the R environment or using the Cluster3.0 software (Hoon et al., 2004). Heatmaps were created with the heatmap3 function in the R environment or using the TreeView (Eisen et al., 1998). For the distance heat map, the distances were calculated using the dist function in R environment after estimating a mean-dispersion relationship of the data using estimateDispersion function with method = 'blind' and transforming the variance with the varianceStabilizingTransformation function in the DESeq2 package (Love et al., 2014). Enriched gene ontology terms were identified using BiNGO plugin for cytoscape (Maere et al., 2005a).

4.9.6 Quality assessment of RNA-seq data

There was certain variation in bacterial enrichment rate among samples and some sequence reads were mapped to neither the *Pto* nor *A. thaliana* genome due to low-quality or contaminations ("Else" in Figure 3C). However, hierarchical clustering of RNA-seq data showed that the bacterial enrichment rate and the sequence depth did not explain the transcriptome pattern (Supplementary figure 2A), suggesting that there are no systematic biases caused by the enrichment method.

4.9.7 Co-expression analysis of *Pto* genes

Co-expression matrix was generated by using `cor` function with the method = 'pearson' in the R environment. The co-expression network was visualized on the Cytoscape (Shannon et al., 2003) using yFiles organic layout. Gene pairs with correlation coefficient greater than 0.8 were used as edges.

4.9.8 Analysis of RNA-seq data of commensal strains

RNA-seq count data were normalized and log-transformed as described in 4.8.5. The genome of each bacterial strain was annotated with KEGG ontology (KO) by BlastKOALA (Kanehisa et al., 2016). Gene expression fold changes between *in vitro* (TSB) and *in planta* (Col-0, 6 hpi) were used for analyses. In case a KO was assigned to multiple genes, the mean expression fold change was used as the KO expression data.

4.9.9 *In planta* bacterial transcriptome method based on customized probes

Pto was grown in the KB medium at 30°C. Plants were grown in a chamber with a 12-h light period, 23°C temperature at day time and 21°C at night time. Two leaves from three to four-and-one-half week-old *A. thaliana* plants were infiltrated with either 0.005% dimethyl sulfoxide (DMSO, Mock) or 500 nM flg22 using a needleless syringe. Plants were inoculated with a suspension of *Pto* at OD₆₀₀ = 0.75 at 20 h after the infiltration of mock or flg22. Seven hours after *Pto* inoculation, leaves were collected for RNA extraction.

RNA was extracted using the TRIzol™ reagent (Thermo Fisher Scientific) and the Direct-zol™ RNA Miniprep kit (Zymo Research). Purified RNA was treated with 10 U of RNase-free DNase I (Roche Applied Science); then RNA was purified with the Direct-zol™ RNA Miniprep kit. Non-organellar 18S and 28S rRNAs, and poly(A) mRNAs were depleted using the MICROBEnrich™ kit (Thermo Fisher Scientific). RNA quality was evaluated using the Agilent 2100 BioAnalyzer and RNA concentration was determined using the Qubit™ RNA HS assay kit (Thermo Fisher Scientific).

RNA-seq libraries were prepared using the Ovation Arabidopsis RNA-seq system 1–16 (NuGEN) with modifications to the manufacturer's protocol. First strand cDNA synthesis used only the first strand primer random mix (the oligo dT primer mix was omitted), while

4. Materials and Methods

on strand selection II, custom insert-dependent adapter cleavage probes (AnyDeplete) with specificity to highly abundant *A. thaliana* chloroplast and nuclear transcripts (361 probes) and *Pto* DC3000 rRNAs (65 probes; 1 μ L of each 2 μ M probe mixture was used; see (Nobori et al., 2018b) for the probe information) were added to the mixture of custom probes for *A. thaliana* cytoplasmic, chloroplast, and mitochondrial rRNA that are included with the kit.

Libraries were sequenced with the Illumina HiSeq 2500 using HiSeq SBS reagents (version 4) to obtain 50 bp single reads. Base calling was done by the Illumina Real Time Analysis software (RTA version 1.18.64).

4.10 *In planta* bacterial proteomics

4.10.1 Bacterial isolation and protein extraction

Bacterial isolation was done as described in 4.7.2. The TriFast solution was mixed with 0.2 volume of chloroform and the organic (lower) phase was isolated by centrifugation. The organic phase was mixed with 4 volume of MeOH 0.01M Ammonium Acetate and incubated at -20°C overnight to precipitate proteins. The precipitated proteins were washed twice with MeOH 0.01M Ammonium Acetate and then washed once with 80% acetone. Proteins were stored in 80% acetone at -20°C.

4.10.2 Sample preparation and fractionation

Proteins were pelleted and re-dissolved in 8M urea 100mM Tris-HCl pH 8.5, then protein mixtures were reduced with dithiothreitol, alkylated with chloroacetamide, and digested first with Lys-C for 3h and subsequently with trypsin o/n. Samples were submitted to SDB-RPS fractionation using a protocol adapted from Borner and Fielding (Cold Spring Harb. Protoc.; doi:10.1101/pdb.prot084137). In brief, stage tips were prepared with 2 layers of SDB-RPS membrane and activated with 100 μ L acetonitrile, followed by equilibration with 100 μ L equilibration buffer (30% (v/v) MeOH, 1% (v/v) TFA) and 100 μ L 0.2% TFA. Then, peptides were immobilized on the membrane and washed with 100 μ L 0.2% TFA. Peptides were eluted into three consecutive fractions using SDS-RPS buffer 1 (100 mM NH_4HCO_2 , 40% (v/v) ACN, 0.5% FA), SDS-RPS buffer 2 (150 mM NH_4HCO_2 , 80% (v/v) ACN, 0.5%

FA) and finally SDS-RPS buffer 3 (5% Ammonia (v/v), 40% (v/V) ACN). The collected fractions were evaporated to dryness to remove residual ammonia.

4.10.3 LC-MS/MS data acquisition

Dried peptides were re-dissolved in 2% ACN, 0.1% TFA for analysis and adjusted to a final concentration of 0.1 µg/µl. Samples were analysed using an EASY-nLC 1200 (Thermo Fisher) coupled to a Q Exactive Plus mass spectrometer (Thermo Fisher) or using an EASY-nLC 1000 (Thermo Fisher) coupled to a Q Exactive mass spectrometer (Thermo Fisher), respectively. Peptides were separated on 16 cm frit-less silica emitters (New Objective, 0.75 µm inner diameter), packed in-house with reversed-phase ReproSil-Pur C18 AQ 1.9 µm resin (Dr. Maisch). Peptides (0.5 µg) were loaded on the column and eluted for 115 min using a segmented linear gradient of 5% to 95% solvent B (80% ACN, 0.1%FA) (0-5 min: 5%, 5-65 min: 20%, 65-90 min: 35%, 90-100 min: 55%, 100-115 min: 95%) at a flow rate of 300 nL/min. Mass spectra were acquired in data-dependent acquisition mode with a TOP15 method. MS spectra were acquired in the Orbitrap analyzer with a mass range of 300–1750 m/z at a resolution of 70,000 FWHM and a target value of 3×10^6 ions. Precursors were selected with an isolation window of 1.3 m/z (Q Exactive Plus) or 2.0 m/z (Q Exactive). HCD fragmentation was performed at a normalized collision energy of 25. MS/MS spectra were acquired with a target value of 10^5 ions at a resolution of 17,500 FWHM, a maximum injection time (max.) of 55 ms and a fixed first mass of m/z 100. Peptides with a charge of +1, greater than 6, or with unassigned charge state were excluded from fragmentation for MS², dynamic exclusion for 30s prevented repeated selection of precursors.

4.10.4 Protein identification and quantification

Raw data were processed using MaxQuant software (version 1.5.7.4, <http://www.maxquant.org/>) (Cox and Mann, 2008) to calculate iBAQ values (Tyanova et al., 2016). MS/MS spectra were searched by the Andromeda search engine against a combined database containing the amino acid sequences of *Pto* (The Pseudomonas Genome Database) and 248 common contaminant proteins and decoy sequences. Trypsin specificity was required and a maximum of two missed cleavages were accepted. Minimal peptide length was set to seven amino acids. Carbamidomethylation of cysteine residues was set as fixed,

4. Materials and Methods

oxidation of methionine and protein N-terminal acetylation as variable modifications. Peptide-spectrum-matches and proteins were retained if they were below a false discovery rate of 1%.

4.10.5 Statistical analysis

iBAQ values were used for the statistical analysis. Protein groups were omitted from the analysis. iBAQ values were normalized by TMM normalization in the package edgeR (Robinson et al., 2010). For this, normalization factors were calculated with the calcNormFactors function with default settings based on expression of proteins with iBAQ values greater than zero in all the samples. When iBAQ values were zero in more than one replicate out of three replicates, the protein was defined as “not detected” and the iBAQ values of all the replicates were converted to NA. TMM normalized iBAQ values were then \log_2 transformed. To each protein, a linear model was fit by using the function lmFit in the limma package with the following terms: $S_{gptr} = GPT_{gpt} + R_{r+} + \epsilon_{gtr}$, where S is the \log_2 count per million, GPT is the host genotype (or liquid medium): *Pto* strain: time point interaction and the random factors, R is the biological replicate, and ϵ is the residual. The eBayes function in the limma package was used for variance shrinkage in the calculation of the *p*-values, which was then used to calculate the false discovery rate (FDR; the Storey’s *q*-values) using the qvalue function in the qvalue package (Storey and Tibshirani, 2003). To determine proteins with significant expression changes, the cutoff of *q*-value < 0.01 and $|\log_2FC| > 2$ was applied. Hierarchical clustering was done using the dist and hclust functions in the R environment or using the Cluster3.0 software (Hoon et al., 2004). Heatmaps were created with the TreeView (Eisen et al., 1998). Enriched gene ontology terms were identified using BiNGO plugin for cytoscape (Maere et al., 2005a).

4.11 Gene ontology based analyses of transcriptome and proteome data

\log_2 -transformed transcriptome or proteome data were standardized by using *z*-score. The genome of *Pto* was annotated with gene ontology (GO) terms and GO expression data were generated by calculating mean *z*-score for each GO term. For each GO category, *t*-test was performed for all possible pair-wise comparisons of 15 conditions. GO terms with large number of significantly different (adjusted *p*-value < 0.01; the Benjamini-Hochberg

method) pairs were curated avoiding redundancy and mean z-scores were used create heatmaps.

4.12 Software and packages used in this study

Table 2: List of software and packages used in this study

Software/Package	Version	Reference	Purpose
BinGO	3.0.3	Maere et al., 2005	GO enrichment
Corrplot	0.77	Murdoch and Chow, 1996	Correlation plots
Cytoscape	3.3.0	Shannon et al., 2003	Run ClueGO
EdgeR	3.14.0	Robinson et al., 2009	Analysing DEGs
Htseq	0.6.0	Anders et al., 2015	Count RNSeq reads
limma	3.28.14	Ritchie et al., 2015	Analysing DEGs
TopHat	2.1.1	Trapnell et al., 2009	Mapping RNA-seq reads
BlastKOALA		Kanehisa et al., 2016)	KO annotation
MaxQuant	1.5.7.4	Cox and Mann, 2008	Proteome analysis

4.13 Primer information.

Table 3: List of primers used in this study

Name	Sequence (5' – 3')	Purpose
avrPto_qF	ATCAACTTGCGGAGTCTGCT	RT-qPCR
avrPto_qR	CCGCCATATCCAGTGTTCTT	RT-qPCR
cmaA_qF	TACACGCTTTCATCGTGCTC	RT-qPCR

4. Materials and Methods

cmaA_qR	GGCTGTAAGGAACGCTTGTC	RT-qPCR
gapA_qF	GTTTCGACACTGTACACGGC	RT-qPCR
gapA_qR	CACCATTGACGGTCAGGCTT	RT-qPCR
hrpL_qF	TCATCAGGTAGAGGGGCATC	RT-qPCR
hrpL_qR	AGCGACACTTCCAGCACTTT	RT-qPCR
katB_qF	CGTACCAACCTGGACAACGA	RT-qPCR
katB_qR	TTGGACTGAACCTGAGCGAC	RT-qPCR
katG_qF	ATAGCTGGCCTGACAACGTC	RT-qPCR
katG_qR	TTTCGGAACCCCAGTACACG	RT-qPCR
16S_qF	CATTGAGACAGGTGCTGCAT	RT-qPCR
16S_qR	CACCGGCAGTCTCCTTAGAG	RT-qPCR
gyrA_qF	TTCAATGCTGATCCCGGAAGAAGG	RT-qPCR
gyrA_qR	ATTCCTCACCATCCAGCACCTGA	RT-qPCR
pvdS_qF	CCAGAAATCTCGCACATCAA	RT-qPCR
pvdS_qR	GCAGGCGATACATCTCGAAC	RT-qPCR

4. Materials and Methods

ActinII_qF	AGTGTCTGGATCGGTGGTTC	RT-qPCR
ActinII_qR	CCCCAGCTTTTTAAGCCTTT	RT-qPCR
PR1_qF	CGGAGCTACGCAGAACAAC	RT-qPCR
PR1_qR	CTCGCTAACCCACATGTTCA	RT-qPCR
PvdS_F	ACAAGCATAAAGCTTTCAGGCTTCGGCAGTGGT	PvdS overexpression
PvdS_R	ACAGGAAACAGCTAAATGACGGAACACGTAATCAC	PvdS overexpression
pLMB426_F	TTAGCTGTTTCCTGTGTGAA	amplifying pLMB426
pLMB426_R	AAGCTTTATGCTTGTAACCG	amplifying pLMB426
avrPto_qF	ATCAACTTGCGGAGTCTGCT	RT-qPCR
avrPto_qR	CCGCCATATCCAGTGTTCTT	RT-qPCR
cmaA_qF	TACACGCTTTCATCGTGCTC	RT-qPCR
cmaA_qR	GGCTGTAAGGAACGCTTGTC	RT-qPCR
gapA_qF	GTTTCGACACTGTACACGGC	RT-qPCR
gapA_qR	CACCATTGACGGTCAGGCTT	RT-qPCR
hrpL_qF	TCATCAGGTAGAGGGGCATC	RT-qPCR

4. Materials and Methods

hrpL_qR	AGCGACACTTCCAGCACTTT	RT-qPCR
katB_qF	CGTACCAACCTGGACAACGA	RT-qPCR
katB_qR	TTGGACTGAACCTGAGCGAC	RT-qPCR
katG_qF	ATAGCTGGCCTGACAACGTC	RT-qPCR
katG_qR	TTTCGGAACCCCAGTACACG	RT-qPCR
16S_qF	CATTGAGACAGGTGCTGCAT	RT-qPCR
16S_qR	CACCGGCAGTCTCCTTAGAG	RT-qPCR
gyrA_qF	TTCAATGCTGATCCCGGAAGAAGG	RT-qPCR
gyrA_qR	ATTCCTCACCATCCAGCACCTGA	RT-qPCR
pvdS_qF	CCAGAAATCTCGCACATCAA	RT-qPCR
pvdS_qR	GCAGGCGATACATCTCGAAC	RT-qPCR
ActinII_qF	AGTGTCTGGATCGGTGGTTC	RT-qPCR
ActinII_qR	CCCCAGCTTTTTAAGCCTTT	RT-qPCR
PR1_qF	CGGAGCTACGCAGAACAAC	RT-qPCR
PR1_qR	CTCGCTAACCCACATGTTCA	RT-qPCR

PvdS_F	ACAAGCATAAAGCTTTCAGGCTTCGGCAGTGGT	PvdS overexpression
PvdS_R	ACAGGAAACAGCTAAATGACGGAACACGTAATCAC	PvdS overexpression
pLMB426_F	TTAGCTGTTTCCTGTGTGAA	amplifying pLMB426
pLMB426_R	AAGCTTTATGCTTGTAACCG	amplifying pLMB426

4.14 RT-qPCR analysis

RT-qPCR was performed using SuperScript One-Step RT-PCR system kit (Invitrogen). As inputs, 3 ng and 300 ng of DNase-treated RNA extracted from infected leaves was used for analyzing plant and bacterial genes, respectively.

Table 4: qRT-PCR master mix

Compound	Volume
10x PCR buffer	2.5 μ l
10 mM dNTPs	0.5 μ l
EvaGreen DNA Dye	1.25 μ l
2.5 μ M primer forward	2 μ l
2.5 μ M primer reverse	2 μ l
Hommade Taq polymerase	0.5 μ l

4. Materials and Methods

4.15 Generation of mutant *Pto* strains

For overexpressing *pvdS*, the *pvdS* coding sequence was amplified from *Pto* genomic DNA by PCR with the primers *pvdS_F* and *pvdS_R*. The amplified fragment was linked with the DNA amplified from pLMB426 plasmid (Rott, 2012) with the primers *pLMB426_F* and *pLMB426_R*, using in-fusion cloning kit (Clontech) to make the circular plasmid. The resulted plasmid was transformed into *Pto* AvrRpt2 by a triparental mating using the helper strain carrying pRK600 and selected with 40 $\mu\text{g ml}^{-1}$ rifampicin, 10 $\mu\text{g ml}^{-1}$ tetracycline, and 50 $\mu\text{g ml}^{-1}$ gentamycin. *Pto* strains overexpressing selected putative transcriptional regulators or predicted target genes were generated by triparental mating of *Pto*, *E. coli* carrying pRK2013, and *E. coli* carrying the plasmid pCPP5040 conjugated with a desired gene and selected with 50 $\mu\text{g/ml}$ rifampicin, 5 $\mu\text{g/ml}$ gentamycin and 35 $\mu\text{g/ml}$ chloramphenicol.

4.16 Bacterial growth assay

Bacterial growth assays were performed as described previously (Tsuda et al., 2009). For Fe co-infiltration study, Na-citrate or Fe-citrate (Sigma) was dissolved in a bacterial suspension at the desired concentration before syringe infiltration.

4.17 Apoplastic and intracellular fluids extraction and iron measurement

Extraction of apoplastic and intracellular fluid was performed following a previous publication with slight modifications (Sasaki et al., 2011). Leaves from four-week-old plants were washed and vacuum infiltrated with cold water twice for 2 min. Apoplastic fluids were collected by centrifugation at 3,000g for 5 min in 50 mL tubes. The leaves were then frozen at -80°C overnight, and thawed at room temperature for 20 min. Intracellular fluids were collected by centrifugation at 12,000g for 10 min from the frozen leaves. For iron measurement, HNO_3 and H_2O_2 were added to the apoplastic and intracellular fluids for final concentrations of 1% (v/v), followed by boiling at 95°C for 10 min. The precipitate was removed by centrifugation at 12,000g for 5 min. The remaining solutions were filtered through 5 μm filters (Millex-SV syringe filter unit; Millipore), followed by measurement with ICP-MS. The concentration of the different elements was determined using an Agilent 7700

4. Materials and Methods

inductively coupled plasma mass spectrometer (ICP-MS) (Agilent Technologies, Waldbronn, Germany) by strictly following the manufacturer's instructions.

5. References

5 References

- Alcázar R, Parker JE. 2011. The impact of temperature on balancing immune responsiveness and growth in *Arabidopsis*. *Trends Plant Sci* **16**:666–75. doi:10.1016/j.tplants.2011.09.001
- Alcázar R, Reymond M, Schmitz G, de Meaux J. 2011. Genetic and evolutionary perspectives on the interplay between plant immunity and development. *Curr Opin Plant Biol* **14**:378–84. doi:10.1016/j.pbi.2011.04.001
- Alonso JM, Hirayama T, Roman G, Nourizadeh S, Ecker JR. 1999. EIN2 , a Bifunctional Transducer of Ethylene and Stress Responses in *Arabidopsis*. *Science* **284**:2148–2153.
- Anders S, Pyl PT, Huber W. 2015. HTSeq-A Python framework to work with high-throughput sequencing data. *Bioinformatics* **31**:166–169. doi:10.1093/bioinformatics/btu638
- Anders S, Pyl PT, Huber W. 2014. HTSeq A Python framework to work with high-throughput sequencing data. *Bioinformatics* **31**:166–169. doi:10.1101/002824
- Anderson JC, Wan Y, Kim YM, Pasa-Tolic L, Metz TO, Peck SC. 2014. Decreased abundance of type III secretion system-inducing signals in *Arabidopsis* *mkp1* enhances resistance against *Pseudomonas syringae*. *Proc Natl Acad Sci USA* **111**:6846–6851. doi:10.1073/pnas.1403248111
- Andolfo G, Jupe F, Witek K, Etherington GJ, Ercolano MR, Jones JDG. 2014. Defining the full tomato NB-LRR resistance gene repertoire using genomic and cDNA RenSeq. *BMC Plant Biol* **14**:120. doi:10.1186/1471-2229-14-120
- Aragón IM, Pérez-Martínez I, Moreno-Pérez A, Cerezo M, Ramos C. 2014. New insights into the role of indole-3-acetic acid in the virulence of *Pseudomonas savastanoi* pv. *savastanoi*. *FEMS Microbiol Lett* **356**:184–192. doi:10.1111/1574-6968.12413
- Aslam SN, Newman MA, Erbs G, Morrissey KL, Chinchilla D, Boller T, Jensen TT, De Castro C, Ierano T, Molinaro A, Jackson RW, Knight MR, Cooper RM. 2008. Bacterial Polysaccharides Suppress Induced Innate Immunity by Calcium Chelation. *Curr Biol* **18**:1078–1083. doi:10.1016/j.cub.2008.06.061
- Avraham R, Haseley N, Brown D, Penaranda C, Jijon HB, Trombetta JJ, Satija R, Shalek AK,

- Xavier RJ, Regev A, Hung DT. 2015. Pathogen Cell-to-Cell Variability Drives Heterogeneity in Host Immune Responses. *Cell* **162**:1309–1321. doi:10.1016/j.cell.2015.08.027
- Aznar a., Dellagi A. 2015. New insights into the role of siderophores as triggers of plant immunity: what can we learn from animals? *J Exp Bot* **66**:3001–3010. doi:10.1093/jxb/erv155
- Bai Y, Kissoudis C, Yan Z, Visser RGF, van der Linden G. 2018. Plant behaviour under combined stress: tomato responses to combined salinity and pathogen stress. *Plant J* **93**:781–793. doi:10.1111/tpj.13800
- Bai Y, Müller DB, Srinivas G, Garrido-Oter R, Potthoff E, Rott M, Dombrowski N, Münch PC, Spaepen S, Remus-Emsermann M, Hüttel B, McHardy AC, Vorholt JA, Schulze-Lefert P. 2015. Functional overlap of the Arabidopsis leaf and root microbiota. *Nature* **1–19**. doi:10.1038/nature16192
- Bakker PAHM, Ran LX, Mercado-Blanco J. 2014. Rhizobacterial salicylate production provokes headaches! *Plant Soil* **382**:1–16. doi:10.1007/s11104-014-2102-0
- Beck M, Wyrsh I, Strutt J, Wimalasekera R, Webb A, Boller T, Robatzek S. 2014. Expression patterns of FLAGELLIN SENSING 2 map to bacterial entry sites in plant shoots and roots. *J Exp Bot* **65**:6487–6498. doi:10.1093/jxb/eru366
- Belkhadir Y, Yang L, Hetzel J, Dangl JL, Chory J. 2014. The growth – defense pivot : crisis management in plants mediated by LRR-RK surface receptors. *Trends Biochem Sci* **39**:447–456. doi:10.1016/j.tibs.2014.06.006
- Bender CL, Alarcón-Chaidez F, Gross DC. 1999. Pseudomonas syringae Phytotoxins : Mode of Action , Regulation , and Biosynthesis by Pseudomonas syringae Phytotoxins : Mode of Action , Regulation , and Biosynthesis by Peptide and Polyketide Synthetases. *Microbiol Mol Biol Rev* **63**:266.
- Bent, A.F. , Kunkel, B.N., Dahibeck D., Brown, K.L., Schmidt, R., Giraudat J., Leung, J., Staskawicz BJ. 1994. RPS2 of Arabidopsis thaliana a leucine-rich repeat class of plant disease resistance genes. *Science* **265**:1856–1860.
- Berens ML, Berry HM, Mine A, Argueso CT, Tsuda K. 2017. Evolution of Hormone Signaling Networks in Plant Defense. *Annu Rev Phytopathol* **55**:401–425.

5. References

- Berens ML, Wolinska KW, Spaepen S, Ziegler J, Nobori T, Nair A, Krüler V, Winkelmüller TM, Wang Y, Mine A, Becker D, Garido-Oter R, Schulze-Lefert P, Tsud K. n.d. Balancing stress trade-offs by leaf age-dependent response prioritization. *Proc Natl Acad Sci USA*.
- Betsuyaku S, Katou S, Takebayashi Y, Sakakibara H, Nomura N, Fukuda H. 2018. Salicylic Acid and Jasmonic Acid Pathways are Activated in Spatially Different Domains around the Infection Site during Effector-Triggered Immunity in *Arabidopsis thaliana*. *Plant Cell Physiol* pcx181-pcx181. doi:10.1093/pcp/pcx181
- Bonardi V, Tang S, Stallmann A, Roberts M, Cherkis K, Dangl JL. 2011. Expanded functions for a family of plant intracellular immune receptors beyond specific recognition of pathogen effectors. *Proc Natl Acad Sci USA* **108**:16463–8. doi:10.1073/pnas.1113726108
- Boutrot F, Zipfel C. 2017. Function , Discovery , and Exploitation of Plant Pattern Recognition Receptors for Broad-Spectrum Disease Resistance. *Annu Rev Phytopathol* **55**:1–30.
- Bronstein P a, Filiatrault MJ, Myers CR, Rutzke M, Schneider DJ, Cartinhour SW. 2008. Global transcriptional responses of *Pseudomonas syringae* DC3000 to changes in iron bioavailability in vitro. *BMC Microbiol* **8**:209. doi:10.1186/1471-2180-8-209
- Brooks DM, Hernández-Guzmán G, Kloek AP, Alarcón-Chaidez F, Sreedharan A, Rangaswamy V, Peñaloza-Vázquez A, Bender CL, Kunkel BN. 2004. Identification and characterization of a well-defined series of coronatine biosynthetic mutants of *Pseudomonas syringae* pv. tomato DC3000. *Mol Plant Microbe Interactoins* **17**:162–174. doi:10.1094/MPMI.2004.17.2.162
- Bulgarelli D, Schlaeppli K, Spaepen S, Ver Loren van Themaat E, Schulze-Lefert P. 2013. Structure and functions of the bacterial microbiota of plants. *Annu Rev Plant Biol* **64**:807–38. doi:10.1146/annurev-arplant-050312-120106
- Butcher BG, Bronstein PA, Myers CR, Stodghill P V., Bolton JJ, Markel EJ, Filiatrault MJ, Swingle B, Gaballa A, Helmann JD, Schneider DJ, Cartinhour SW. 2011. Characterization of the Fur regulon in *Pseudomonas syringae* pv. tomato DC3000. *J Bacteriol* **193**:4598–4611. doi:10.1128/JB.00340-11
- Büttner D, He S-Y. 2009. Type III Protein Secretion in Plant Pathogenic Bacteria. *Plant*

- Physiol* **150**:1656–1664. doi:10.1104/pp.109.139089
- Campos ML, Yoshida Y, Major IT, Ferreira D de O, Weraduwege SM, Froehlich JE, Johnson BF, Kramer DM, Jander G, Sharkey TD, Howe GA. 2016. Rewiring of jasmonate and phytochrome B signalling uncouples plant growth-defense tradeoffs. *Nat Commun* **129**:11–12.
- Cao H, Glazebrook J, Clarke JD, Volko S, Dong X. 1997. The Arabidopsis NPR1 gene that controls systemic acquired resistance encodes a novel protein containing ankyrin repeats. *Cell* **88**:57–63.
- Cao Y, Halane MK, Gassmann W, Stacey G. 2017. The Role of Plant Innate Immunity in the Legume-Rhizobium Symbiosis. *Annu Rev Plant Biol* **68**:535–561. doi:10.1146/annurev-arplant-042916-041030
- Carviel JL, Wilson DC, Isaacs M, Carella P, Catana V, Golding B, Weretilnyk E a, Cameron RK. 2014. Investigation of intercellular salicylic acid accumulation during compatible and incompatible arabidopsis-pseudomonas syringae interactions using a fast neutron-generated mutant allele of EDS5 identified by genetic mapping and whole-genome sequencing. *PLoS One* **9**:e88608. doi:10.1371/journal.pone.0088608
- Castel B, Ngou P, Cevik V, Jones A, Kim RD, Yang Y, Ding P, D.G J. 2018. Diverse NLR immune receptors activate defence via the RPW8-NLR NRG1. *New Phytol.* doi:10.1111/nph.15659
- Castillo-Lizardo MG, Aragón IM, Carvajal V, Matas IM, Pérez-Bueno ML, Gallegos M-T, Barón M, Ramos C. 2015. Contribution of the non-effector members of the HrpL regulon, *iaaL* and *matE*, to the virulence of *Pseudomonas syringae* pv. *tomato* DC3000 in tomato plants. *BMC Microbiol* **15**:165. doi:10.1186/s12866-015-0503-8
- Castrillo G, Teixeira PJPL, Herrera Paerdes S, Law TF, de Lorenzo L, Feltcher ME, Finkel OM, Breakfield N, Mieczkowski P, Jones CD, Paz-Ares J, Dangl JL. 2017. Direct integration of phosphate starvation and immunity in response to a root microbiome. *Nature* **543**:513–518. doi:10.1038/nature21417
- Cha JY, Lee JS, Oh J Il, Choi JW, Baik HS. 2008. Functional analysis of the role of Fur in the virulence of *Pseudomonas syringae* pv. *tabaci* 11528: Fur controls expression of genes involved in quorum-sensing. *Biochem Biophys Res Commun* **366**:281–287.

5. References

doi:10.1016/j.bbrc.2007.11.021

- Chandrangsu P, Rensing C, Helmann JD. 2017. Metal homeostasis and resistance in bacteria. *Nat Rev Microbiol* **15**:338–350.
- Chapelle E, Alunni B, Malfatti P, Solier L, Pédrón J, Kraepiel Y, Van Gijsegem F. 2015. A straightforward and reliable method for bacterial in planta transcriptomics: application to the *Dickeya dadantii*/ *Arabidopsis thaliana* pathosystem. *Plant J* **82**(2):352–362.
- Chatnaparat T, Prathuangwong S, Lindow SE. 2016. Global Pattern of Gene Expression of *Xanthomonas axonopodis* pv. *glycines* Within Soybean Leaves. *Mol Plant-Microbe Interact* **29**:508–522. doi:10.1094/MPMI-01-16-0007-R
- Chen H, Xue L, Chintamanani S, Germain H, Lin H, Cui H, Cai R, Zuo J, Tang X, Li X, Guo H, Zhou J-M. 2009. ETHYLENE INSENSITIVE3 and ETHYLENE INSENSITIVE3-LIKE1 repress SALICYLIC ACID INDUCTION DEFICIENT2 expression to negatively regulate plant innate immunity in *Arabidopsis*. *Plant Cell* **21**:2527–2540. doi:10.1105/tpc.108.065193
- Chen Z, Agnew JL, Cohen JD, He P, Shan L, Sheen J, Kunkel BN. 2007. *Pseudomonas syringae* type III effector AvrRpt2 alters *Arabidopsis thaliana* auxin physiology. *Proc Natl Acad Sci USA* **104**:20131–20136. doi:10.1073/pnas.0704901104
- Choo JH, Rukayadi Y, Hwang J. 2006. Inhibition of bacterial quorum sensing by vanilla extract. *Lett Appl Microbiol* **42**:637–641. doi:10.1111/j.1472-765X.2006.01928.x
- Cole BJ, Feltcher ME, Waters RJ, Wetmore KM, Mucyn TS, Ryan EM, Wang G, Ul-Hasan S, McDonald M, Yoshikuni Y, Malmstrom RR, Deutschbauer AM, Dangl JL, Visel A. 2017. Genome-wide identification of bacterial plant colonization genes. *PLOS Biol* **15**:e2002860. doi:10.1371/journal.pbio.2002860
- Collier SM, Hamel L, Moffett P. 2011. Cell Death Mediated by the N-Terminal Domains of a Unique and Highly Conserved Class of NB-LRR Protein. *Mol Plant Microbe Interact* **24**:918–931.
- Collmer A, Badel JL, Charkowski AO, Deng W-L, Fouts DE, Ramos AR, Rehm AH, Anderson DM, Schneewind O, Dijk K van, Alfano JR. 2000. *Pseudomonas syringae* Hrp type III secretion system and effector proteins. *Proc Natl Acad Sci USA* **97**:8770–8777. doi:97/16/8770 [pii]

- Corral-Lugo A, Daddaoua A, Ortega A, Espinosa-Urgel M, Krell T. 2016. Rosmarinic acid is a homoserine lactone mimic produced by plants that activates a bacterial quorum-sensing regulator. *Sci Signal* **9**:ra1. doi:10.1126/scisignal.aaa8271
- Cox J, Mann M. 2008. MaxQuant enables high peptide identification rates, individualized p.p.b.-range mass accuracies and proteome-wide protein quantification. *Nat Biotechnol* **26**:1367–1372. doi:10.1038/nbt.1511
- Crabill E, Joe A, Block A, van Rooyen JM, Alfano JR. 2010a. Plant Immunity Directly or Indirectly Restricts the Injection of Type III Effectors by the *Pseudomonas syringae* Type III Secretion System. *Plant Physiol* **154**:233–244. doi:10.1104/pp.110.159723
- Crabill E, Joe A, Block A, van Rooyen JM, Alfano JR. 2010b. Plant immunity directly or indirectly restricts the injection of type III effectors by the *Pseudomonas syringae* type III secretion system. *Plant Physiol* **154**:233–244. doi:10.1104/pp.110.159723
- Cui H, Tsuda K, Parker JE. 2014. Effector-Triggered Immunity: From Pathogen Perception to Robust Defense. *Annu Rev Plant Biol* **66**:487–511.
- de Torres-Zabala M, Truman W, Bennett MH, Lafforgue G, Mansfield JW, Rodriguez Egea P, Bögre L, Grant M. 2007. *Pseudomonas syringae* pv. tomato hijacks the Arabidopsis abscisic acid signalling pathway to cause disease. *EMBO J* **26**:1434–1443. doi:10.1038/sj.emboj.7601575
- Degrassi G, Devescovi G, Solis R, Steindler L, Venturi V. 2007. *Oryza sativa* rice plants contain molecules that activate different quorum-sensing N-acyl homoserine lactone biosensors and are sensitive to the specific AiiA lactonase. *FEMS Microbiol Lett* **269**:213–220. doi:10.1111/j.1574-6968.2006.00624.x
- Doares SH, Narvaez-Vasquez J, Conconi A, Ryan CA. 1995. Salicylic Acid Inhibits Synthesis of Proteinase Inhibitors in Tomato Leaves Induced by Systemin and Jasmonic Acid. *Plant Physiol* **108**:1741–1746. doi:10.1104/pp.108.4.1741
- Dulla GFJ, Krasileva K V., Lindow SE. 2010. Interference of quorum sensing in *Pseudomonas syringae* by bacterial epiphytes that limit iron availability. *Environ Microbiol* **12**:1762–1774. doi:10.1111/j.1462-2920.2010.02261.x
- Duran P, Thiergart T, Garrido-Oter R, Agler M, Kemen E, Schulze-Lefert P, Hacquard S. 2018. Microbial interkingdom interactions in roots promote Arabidopsis survival. *Cell*

5. References

354167. doi:10.1101/354167
- Efroni I, Birnbaum KD. 2016. The potential of single-cell profiling in plants. *Genome Biol* **17**:65. doi:10.1186/s13059-016-0931-2
- Eisen MB, Spellman PT, Brown PO, Botstein D. 1998. Cluster analysis and display of genome-wide expression patterns. *Proc Natl Acad Sci USA* **95**:12930–12933.
- Evans SS, Repasky EA, Fisher DT. 2015. Fever and the thermal regulation of immunity: the immune system feels the heat. *Nat Rev Immunol* **15**:335–349. doi:10.1038/nri3843
- Fahad S, Hussain S, Bano A, Saud S, Hassan S, Shan D, Khan FA, Khan F, Chen Y, Wu C, Tabassum MA, Chun MX, Afzal M, Jan A, Jan MT, Huang J. 2015. Potential role of phytohormones and plant growth-promoting rhizobacteria in abiotic stresses: consequences for changing environment. *Environ Sci Pollut Res* **22**:4907–4921. doi:10.1007/s11356-014-3754-2
- Farley RA, Fitter AH. 1999. Temporal and spatial variation in soil resources in a deciduous woodland. *J Ecol* **87**:688–696. doi:10.1046/j.1365-2745.1999.00390.x
- Ferluga S, Bigirimana J, Höfte M, Venturi V. 2007. A LuxR homologue of *Xanthomonas oryzae* pv. *oryzae* is required for optimal rice virulence. *Mol Plant Pathol* **8**:529–538. doi:10.1111/j.1364-3703.2007.00415.x
- Ferluga S, Venturi V. 2009. OryR is a LuxR-family protein involved in interkingdom signaling between pathogenic *Xanthomonas oryzae* pv. *oryzae* and Rice. *J Bacteriol* **191**:890–897. doi:10.1128/JB.01507-08
- Fones H, Preston GM. 2013. The impact of transition metals on bacterial plant disease. *FEMS Microbiol Rev* **37**:495–519.
- Foss EJ, Radulovic D, Shaffer SA, Ruderfer DM, Bedalov A, Goodlett DR, Kruglyak L. 2007. Genetic basis of proteome variation in yeast. *Nat Genet* **39**:1369–1375. doi:10.1038/ng.2007.22
- Fouts DE, Abramovitch RB, Alfano JR, Baldo AM, Buell CR, Cartinhour S, Chatterjee AK, Ascenzo MD, Gwinn ML, Lazarowitz SG, Lin N, Martin GB, Rehm AH, Schneider DJ, Dijk K Van, Tang X, Collmer A. 2002. Genomewide identification of *Pseudomonas syringae* pv. *tomato* DC3000 promoters controlled by the HrpL alternative sigma factor.

- Proc Natl Acad Sci USA* **99**:2275–2280.
- Gao M, Teplitski M, Robinson JB, Bauer WD. 2003. Production of Substances by *Medicago truncatula* that Affect Bacterial Quorum Sensing. *Mol Plant-Microbe Interact* **16**:827–834. doi:10.1094/MPMI.2003.16.9.827
- Garrido-Oter R, Nakano RT, Dombrowski N, Ma KW, McHardy AC, Schulze-Lefert P. 2018. Modular Traits of the Rhizobiales Root Microbiota and Their Evolutionary Relationship with Symbiotic Rhizobia. *Cell Host Microbe* **24**:155–167.e5. doi:10.1016/j.chom.2018.06.006
- Gassmann W, Hinsch ME, Staskawicz BJ. 1999. The Arabidopsis RPS4 bacterial-resistance gene is a member of the TIR-NBS-LRR family of disease-resistance genes. *Plant J* **20**:265–277. doi:10.1046/j.1365-313X.1999.00600.x
- Ghazalpour A, Bennett B, Petyuk VA, Orozco L, Hagopian R, Mungrue IN, Farber CR, Sinsheimer J, Kang HM, Furlotte N, Park CC, Wen PZ, Brewer H, Weitz K, Camp DG, Pan C, Yordanova R, Neuhaus I, Tilford C, Siemers N, Gargalovic P, Eskin E, Kirchgessner T, Smith DJ, Smith RD, Lulis AJ. 2011. Comparative analysis of proteome and transcriptome variation in mouse. *PLoS Genet* **7**. doi:10.1371/journal.pgen.1001393
- Gimenez-Ibanez S, Boter M, Fernández-Barbero G, Chini A, Rathjen JP, Solano R. 2014. The bacterial effector HopX1 targets JAZ transcriptional repressors to activate jasmonate signaling and promote infection in Arabidopsis. *PLoS Biol* **12**:e1001792. doi:10.1371/journal.pbio.1001792
- Gimenez-Ibanez S, Ntoukakis V, Rathjen JP. 2009. The LysM receptor kinase CERK1 mediates bacterial perception in Arabidopsis. *Plant Signal Behav* **4**:539–41. doi:10.1016/j.cub.2009.01.054
- Glazebrook J. 2005. Contrasting mechanisms of defense against biotrophic and necrotrophic pathogens. *Annu Rev Phytopathol* **43**:205–27. doi:10.1146/annurev.phyto.43.040204.135923
- Gnonlonfin GJB, Sanni A, Brimer L. 2012. Review Scopoletin - A Coumarin Phytoalexin with Medicinal Properties. *CRC Crit Rev Plant Sci* **31**:47–56. doi:10.1080/07352689.2011.616039
- Göhre V, Spallek T, Häweker H, Mersmann S, Mentzel T, Boller T, de Torres M, Mansfield

5. References

- JW, Robatzek S. 2008. Plant pattern-recognition receptor FLS2 is directed for degradation by the bacterial ubiquitin ligase AvrPtoB. *Curr Biol* **18**:1824–32. doi:10.1016/j.cub.2008.10.063
- Goldmann O, Beineke A, Medina E. 2017. Host-inherent variability influences the aureus during in vivo infection. *Nat Commun* **8**:14268. doi:10.1038/ncomms14268
- González JF, Myers MP, Venturi V. 2013. The inter-kingdom solo OryR regulator of *Xanthomonas oryzae* is important for motility. *Mol Plant Pathol* **14**:211–221. doi:10.1111/j.1364-3703.2012.00843.x
- González JF, Venturi V. 2013. A novel widespread interkingdom signaling circuit. *Trends Plant Sci* **18**:167–174. doi:10.1016/j.tplants.2012.09.007
- Gygi SP, Rochon Y, Franza BR, Aebersold R. 1999. Correlation between Protein and mRNA Abundance in Yeast. *Mol Cell Biol* **19**:1720–1730.
- Hacquard S, Garrido-Oter R, González A, Spaepen S, Ackermann G, Lebeis S, McHardy AC, Dangl JL, Knight R, Ley R, Schulze-Lefert P. 2015. Microbiota and Host Nutrition across Plant and Animal Kingdoms. *Cell Host Microbe* **17**:603–616. doi:10.1016/j.chom.2015.04.009
- Hacquard S, Spaepen S, Garrido-oter R, Schulze-lefert P. 2017. Interplay Between Innate Immunity and the Plant Microbiota. *Annu Rev Phytopathol* **55**:565–589.
- Hatsugai N, Igarashi D, Mase K, Lu Y, Tsuda Y, Chakravarthy S, Wei H, Foley JW, Collmer A, Glazebrook J, Katagiri F. 2017. A plant effector-triggered immunity signaling sector is inhibited by pattern-triggered immunity. *EMBO J* **36**:2758–2769. doi:10.15252/embj.201796529
- Hauck P, Thilmony R, He SY. 2003. A *Pseudomonas syringae* type III effector suppresses cell wall-based extracellular defense in susceptible *Arabidopsis* plants. *Proc Natl Acad Sci USA* **100**:8577–8582. doi:10.1073/pnas.1431173100
- Heil M, Baldwin IT. 2002. Fitness costs of induced resistance: Emerging experimental support for a slippery concept. *Trends Plant Sci* **7**:61–67. doi:10.1016/S1360-1385(01)02186-0
- Helfrich EJN, Vogel CM, Ueoka R, Schäfer M, Ryffel F, Müller DB, Probst S, Kreuzer M, Piel J, Vorholt JA. 2018. Bipartite interactions, antibiotic production and biosynthetic

- potential of the Arabidopsis leaf microbiome. *Nat Microbiol*. doi:10.1038/s41564-018-0200-0
- Henke J, Bassler B. 2004. Quorum sensing regulates type III secretion in *Vibrio harveyi* and *Vibrio parahaemolyticus*. *J Bacteriol* **186**:3794–3805. doi:10.1128/JB.186.12.3794
- Hilleary R, Choi W-G, Kim S-H, Lim SD, Gilroy S. 2018. Sense and sensibility: the use of fluorescent protein-based genetically encoded biosensors in plants. *Curr Opin Plant Biol* **46**:32–38. doi:10.1016/j.pbi.2018.07.004
- Hillmer RA, Tsuda K, Rallapalli G, Asai S, Truman W, Papke MD, Sakakibara H, Jones JDG, Myers CL, Katagiri F. 2017. The highly buffered Arabidopsis immune signaling network conceals the functions of its components. *PLoS Genet* **13**:e1006639.
- Hoon MJL De, Imoto S, Nolan J, Miyano S. 2004. Open source clustering software. *Bioinformatics* **20**:1453–1454. doi:10.1093/bioinformatics/bth078
- Huot B, Castroverde CDM, Velásquez A, Hubbard E, Pulman JA, Yoshida Y, Yao J, Howe GA, Childs KL, Tsuda K, Montgomery BL, He SY. 2017. Dual impact of elevated temperature on plant defence and bacterial virulence in Arabidopsis. *Nat Commun* **8**:1808. doi:10.1038/s41467-017-01674-2
- Huot B, Yao J, Montgomery BL, He SY. 2014. Growth-Defense Tradeoffs in Plants: A Balancing Act to Optimize Fitness. *Mol Plant* **7**:1267–1287. doi:10.1093/mp/ssu049
- Huynh T V, Dahlbeck D, Staskawicz BJ. 1989. Bacterial blight of soybean: regulation of a pathogen gene determining host cultivar specificity. *Science* **29**:1374–1377. doi:10.1126/science.2781284
- Jackson RB, Caldwell MM. 1993. The Scale of Nutrient Heterogeneity Around Individual Plants and Its Quantification with Geostatistics. *Ecology* **74**(2):612–614.
- Jiang S, Yao J, Ma K-W, Zhou H, Song J, He SY, Ma W. 2013. Bacterial effector activates jasmonate signaling by directly targeting JAZ transcriptional repressors. *PLoS Pathog* **9**:e1003715. doi:10.1371/journal.ppat.1003715
- Jirage D, Tootle TL, Reuber TL, Frost LN, Feys BJ, Parker JE, Ausubel FM, Glazebrook J. 1999. Arabidopsis thaliana PAD4 encodes a lipase-like gene that is important for salicylic acid signaling. *Proc Natl Acad Sci USA* **96**(23):13583–13588.

5. References

- Jones AM, Lindow SE, Wildermuth MC. 2007. Salicylic acid, yersiniabactin, and pyoverdinin production by the model phytopathogen *Pseudomonas syringae* pv. tomato DC3000: Synthesis, regulation, and impact on tomato and Arabidopsis host plants. *J Bacteriol* **189**:6773–6786. doi:10.1128/JB.00827-07
- Jones AM, Wildermuth MC. 2011. The phytopathogen *Pseudomonas syringae* pv. tomato DC3000 has three high-affinity iron-scavenging systems functional under iron limitation conditions but dispensable for pathogenesis. *J Bacteriol* **193**:2767–2775. doi:10.1128/JB.00069-10
- Kanehisa M, Sato Y, Morishima K. 2016. BlastKOALA and GhostKOALA: KEGG Tools for Functional Characterization of Genome and Metagenome Sequences. *J Mol Biol* **428**:726–731. doi:10.1016/j.jmb.2015.11.006
- Karasov TL, Chae E, Herman JJ, Bergelson J. 2017. Mechanisms to Mitigate the Tradeoff between Growth and Defense. *Plant Cell* **29**:666–680. doi:10.1105/tpc.16.00931
- Katagiri F. 2018. Review: Plant immune signaling from a network perspective. *Plant Sci* **276**:14–21. doi:10.1016/j.plantsci.2018.07.013
- Kazan K, Lyons R. 2014. Intervention of Phytohormone Pathways by Pathogen Effectors. *Plant Cell* **26**:2285–2309. doi:10.1105/tpc.114.125419
- Keshavan ND, Chowdhary PK, Donovan C, González JE. 2005. l-Canavanine Made by *Medicago sativa* Interferes with Quorum Sensing in *Sinorhizobium meliloti* L - Canavanine Made by *Medicago sativa* Interferes with Quorum Sensing in *Sinorhizobium meliloti*. *J Bacteriol* **187**:8427–8436. doi:10.1128/JB.187.24.8427
- Kim D, Perteza G, Trapnell C, Pimentel H, Kelley R, Salzberg SL. 2013. TopHat2: accurate alignment of transcriptomes in the presence of insertions, deletions and gene fusions. *Genome Biol* **14**:14–36.
- Kim Y, Tsuda K, Igarashi D, Hillmer R a, Sakakibara H, Myers CL, Katagiri F. 2014. Mechanisms underlying robustness and tunability in a plant immune signaling network. *Cell Host Microbe* **15**:84–94. doi:10.1016/j.chom.2013.12.002
- Kim YJ, Lin N, Martin GB. 2002. Interact with the Pto Kinase and Activate Plant Immunity. *Cell* **109**:589–598.

- Kourelis J, Van Der Hoorn RAL. 2018. Defended to the Nines: 25 years of Resistance Gene Cloning Identifies Nine Mechanisms for R Protein Function. *Plant Cell*. doi:10.1105/tpc.17.00579
- Kunkel BN, Harper CP. 2017. The roles of auxin during interactions between bacterial plant pathogens and their hosts. *J Exp Bot* **69**:245–254. doi:10.1093/jxb/erx447
- Kvitko BH, Ramos AR, Morello JE, Oh HS, Collmer A. 2007. Identification of harpins in *Pseudomonas syringae* pv. tomato DC3000, which are functionally similar to HrpK1 in promoting translocation of type III secretion system effectors. *J Bacteriol* **189**:8059–8072. doi:10.1128/JB.01146-07
- Kwak M-J, Kong HG, Choi K, Kwon S-K, Song JY, Lee J, Lee PA, Choi SY, Seo M, Lee HJ, Jung EJ, Park H, Roy N, Kim H, Lee MM, Rubin EM, Lee S-W, Kim JF. 2018. Rhizosphere microbiome structure alters to enable wilt resistance in tomato. *Nat Biotechnol* **36**(11):1100. doi:10.1038/nbt.4232
- La M Van, Raoult D, Renesto P. 2008. Regulation of whole bacterial pathogen transcription within infected hosts. *FEMS Microbiol Rev* **32**:440–460. doi:10.1111/j.1574-6976.2008.00103.x
- Lan P, Li W, Schmidt W. 2012. Complementary Proteome and Transcriptome Profiling in Phosphate-deficient Arabidopsis Roots Reveals Multiple Levels of Gene Regulation. *Mol Cell Proteomics* **11**:1156–1166. doi:10.1074/mcp.M112.020461
- Langmead B, Salzberg SL. 2012. Fast gapped-read alignment with Bowtie 2. *Nat Methods* **9**:357–360. doi:10.1038/nmeth.1923
- Lark RM, Milne AE, Addiscott TM, Goulding KWT, Webster CP, O’Flaherty S. 2004. Scale- and location-dependent correlation of nitrous oxide emissions with soil properties: An analysis using wavelets. *Eur J Soil Sci* **55**:611–627. doi:10.1111/j.1365-2389.2004.00620.x
- Leach JE, Triplett LR, Argueso CT, Trivedi P. 2017. Communication in the Phytobiome. *Cell* **169**:587–596. doi:10.1016/j.cell.2017.04.025
- Lebeis SL, Paredes SH, Lundberg DS, Breakfield N, Gehring J, McDonald M, Malfatti S, Glavina del Rio T, Jones CD, Tringe SG, Dangl JL. 2015. Salicylic acid modulates colonization of the root microbiome by specific bacterial taxa. *Science* **349**:860–864. doi:10.1126/science.aaa8764

5. References

- Levy A, Conway JM, Dangl JL, Woyke T. 2018. Elucidating Bacterial Gene Functions in the Plant Microbiome. *Cell Host Microbe* **24**:475–485. doi:10.1016/j.chom.2018.09.005
- Levy A, Gonzalez IS, Mittelviefhaus M, Clingenpeel S, Paredes SH, Miao J, Wang K, Devescovi G, Lebeis S, Jin Z, McDonald M, Klein AP, Meghan E. 2017. Genomic features of bacterial adaptation to plants. *Nat Genet* **50**:138–150. doi:10.1038/s41588-017-0012-9
- Levy M, Kolodziejczyk AA, Thaiss CA, Elinav E. 2017. Dysbiosis and the immune system. *Nat Rev Immunol* **17**:219–232. doi:10.1038/nri.2017.7
- Li L, Kim P, Yu L, Cai G, Chen S, Alfano JR, Zhou J-M. 2016. Activation-Dependent Destruction of a Co-receptor by a *Pseudomonas syringae* Effector Dampens Plant Immunity. *Cell Host Microbe* **20**:504–514. doi:10.1016/j.chom.2016.09.007
- Lindeberg M, Cunnac S, Collmer A. 2009. The evolution of *Pseudomonas syringae* host specificity and type III effector repertoires. *Mol Plant Pathol* **10**:767–775. doi:10.1111/j.1364-3703.2009.00587.x
- Ling T, Bellin D, Vandelle E, Imanifard Z, Delledonne M. 2017. Host-Mediated S - Nitrosylation Disarms the Bacterial Effector HopAI1 to Reestablish Immunity. *Plant cellHost target Modif as a Strateg to Count Pathog hijacking jasmonate Horm Recept* **29**:2871–2881. doi:10.1105/tpc.16.00557
- Liu H, Coulthurst SJ, Pritchard L, Hedley PE, Ravensdale M, Humphris S, Burr T, Takle G, Brurberg MB, Birch PRJ, Salmond GPC, Toth IK. 2008. Quorum sensing coordinates brute force and stealth modes of infection in the plant pathogen *Pectobacterium atrosepticum*. *PLoS Pathog* **4**. doi:10.1371/journal.ppat.1000093
- Llamas A, Imperi F, Visca P, Lamont IL. 2014. Cell-surface signaling in *Pseudomonas* : stress responses, iron transport, and pathogenicity. *FEMS Microbiol Rev* **38**:569–597. doi:10.1111/1574-6976.12078
- Lorang J, Kidarsa T, Bradford CS, Gilbert B, Curtis M, Tzeng S-C, Maier CS, Wolpert TJ. 2012. Tricking the guard: exploiting plant defense for disease susceptibility. *Science* **338**:659–62. doi:10.1126/science.1226743
- Love MI, Huber W, Anders S. 2014. Moderated estimation of fold change and dispersion for RNA-seq data with DESeq2. *Genome Biol* **15**:550. doi:10.1186/s13059-014-0550-8

- Macho AP, Schwessinger B, Ntoukakis V, Brutus A, Segonzac C, Roy S, Kadota Y, Oh M-H, Sklenar J, Derbyshire P, Lozano-Durán R, Malinovsky FG, Monaghan J, Menke FL, Huber SC, He SY, Zipfel C. 2014. A bacterial tyrosine phosphatase inhibits plant pattern recognition receptor activation. *Science* **343**:1509–12. doi:10.1126/science.1248849
- Mackey D, Belkhadir Y, Alonso JM, Ecker JR, Dangl JL. 2003. Arabidopsis RIN4 is a target of the type III virulence effector AvrRpt2 and modulates RPS2-mediated resistance. *Cell* **112**:379–389.
- Mackey D, Holt BF, Wiig A, Dangl JL. 2002. RIN4 interacts with *Pseudomonas syringae* type III effector molecules and is required for RPM1-mediated resistance in Arabidopsis. *Cell* **108**:743–54.
- Maere S, Heymans K, Kuiper M. 2005a. Systems biology BiNGO: a Cytoscape plugin to assess overrepresentation of Gene Ontology categories in Biological Networks. *Bioinformatics* **21**:3448–3449. doi:10.1093/bioinformatics/bti551
- Maere S, Heymans K, Kuiper M. 2005b. BiNGO: A Cytoscape plugin to assess overrepresentation of Gene Ontology categories in Biological Networks. *Bioinformatics* **21**:3448–3449. doi:10.1093/bioinformatics/bti551
- Malek B von, Graaff E van der, Schneitz K, Keller B. 2002. The Arabidopsis male-sterile mutant *dde2-2* is defective in the ALLENE OXIDE SYNTHASE gene encoding one of the key enzymes of the jasmonic acid biosynthesis pathway. *Planta* **216**:187–192.
- Mandlik A, Livny J, Robins WP, Ritchie JM, Mekalanos JJ, Waldor MK. 2011. RNA-seq-based monitoring of infection-linked changes in vibrio cholerae gene expression. *Cell Host Microbe* **10**:165–174. doi:10.1016/j.chom.2011.07.007
- Marguerat S, Schmidt A, Codlin S, Chen W, Aebersold R, Bähler J. 2012. Quantitative analysis of fission yeast transcriptomes and proteomes in proliferating and quiescent cells. *Cell* **151**:671–683. doi:10.1016/j.cell.2012.09.019
- Markel E, Butcher BG, Myers CR, Stodghill P, Cartinhour S, Swingle B. 2013. Regulons of three *Pseudomonas syringae* pv. tomato DC3000 iron starvation sigma factors. *Appl Environ Microbiol* **79**:725–727. doi:10.1128/AEM.02801-12
- Markel E, Stodghill P, Bao Z, Myers CR, Swingle B. 2016. AlgU Controls Expression of Virulence Genes in *Pseudomonas syringae* pv. tomato DC3000. *J Bacteriol* **198**:2330–

5. References

2344. doi:10.1128/JB.00276-16.Editor
- Martin M. 2011. Cutadapt Removes Adapter Sequences From High-Throughput Sequencing Reads. *EMBnet J* **17**:10–12.
- Martínez-Medina A, Van Wees SCM, Pieterse CMJ. 2017. Airborne signals from Trichoderma fungi stimulate iron uptake responses in roots resulting in priming of jasmonic acid-dependent defences in shoots of Arabidopsis thaliana and Solanum lycopersicum. *Plant Cell Environ* **40**:2691–2705. doi:10.1111/pce.13016
- Martinière A, Gibrat R, Sentenac H, Dumont X, Gaillard I, Paris N. 2018. Uncovering pH at both sides of the root plasma membrane interface using noninvasive imaging. *Proc Natl Acad Sci USA* 201721769. doi:10.1073/pnas.1721769115
- Mathesius U, Mulders S, Gao M, Teplitski M, Caetano-Anolles G, Rolfe BG, Bauer WD. 2003. Extensive and specific responses of a eukaryote to bacterial quorum-sensing signals. *Proc Natl Acad Sci USA* **100**:1444–1449. doi:10.1073/pnas.262672599
- Matsui H, Nomura Y, Egusa M, Hamada T, Hyon G, Kaminaka H, Watanabe Y, Ueda T, Trujillo M, Shirasu K, Nakagami H. 2017. The GYF domain protein PSIG1 dampens the induction of cell death during plant-pathogen interactions. *PLoS Genet* **13**:e1007037.
- McClerklin SA, Lee SG, Harper CP, Nwumeh R, Jez JM, Kunkel BN. 2018. Indole-3-acetaldehyde dehydrogenase-dependent auxin synthesis contributes to virulence of Pseudomonas syringae strain DC3000. *PLOS Pathog* **14**:e1006811. doi:10.1371/journal.ppat.1006811
- Melotto M, Zhang L, Oblessuc PR, He SY. 2017. Stomatal Defense a Decade Later. *Plant Physiol* **174**:561–571. doi:10.1104/pp.16.01853
- Meng X, Zhang S. 2013. MAPK cascades in plant disease resistance signaling. *Annu Rev Phytopathol* **51**:245–66. doi:10.1146/annurev-phyto-082712-102314
- Mengiste T. 2012. Plant immunity to necrotrophs. *Annu Rev Phytopathol* **50**:267–94. doi:10.1146/annurev-phyto-081211-172955
- Miao C, Liu F, Zhao Q, Jia Z, Song S. 2012. Biochemical and Biophysical Research Communications A proteomic analysis of Arabidopsis thaliana seedling responses to 3-oxo-octanoyl-homoserine lactone, a bacterial quorum-sensing signal. *Biochem Biophys*

- Res Commun* **427**:293–298. doi:10.1016/j.bbrc.2012.09.044
- Mikkelsen MD, Hansen CH, Wittstock U, Halkier BA. 2000. Cytochrome P450 CYP79B2 from *Arabidopsis* catalyzes the conversion of tryptophan to indole-3-acetaldoxime, a precursor of indole glucosinolates and indole-3-acetic acid. *J Biol Chem* **275**:33712–33717. doi:10.1074/jbc.M001667200
- Mindrinos M, Katagiri F, Yu GL, Ausubel FM. 1994. The *A. thaliana* disease resistance gene RPS2 encodes a protein containing a nucleotide-binding site and leucine-rich repeats. *Cell* **78**:1089–1099. doi:10.1016/0092-8674(94)90282-8
- Mine A, Berens ML, Nobori T, Anver S, Fukumoto K, Winkel Müller TM. 2017a. Pathogen exploitation of an abscisic acid- and jasmonate-inducible MAPK phosphatase and its interception by *Arabidopsis* immunity. *Proc Natl Acad Sci USA* **114**:7456–7461.
- Mine A, Nobori T, Salazar-rondon MC, Winkel Müller TM, Anver S, Becker D, Tsuda K. 2017b. An incoherent feed-forward loop mediates robustness and tunability in a plant immune network. *EMBO Rep* **18**:464–476. doi:10.15252/embr.201643051
- Mine A, Sato M, Tsuda K. 2014. Toward a systems understanding of plant–microbe interactions. *Front Plant Sci* **5**:423. doi:10.3389/fpls.2014.00423
- Mine A, Seyfferth C, Barbara Kracher¹, Matthias L. Berens¹ DB and, Tsuda K. 2018. The Defense Phytohormone Signaling Network Enables Rapid, High- amplitude Transcriptional Reprogramming During Effector-Triggered Immunity. *Plant Cell*. doi:10.1105/tpc.1
- Mittal S, Davis KR. 1995. Role of the phytotoxin coronatine in the infection of *Arabidopsis thaliana* by *Pseudomonas syringae* pv. tomato. *Mol Plant Microbe Interact* **8**:165–171.
- Mole BM, Baltrus DA, Dangl JL, Grant SR. 2007. Global virulence regulation networks in phytopathogenic bacteria. *Trends Microbiol* **15**:363–371. doi:10.1016/j.tim.2007.06.005
- Mucyn TS, Yourstone S, Lind AL, Biswas S, Nishimura MT, Baltrus D a, Cumbie JS, Chang JH, Jones CD, Dangl JL, Grant SR. 2014. Variable suites of non-effector genes are co-regulated in the type III secretion virulence regulon across the *Pseudomonas syringae* phylogeny. *PLoS Pathog* **10**:e1003807. doi:10.1371/journal.ppat.1003807

5. References

- Müller DB, Schubert OT, Röst H, Aebersold R, Vorholt JA. 2016. Systems-level proteomics of two ubiquitous leaf commensals reveals complementary adaptive traits for phyllosphere colonization. *Mol Cell Proteomics* **mcp-M116**. doi:10.1074/mcp.M116.058164
- Murdoch DJ, Chow ED. 1996. COMPUTING A Graphical Display of Large Correlation Matrices. *Am Stat* **50**:178–180.
- Mustilli a.-C. 2002. Arabidopsis OST1 Protein Kinase Mediates the Regulation of Stomatal Aperture by Abscisic Acid and Acts Upstream of Reactive Oxygen Species Production. *Plant Cell* **14**:3089–3099. doi:10.1105/tpc.007906
- Nagel R, Peters RJ. 2017. Investigating the Phylogenetic Range of Gibberellin Biosynthesis in Bacteria. *Mol Plant Microbe Interactoins* **30**:343–349.
- Narusaka M, Shirasu K, Noutoshi Y, Kubo Y, Shiraishi T, Iwabuchi M, Narusaka Y. 2009. RRS1 and RPS4 provide a dual Resistance-gene system against fungal and bacterial pathogens. *Plant J* **60**:218–226. doi:10.1111/j.1365-313X.2009.03949.x
- Návarová H, Bernsdorff F, Döring A-C, Zeier J. 2012. Pipecolic acid, an endogenous mediator of defense amplification and priming, is a critical regulator of inducible plant immunity. *Plant Cell* **24**:5123–41. doi:10.1105/tpc.112.103564
- Nietzel T, Elsässer M, Ruberti C, Steinbeck J, Ugalde JM, Fuchs P, Wagner S, Ostermann L, Moseler A, Lemke P, Fricker MD, Müller-Schüssele SJ, Moerschbacher BM, Costa A, Meyer AJ, Schwarzländer M. 2018. The fluorescent protein sensor roGFP2-Orp1 monitors in vivo H₂O₂ and thiol redox integration and elucidates intracellular H₂O₂ dynamics at elicitor-induced oxidative burst in Arabidopsis. *New Phytol.* doi:10.1111/nph.15550
- Nishimura MT, Stein M, Hou B-H, Vogel JP, Edwards H, Somerville SC. 2003. Loss of a callose synthase results in salicylic acid-dependent disease resistance. *Science* **301**:969–972. doi:10.1126/science.1086716
- Nobori T, Mine A, Tsuda K. 2018a. Molecular networks in plant – pathogen holobiont. *FEBS Lett* 1–17. doi:10.1002/1873-3468.13071
- Nobori T, Tsuda K. 2018. In planta Transcriptome Analysis of Pseudomonas syringae. *Bio-Protocol* **8**:1–8. doi:10.21769/BioProtoc.2987

- Nobori T, Velásquez AC, Wu J, Kvitko BH, Kremer JM, Wang Y, He SY, Tsuda K. 2018b. Transcriptome landscape of a bacterial pathogen under plant immunity. *Proc Natl Acad Sci USA* **115**:E3055–E3064. doi:10.1073/pnas.1800529115
- Nomura K, Mecey C, Lee Y-N, Imboden LA, Chang JH, He SY. 2011. Effector-triggered immunity blocks pathogen degradation of an immunity-associated vesicle traffic regulator in *Arabidopsis*. *Proc Natl Acad Sci USA* **108**:10774–10779. doi:10.1073/pnas.1103338108
- Nuss AM, Beckstette M, Pimenova M, Schmühl C, Opitz W, Pisano F, Heroven AK, Dersch P. 2017. Tissue dual RNA-seq allows fast discovery of infection-specific functions and riboregulators shaping host–pathogen transcriptomes. *Proc Natl Acad Sci USA* 201613405. doi:10.1073/pnas.1613405114
- O’Leary BM, Neale HC, Geilfus C-M, Jackson RW, Arnold DL, Preston GM. 2016. Early changes in apoplast composition associated with defence and disease in interactions between *Phaseolus vulgaris* and the halo blight pathogen *Pseudomonas syringae* Pv. *phaseolicola*. *Plant Cell Environ* **39**:2172–2184. doi:10.1111/pce.12770
- O’Neill EM, Mucyn TS, Patteson JB, Finkel OM, Chung E-H, Baccile JA, Massolo E, Schroeder FC, Dangl JL, Li B. 2018. Phevamine A, a small molecule that suppresses plant immune responses. *Proc Natl Acad Sci* **115**:201803779. doi:10.1073/PNAS.1803779115
- Oh H-S, Park DH, Collmer A. 2010. Components of the *Pseudomonas syringae* type III secretion system can suppress and may elicit plant innate immunity. *Mol Plant Microbe Interact* **23**:727–739. doi:10.1094/MPMI-23-6-0727
- Papenfert K, Bassler BL. 2016. Quorum sensing signal–response systems in Gram-negative bacteria. *Nat Rev Microbiol* **14**:576–588. doi:10.1038/nrmicro.2016.89
- Patankar A V, Gonz’alez JE. 2009. Orphan LuxR regulators of quorum sensing. *FEMS Microbiol Rev* **33**:739–756. doi:10.1111/j.1574-6976.2009.00163.x
- Petnicki-ocwieja T, Alfano JR. 2005. The hrpK Operon of *Pseudomonas syringae* pv. *tomato* DC3000 Encodes Two Proteins Secreted by the Type III (Hrp) Protein Secretion System: HopB1 and HrpK, a Putative Type III Translocator. *Society* **187**:649–663. doi:10.1128/JB.187.2.649
- Piasecka A, Jedrzejczak-rey N. 2015. Secondary metabolites in plant innate immunity :

5. References

- conserved function of divergent chemicals. *New Phytol* **206(3)**:948–964.
- Pieterse CMJ, Van der Does D, Zamioudis C, Leon-Reyes A, Van Wees SCM. 2012. Hormonal modulation of plant immunity. *Annu Rev Cell Dev Biol* **28**:489–521. doi:10.1146/annurev-cellbio-092910-154055
- Prithiviraj B, Bais HP, Weir T, Suresh B, Najarro EH, Dayakar V, Schweizer HP, Vivanco JM, Dayakar B. 2005. Down regulation of virulence factors of *Pseudomonas aeruginosa* by salicylic acid attenuates its virulence on *Arabidopsis thaliana* and *Caenorhabditis elegans*. *Infect Immun* **73**:5319–5328. doi:10.1128/IAI.73.9.5319
- Qi T, Seong K, Thomazella DPT, Ryan J, Pham J, Seo E. 2018. NRG1 functions downstream of EDS1 to regulate TIR-NLR-mediated plant immunity in *Nicotiana benthamiana*. *Proc Natl Acad Sci USA* **115**. doi:10.1073/pnas.1814856115
- Quiñones B, Dulla G, Lindow SE. 2005. Quorum sensing regulates exopolysaccharide production, motility, and virulence in *Pseudomonas syringae*. *Mol Plant Microbe Interact* **18**:682–693. doi:10.1094/MPMI-18-0682
- Rajniak J, Barco B, Clay NK, Sattely ES. 2015. A new cyanogenic metabolite in *Arabidopsis* required for inducible pathogen defence. *Nature* **525**:376–379. doi:10.1038/nature14907
- Rasmussen TB, Givskov M. 2006. Quorum sensing inhibitors: a bargain of effects. *Microbiology* 895–904. doi:10.1099/mic.0.28601-0
- Rich C, Reitz MU, Eichmann R, Hermann S, Jenkins DJ, Kogel K-H, Esteban E, Ott S, Schäfer P. 2018. Cell type identity determines transcriptomic immune responses in *Arabidopsis thaliana* roots, bioRxiv.
- Rico A, Preston GM. 2008. *Pseudomonas syringae* pv. tomato DC3000 uses constitutive and apoplast-induced nutrient assimilation pathways to catabolize nutrients that are abundant in the tomato apoplast. *Mol Plant Microbe Interact* **21**:269–282. doi:10.1094/MPMI-21-2-0269
- Ritchie ME, Phipson B, Wu D, Hu Y, Law CW, Shi W, Smyth GK. 2015. limma powers differential expression analyses for RNA-sequencing and microarray studies. *Nucleic Acids Res* **43**:e47. doi:10.1093/nar/gkv007
- Robinson MD, McCarthy DJ, Smyth GK. 2010. edgeR: a Bioconductor package for

- differential expression analysis of digital gene expression data. *Bioinformatics* **26**:139–140. doi:10.1093/bioinformatics/btp616
- Robinson MD, McCarthy DJ, Smyth GK. 2009. edgeR: A Bioconductor package for differential expression analysis of digital gene expression data. *Bioinformatics* **26**:139–140. doi:10.1093/bioinformatics/btp616
- Ronald P, Joe A. 2017. Molecular mimicry modulates plant host responses to pathogens. *Ann Bot* **121**:17–23. doi:10.1093/aob/mcx125
- Rott M. 2012. Structure and assembly cues of Arabidopsis root-inhabiting bacterial communities and comparative genomics of selected Rhizobium members. *Diss Univ Col.*
- Rufián JS, Sánchez-Romero M-A, López-Márquez D, Macho AP, Mansfield JW, Arnold DL, Ruiz-Albert J, Casadesús J, Beuzón CR. 2016. *Pseudomonas syringae* Differentiates into Phenotypically Distinct Subpopulations During Colonization of a Plant Host. *Environ Microbiol* **18**:3593–3605. doi:10.1111/1462-2920.13497
- Russell AB, Peterson SB, Mougous JD. 2014. Type VI secretion system effectors: poisons with a purpose. *Nat Rev Microbiol* **12**:137–148. doi:10.1038/nrmicro3185
- Ryffel F, Helfrich EJN, Kiefer P, Peyriga L, Portais J, Piel J, Vorholt JA. 2015. Metabolic footprint of epiphytic bacteria on Arabidopsis thaliana leaves. *ISME J* **10**:632–643. doi:10.1038/ismej.2015.141
- Sasaki A, Yamaji N, Xia J, Jian Feng Ma. 2011. OsYSL6 Is Involved in the Detoxification of Excess. *Plant Physiol* **157**:1832–1840. doi:10.1104/pp.111.186031
- Schenk A, Weingart H, Ullrich MS. 2008. Extraction of high-quality bacterial RNA from infected leaf tissue for bacterial in planta gene expression analysis by multiplexed fluorescent Northern hybridization. *Mol Plant Pathol* **9**:227–235. doi:10.1111/j.1364-3703.2007.00452.x
- Schenk ST, Hernandez-Reyes C, Samans B, Stein E, Neumann C, Schikora M, Reichelt M, Mithofer A, Becker A, Kogel K-H, Schikora A. 2014. N-Acyl-Homoserine Lactone Primes Plants for Cell Wall Reinforcement and Induces Resistance to Bacterial Pathogens via the Salicylic Acid/Oxylipin Pathway. *Plant Cell* **26**:2708–2723. doi:10.1105/tpc.114.126763

5. References

- Seyfferth C, Tsuda K. 2014. Salicylic acid signal transduction : the initiation of biosynthesis , perception and transcriptional reprogramming. *Front Plant Sci* **5**:697. doi:10.3389/fpls.2014.00697
- Shan L, He P, Li J, Heese A, Peck SC, Nu T, Martin GB. 2008. Bacterial Effectors Target the Common Signaling Partner BAK1 to Disrupt Multiple MAMP Receptor- Signaling Complexes and Impede Plant Immunity. *Cell Host Microbe* **4**:17–27. doi:10.1016/j.chom.2008.05.017
- Shannon P, Markiel A, Ozier O, Baliga NS, Wang JT, Ramage D, Amin N, Schwikowski B, Ideker T. 2003. Cytoscape: A software Environment for integrated models of biomolecular interaction networks. *Genome Res* **13**:2498–2504. doi:10.1101/gr.1239303
- Shen Q, Liu Y, Naqvi NI. 2018. Fungal effectors at the crossroads of phytohormone signaling. *Curr Opin Microbiol* **46**:1–6. doi:10.1016/j.mib.2018.01.006
- Shi G, Zhang Z, Friesen TL, Raats D, Fahima T, Brueggeman RS, Lu S, Trick HN, Liu Z, Chao W, Frenkel Z, Xu SS, Rasmussen JB, Faris JD. 2016. The hijacking of a receptor kinase – driven pathway by a wheat fungal pathogen leads to disease. *Sci Adv* **2**:e1600822.
- Shigenaga AM, Berens ML, Tsuda K, Argueso CT. 2017. Towards engineering of hormonal crosstalk in plant immunity. *Curr Opin Plant Biol* **38**:164–172. doi:10.1016/j.pbi.2017.04.021
- Smakowska-luzan E, Mott GA, Stolt-bergner P, Provart NJ, Mukhtar MS, Zipfel C. 2018. An extracellular network of Arabidopsis leucine-rich repeat receptor kinases. *Nature* **533**:342–346. doi:10.1038/nature25184
- Smakowska E, Kong J, Busch W, Belkhadir Y. 2016. Organ-specific regulation of growth-defense tradeoffs by plants. *Curr Opin Plant Biol* **29**:129–137. doi:10.1016/j.pbi.2015.12.005
- Smyth GK. 2005. limma: Linear Models for Microarray Data. *Bioinforma Comput Biol Solut Using R Bioconductor* 397–420.
- Spoel SH, Johnson JS, Dong X. 2007. Regulation of tradeoffs between plant defenses against pathogens with different lifestyles. *Proc Natl Acad Sci USA* **104**:18842–18847. doi:10.1073/pnas.0708139104

- Sreedharan A, Penaloza-Vazquez A, Kunkel BN, Bender CL. 2006. CorR regulates multiple components of virulence in *Pseudomonas syringae* pv. tomato DC3000. *Mol Plant Microbe Interact* **19**:768–779. doi:10.1094/MPMI-19-0768
- Stapels D, Hill P, Westermann A, Fisher R, Saliba E, Blommestein I, Vogel J, Helaine S. 2018. Salmonella persists undermine host immune defenses during antibiotic treatment. *Science* **1160**:1156–1160. doi:10.1007/s10035-011-0292-1
- Storey JD, Tibshirani R. 2003. Statistical significance for genomewide studies. *Proc Natl Acad Sci USA* **100**:9440–9445. doi:10.1073/pnas.1530509100
- Stringlis IA, Yu K, Feussner K, Jonge R De, Bentum S Van, Verk MC Van. 2018. MYB72-dependent coumarin exudation shapes root microbiome assembly to promote plant health. *Proc Natl Acad Sci*. doi:10.1073/pnas.1722335115
- Sun J, Li L, Wang P, Zhang S, Wu J. 2017. Genome-wide characterization, evolution, and expression analysis of the leucine-rich repeat receptor-like protein kinase (LRR-RLK) gene family in Rosaceae genomes. *BMC Genomics* **18**:763. doi:10.1186/s12864-017-4155-y
- Swingle B, Thete D, Moll M, Myers CR, Schneider DJ, Cartinhour S. 2008. Characterization of the PvdS-regulated promoter motif in *Pseudomonas syringae* pv. tomato DC3000 reveals regulon members and insights regarding PvdS function in other pseudomonads. *Mol Microbiol* **68**:871–889. doi:10.1111/j.1365-2958.2008.06209.x
- Taguchi F, Suzuki T, Inagaki Y, Toyoda K, Shiraishi T, Ichinose Y. 2010. The siderophore pyoverdine of *Pseudomonas syringae* pv. tabaci 6605 is an intrinsic virulence factor in host tobacco infection. *J Bacteriol* **192**:117–126. doi:10.1128/JB.00689-09
- Tang X, Xiao Y, Zhou J-M. 2006. Regulation of the type III secretion system in phytopathogenic bacteria. *Mol Plant Microbe Interact* **19**:1159–1166. doi:10.1094/MPMI-19-1159
- Teplitski M, Chen H, Rajamani S, Gao M, Merighi M, Sayre RT, Robinson JB, Rolfe BG, Bauer WD. 2004. *Chlamydomonas reinhardtii* Secretes Compounds That Mimic Bacterial Signals and Interfere with Quorum Sensing Regulation in Bacteria 1. *Plant Physiol* **134**:137–146. doi:10.1104/pp.103.029918.bacteria
- Teplitski M, Robinson JB, Bauer WD. 2000. Plants secrete substances that mimic bacterial N-

5. References

- acyl homoserine lactone signal activities and affect population density-dependent behaviors in associated bacteria. *Mol Plant Microbe Interact* **13**:637–48. doi:10.1094/MPMI.2000.13.6.637
- Thaler JS, Humphrey PT, Whiteman NK. 2012. Evolution of jasmonate and salicylate signal crosstalk. *Trends Plant Sci* **17**:260–270. doi:10.1016/j.tplants.2012.02.010
- Toruño TY, Stergiopoulos I, Coaker G. 2016. Plant-Pathogen Effectors: Cellular Probes Interfering with Plant Defenses in Spatial and Temporal Manners. *Annu Rev Phytopathol* **54**:419–441. doi:10.1146/annurev-phyto-080615-100204
- Trapnell C, Pachter L, Salzberg SL. 2009. TopHat: Discovering splice junctions with RNA-Seq. *Bioinformatics* **25**:1105–1111. doi:10.1093/bioinformatics/btp120
- Troxell B, Hassan HM. 2013. Transcriptional regulation by Ferric Uptake Regulator (Fur) in pathogenic bacteria. *Front Cell Infect Microbiol* **3**:1–13. doi:10.3389/fcimb.2013.00059
- Tsuda K. 2018. Division of tasks - Defense by the spatial separation of antagonistic hormone activities. *Plant Cell Physiol* **59**:3–4. doi:10.1093/pcp/pcx208/4774332
- Tsuda K, Mine A, Bethke G, Igarashi D, Botanga CJ, Tsuda Y, Glazebrook J, Sato M, Katagiri F. 2013. Dual Regulation of Gene Expression Mediated by Extended MAPK Activation and Salicylic Acid Contributes to Robust Innate Immunity in *Arabidopsis thaliana*. *PLoS Genet* **9**:e1004015. doi:10.1371/journal.pgen.1004015
- Tsuda K, Sato M, Glazebrook J, Cohen JD, Katagiri F. 2008. Interplay between MAMP-triggered and SA-mediated defense responses. *Plant J* **53**:763–775. doi:10.1111/j.1365-313X.2007.03369.x
- Tsuda K, Sato M, Stoddard T, Glazebrook J, Katagiri F. 2009. Network properties of robust immunity in plants. *PLOS Genet* **5**:e1000772.
- Tyanova S, Temu T, Cox J. 2016. The MaxQuant computational platform for mass spectrometry-based shotgun proteomics. *Nat Protoc* **11**:2301–2319. doi:10.1038/nprot.2016.136
- Van der Ent S, Verhagen BWM, Van Doorn R, Bakker D, Verlaan MG, Pel MJC, Joosten RG, Proveniers MCG, Van Loon LC, Ton J, Pieterse CMJ. 2008. MYB72 Is Required in Early Signaling Steps of Rhizobacteria-Induced Systemic Resistance in *Arabidopsis*. *Plant*

- Physiol* **146**:1293–1304. doi:10.1104/pp.107.113829
- Vargas P, Farias G a., Nogales J, Prada H, Carvajal V, Barón M, Rivilla R, Martín M, Olmedilla A, Gallegos MT. 2013. Plant flavonoids target *Pseudomonas syringae* pv. tomato DC3000 flagella and type III secretion system. *Environ Microbiol Rep* **5**:841–850. doi:10.1111/1758-2229.12086
- Velasquez AC, Castroverde CDM, He SY. 2018. Plant-Pathogen Warfare under Changing Climate Conditions. *Curr Biol* **28**:619–634. doi:10.1016/j.cub.2018.03.054
- Venturi V, Fuqua C. 2013. Chemical signaling between plants and plant-pathogenic bacteria. *Annu Rev Phytopathol* **51**:17–37. doi:10.1146/annurev-phyto-082712-102239
- Verbon EH, Trapet PL, Stringlis IA, Kruijs S, Bakker PAHM, Pieterse MJ. 2017. Iron and Immunity. *Annu Rev Phytopathol* **55**:355–375.
- Verhagen BWM, Glazebrook J, Zhu T, Chang H-S, van Loon LC, Pieterse CMJ. 2004. The Transcriptome of Rhizobacteria-Induced Systemic Resistance in *Arabidopsis*. *Mol Plant-Microbe Interact* **17**:895–908. doi:10.1094/MPMI.2004.17.8.895
- Vikram A, Jayaprakasha GK, Jesudhasan PR, Pillai SD, Patil BS. 2010. Suppression of bacterial cell-cell signalling, biofilm formation and type III secretion system by citrus flavonoids. *J Appl Microbiol* **109**:515–527. doi:10.1111/j.1365-2672.2010.04677.x
- Vorholt J a. 2012. Microbial life in the phyllosphere. *Nat Rev Microbiol* **10**:828–40. doi:10.1038/nrmicro2910
- Vranova V, Lojkova L, Rejsek K, Formanek P. 2013. Significance of the Natural Occurrence of L-Versus D-Pipecolic Acid: A Review. *Chirality* **26**:553–562. doi:10.1002/chir
- Wang C, Liu Y, Li S-S, Han G-Z. 2015. Insights into the Origin and Evolution of the Plant Hormone Signaling Machinery. *Plant Physiol* **167**:872–886. doi:10.1104/pp.114.247403
- Wei H-L, Chakravarthy S, Mathieu J, Helmann TC, Stodghill P, Swingle B, Martin GB, Collmer A. 2015. *Pseudomonas syringae* pv. tomato DC3000 Type III Secretion Effector Polymutants Reveal an Interplay between HopAD1 and AvrPtoB. *Cell Host Microbe* **17**:752–762. doi:10.1016/j.chom.2015.05.007
- West SA, Cooper GA. 2016. Division of labour in microorganisms: an evolutionary perspective. *Nat Rev Microbiol* **14**(11):716. doi:10.1038/nrmicro.2016.111

5. References

- Westermann AJ, Barquist L, Vogel J. 2017. Resolving host–pathogen interactions by dual RNA-seq. *PLoS Pathog* **13**:e1006033. doi:10.1371/JOURNAL.PPAT.1006033
- Westermann AJ, Förstner KU, Amman F, Barquist L, Chao Y, Schulte LN, Müller L, Reinhardt R, Stadler PF, Vogel J. 2016. Dual RNA-seq unveils noncoding RNA functions in host–pathogen interactions. *Nature* **529**:496–501. doi:10.1038/nature16547
- Westermann AJ, Gorski S a, Vogel J. 2012. Dual RNA-seq of pathogen and host. *Nat Rev Microbiol* **10**:618–30. doi:10.1038/nrmicro2852
- Wildermuth MC, Dewdney J, Wu G, Ausubel FM. 2001. Isochorismate synthase is required to synthesize salicylic acid for plant defence. *Nature* **414**:562–565. doi:10.1038/417571a
- Wolpert TJ, Lorang JM. 2016. Victoria Blight, defense turned upside down. *Physiol Mol Plant Pathol* **95**:8–13. doi:10.1016/j.pmpp.2016.03.006
- Wu C-H, Abd-El-Haliem A, Bozkurt TO, Belhaj K, Terauchi R, Vossen JH, Kamoun S. 2017. NLR network mediates immunity to diverse plant pathogens. *Proc Natl Acad Sci USA* **114**:8113–8118. doi:10.1073/pnas.1702041114
- Wu C-H, Belhaj K, Bozkurt TO, Kamoun S. 2016. The NLR helper protein NRC3 but not NRC1 is required for Pto-mediated cell death in *Nicotiana benthamiana*. *New Phytol* **209**:1344–1352. doi:http://dx.doi.org/10.1101/015479
- Wu Z, Li M, Dong OX, Xia S, Liang W, Bao Y, Wasteneys G, Li and X. 2018. Differential regulation of TNL-mediated immune signaling by redundant helper CNLs. *New Phytol* **1**. doi:10.1111/nph.15665
- Xiang T, Zong N, Zou Y, Wu Y, Zhang J, Xing W, Li Y, Tang X, Zhu L, Chai J, Zhou J-M. 2008. *Pseudomonas syringae* effector AvrPto blocks innate immunity by targeting receptor kinases. *Curr Biol* **18**:74–80. doi:10.1016/j.cub.2007.12.020
- Xiao F, Goodwin SM, Xiao Y, Sun Z, Baker D, Tang X, Jenks M a, Zhou J-M. 2004. Arabidopsis CYP86A2 represses *Pseudomonas syringae* type III genes and is required for cuticle development. *EMBO J* **23**:2903–2913. doi:10.1038/sj.emboj.7600290
- Xin X-F, Nomura K, Aung K, Velásquez AC, Yao J, Boutrot F, Chang JH, Zipfel C, He SY. 2016. Bacteria establish an aqueous living space in plants crucial for virulence. *Nature* **539**:524–529. doi:10.1038/nature20166

5. References

- Yamada K, Kanai M, Osakabe Y, Ohiraki H, Shinozaki K, Yamaguchi-Shinozaki K. 2011. Monosaccharide absorption activity of Arabidopsis roots depends on expression profiles of transporter genes under high salinity conditions. *J Biol Chem* **286**:43577–43586. doi:10.1074/jbc.M111.269712
- Yamada K, Saijo Y, Nakagami H, Takano Y. 2016. Regulation of sugar transporter activity for antibacterial defense in Arabidopsis. *Science* **354**:1427–1430.
- Yamada K, Yamashita-yamada M, Hirase T, Fujiwara T, Tsuda K, Hiruma K, Saijo Y. 2015. Danger peptide receptor signaling in plants ensures basal immunity upon pathogen-induced depletion of BAK 1. *EMBO J* **35**:46 – 61.
- Yang L, Teixeira PJPL, Biswas S, Finkel OM, He Y, Salas-Gonzalez I, English ME, Epple P, Mieczkowski P, Dangl JL. 2017. Pseudomonas syringae Type III Effector HopBB1 Promotes Host Transcriptional Repressor Degradation to Regulate Phytohormone Responses and Virulence. *Cell Host Microbe* **21**:156–168. doi:10.1016/j.chom.2017.01.003
- Yang S, Zhang Q, Guo J, Charkowski AO, Glick BR, Ibekwe AM, Cooksey DA, Yang C. 2007. Global Effect of Indole-3-Acetic Acid Biosynthesis on Multiple Virulence Factors of Erwinia chrysanthemi 3937. *Appl Environmental Microbiol* **73**:1079–1088. doi:10.1128/AEM.01770-06
- Yasuda M, Ishikawa A, Jikumaru Y, Seki M, Umezawa T, Asami T, Maruyama-Nakashita A, Kudo T, Shinozaki K, Yoshida S, Nakashita H. 2008. Antagonistic interaction between systemic acquired resistance and the abscisic acid-mediated abiotic stress response in Arabidopsis. *Plant Cell* **20**:1678–92. doi:10.1105/tpc.107.054296
- Yasuda S, Okada K, Saijo Y. 2017. A look at plant immunity through the window of the multitasking coreceptor BAK1. *Curr Opin Plant Biol* **38**:10–18. doi:10.1016/j.pbi.2017.04.007
- Yorgey P, Rahme LG, Tan MW, Ausubel FM. 2001. The roles of mucD and alginate in the virulence of Pseudomonas aeruginosa in plants, nematodes and mice. *Mol Microbiol* **41**:1063–1076. doi:10.1046/j.1365-2958.2001.02580.x
- Yu J, Penaloza-Vázquez A, Chakrabarty AM, Bender CL. 1999. Involvement of the exopolysaccharide alginate in the virulence and epiphytic fitness of Pseudomonas

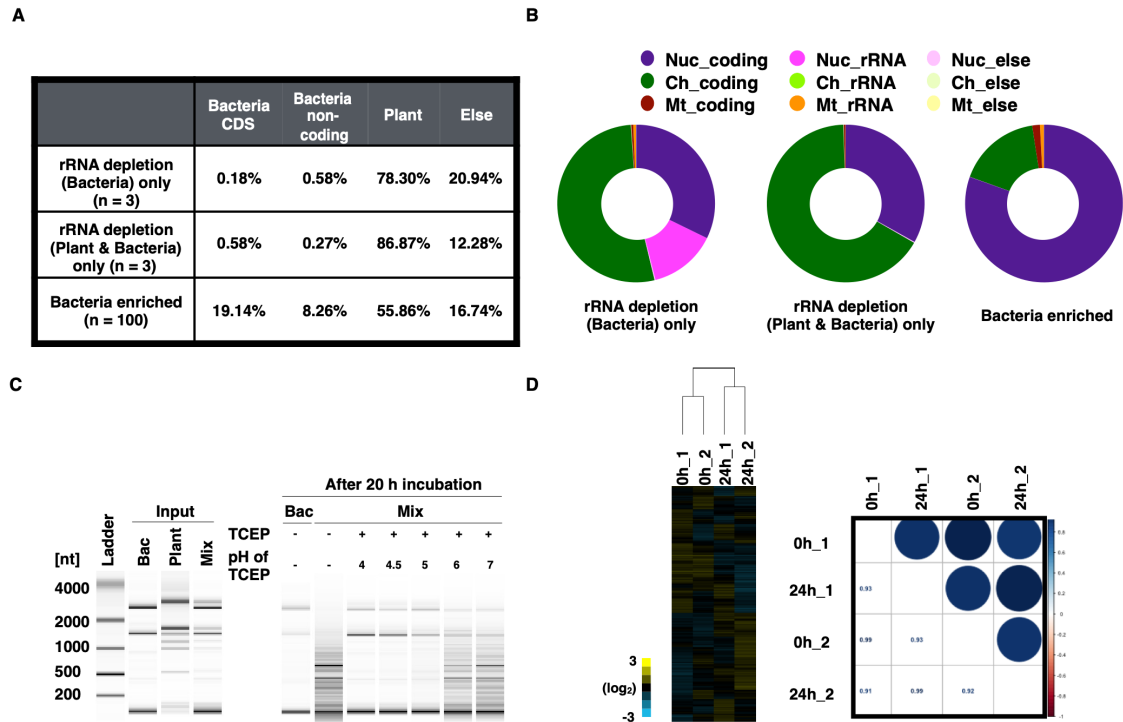
5. References

- syringae pv. syringae. *Mol Microbiol* **33**:712–720. doi:10.1046/j.1365-2958.1999.01516.x
- Yu X, Lund SP, Greenwald JW, Records AH, Scott RA, Nettleton D, Lindow SE, Gross DC, Beattie A. 2014. Transcriptional Analysis of the Global Regulatory Networks Active in *Pseudomonas syringae* during Leaf Colonization. *MBio* **5**:01614– e01683. doi:10.1128/mBio.01683-14.Editor
- Yu X, Lund SP, Scott R a, Greenwald JW, Records AH, Nettleton D, Lindow SE, Gross DC, Beattie G a. 2013. Transcriptional responses of *Pseudomonas syringae* to growth in epiphytic versus apoplastic leaf sites. *Proc Natl Acad Sci USA* **110**:E425–E434. doi:10.1073/pnas.1221892110
- Yuan ZC, Haudecoeur E, Faure D, Kerr KF, Nester EW. 2008. Comparative transcriptome analysis of *Agrobacterium tumefaciens* in response to plant signal salicylic acid, indole-3-acetic acid and γ -amino butyric acid reveals signalling cross-talk and *Agrobacterium*-plant co-evolution. *Cell Microbiol* **10**:2339–2354. doi:10.1111/j.1462-5822.2008.01215.x
- Yue J, Hu X, Huang J. 2014. Origin of plant auxin biosynthesis. *Trends Plant Sci* **19**:764–770. doi:10.1016/j.tplants.2014.07.004
- Zamioudis C, Hanson J, Pieterse CMJ. 2014. β -Glucosidase BGLU42 is a MYB72-dependent key regulator of rhizobacteria-induced systemic resistance and modulates iron deficiency responses in *Arabidopsis* roots. *New Phytol* **204**:368–379. doi:10.1111/nph.12980
- Zhang L, Yao J, Withers J, Xin X-F, Banerjee R, Fariduddin Q, Nakamura Y, Nomura K, Howe GA, Boland W, Yan H, He SY. 2015. Host target modification as a strategy to counter pathogen hijacking of the jasmonate hormone receptor. *Proc Natl Acad Sci USA* **112**:14354–14359. doi:10.1073/pnas.1510745112
- Zhang L, Zhang F, Melotto M, Yao J, He SY. 2017. Jasmonate signaling and manipulation by pathogens and insects. *J Exp Bot* **68**:1371–1385. doi:10.1093/jxb/erw478
- Zhao Y, Hull AK, Ecker JR, Normanly J, Chory J, Celenza JL. 2002. Trp-dependent auxin biosynthesis in *Arabidopsis*: involvement of cytochrome P450s CYP79B2 and CYP79B3. *Genes Dev* **16**:3100–3112.
- Zheng X-Y, Spivey NW, Zeng W, Liu P-P, Fu ZQ, Klessig DF, He SY, Dong X. 2012. Coronatine promotes *Pseudomonas syringae* virulence in plants by activating a signaling

5. References

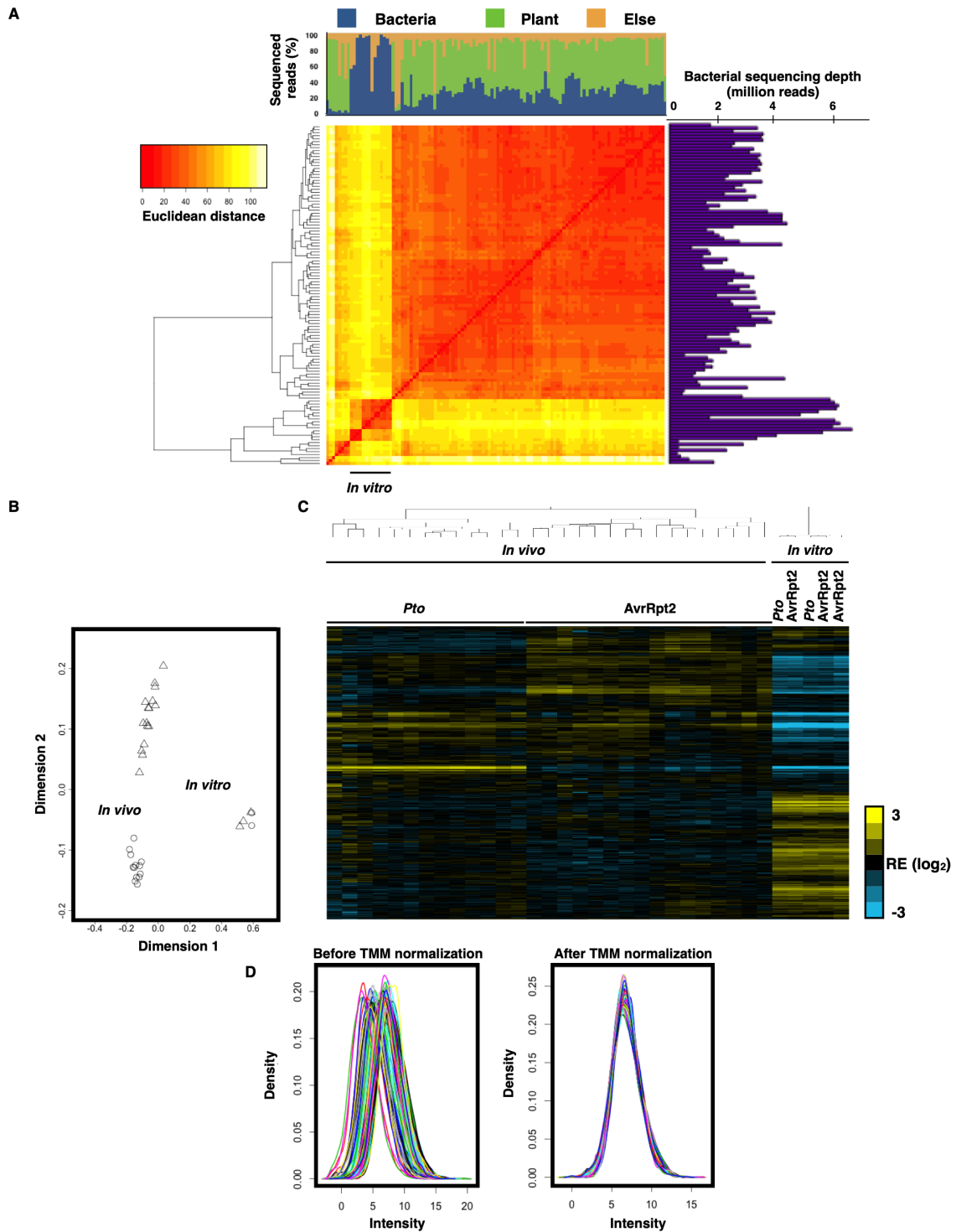
- cascade that inhibits salicylic acid accumulation. *Cell Host Microbe* **11**:587–96. doi:10.1016/j.chom.2012.04.014
- Zhou J, Wu S, Chen X, Liu C, Sheen J, Shan L, He P. 2014. The *Pseudomonas syringae* effector HopF2 suppresses Arabidopsis immunity by targeting BAK1. *Plant J* **2**:235–245. doi:10.1111/tpj.12381
- Zhou Z, Wu Y, Yang Y, Du M, Zhang X, Guo Y, Li C, Zhou J-M. 2015. An Arabidopsis Plasma Membrane Proton ATPase Modulates JA Signaling and Is Exploited by the *Pseudomonas syringae* Effector Protein AvrB for Stomatal Invasion. *Plant Cell* **27**:2032–2041. doi:10.1105/tpc.15.00466
- Zipfel C, Robatzek S, Navarro L, Oakeley EJ, Jones JDG, Felix G, Boller T. 2004. Bacterial disease resistance in Arabidopsis through flagellin perception. *Nature* **428**:764–767.

6 Supplementary figures



Supplementary figure 1: Bacterial enrichment and quality of RNA extraction in *in planta* bacterial transcriptome

(A) Proportion of the sequencing reads mapped on *P. syringae* pv. *tomato* DC3000 (*Pto*; Bacteria) coding sequence (CDS), *Pto* non-coding sequence, *A. thaliana* (Plant) genome, and else. (B) Proportion of the RNA-seq reads mapped on the *A. thaliana* genome. Left and middle: RNA extracted from the infected leaves, followed by bacterial rRNA depletion and bacterial and plant rRNA depletion, respectively (n = 3). Right: RNA extracted from the bacteria enriched samples, followed by bacterial and plant rRNA depletion (Bacteria enriched; n = 8; a subset of all 100 *in planta* samples were randomly selected). Protein coding RNA (coding), ribosomal RNA (rRNA), and other RNA (else) encoded in the nucleus (Nuc), chloroplast (Ch), and mitochondrion (Mt) are shown. (C) Assessment of RNA integrity with the 2100 Bioanalyzer (Agilent). Total RNA from *Pto* (Bac.), *A. thaliana* leaves (Plant), and the mixtures of both (Mix) were analyzed (left panel). Bacterial cells were incubated with crushed *A. thaliana* leaves in RNA stabilizing buffer (9.5% ethanol and 0.5% phenol) without or with Tris(2-carboxyethyl)phosphine (TCEP) at different pHs for 20 h at 4 °C. Then, total RNA was extracted and analyzed (right panel). (D) Bacterial isolation buffer fixes bacterial transcriptome. *Pto* (OD₆₀₀ = 0.65) was incubated in bacterial isolation buffer for 0 h or 24 h, followed by RNA extraction and RNA-seq. Hierarchical clustering (left) and Pearson correlation plot (right) of all the genes detected are shown (n = 2 biological replicates from two independent experiments). This figure was adopted from (Nobori et al., 2018b).

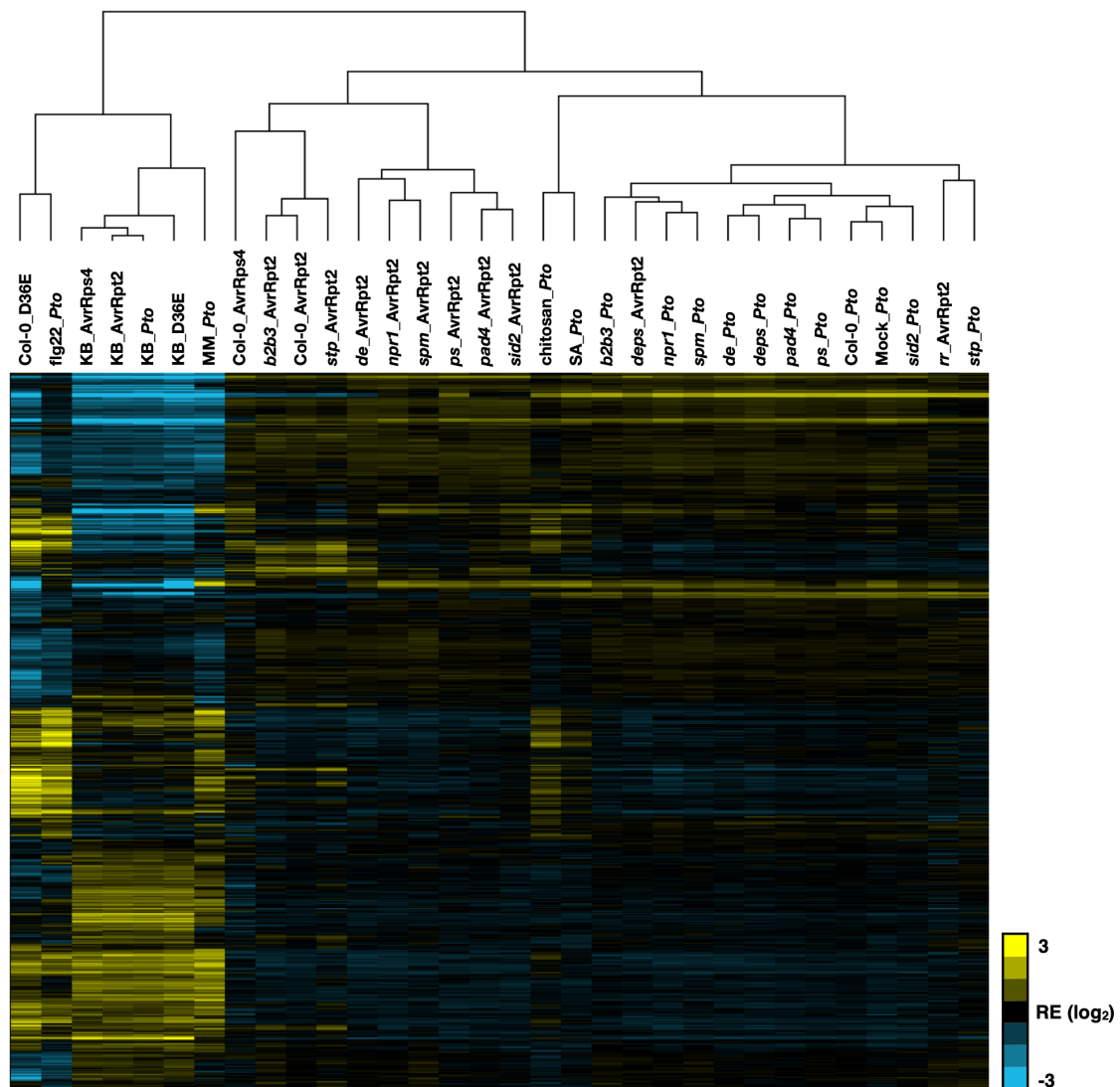


Supplementary figure 2: Normalization and quality control of RNA-seq data

(A) Heatmap of Euclidean distances between RNA-seq data of each sample. The top panel shows the ratio of sequencing reads mapped on the bacterial genome (blue), plant genome (green), and else (orange) in each sample. The right panel shows the sequencing depth of bacterial RNA in each sample. (B) Multidimensional scaling (MDS) plot of the RNA-seq data of *Pto* (circle) and *Pto* AvrRpt2 (triangle) profiled in *in vivo* (Col-0) and *in vitro* (KB medium) conditions. Distances represent leading \log_2 differences between samples. (C) Hierarchical clustering of the relative expression (RE) of the RNA-seq data of *Pto* and *Pto* AvrRpt2 profiled in *in vivo* (Col-0) and *in vitro* (KB medium)

6. Supplementary figures

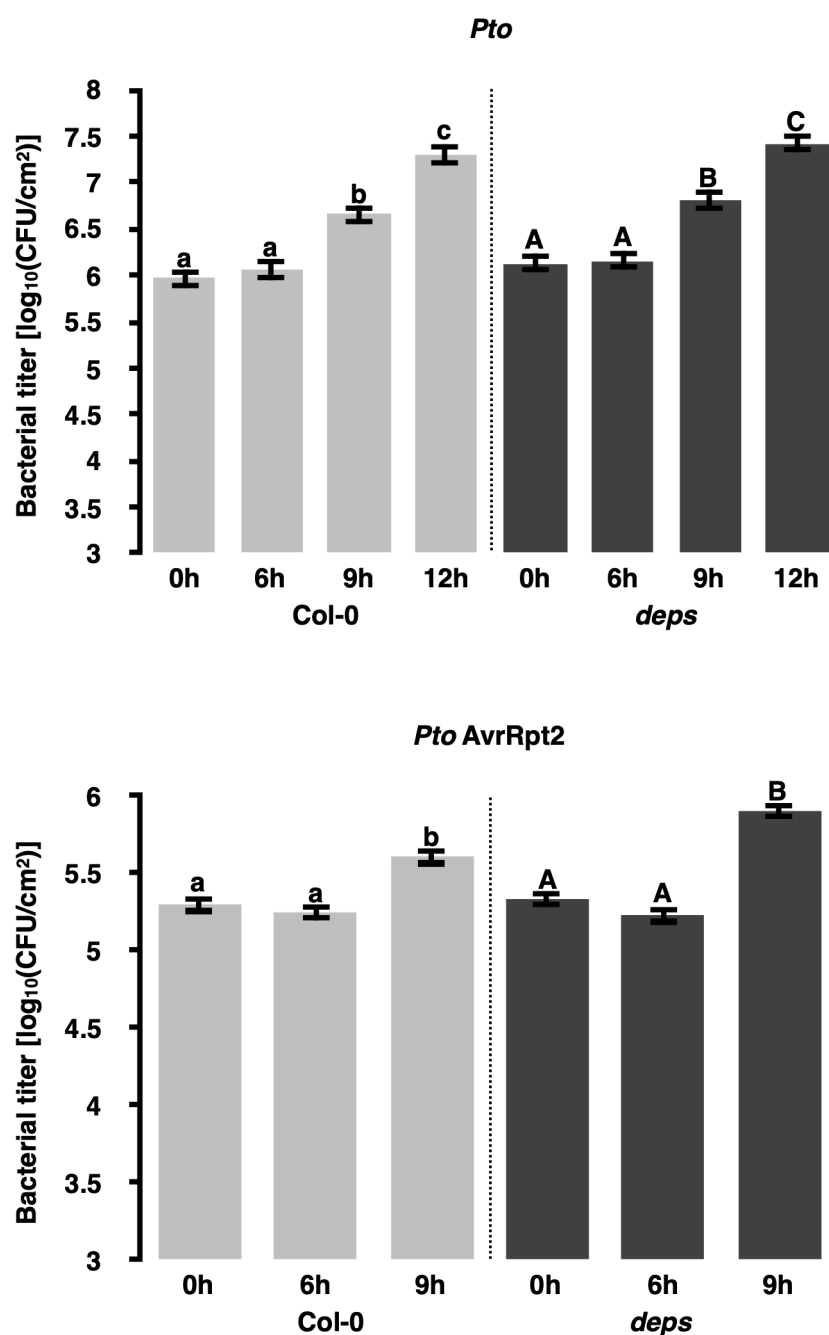
conditions. (D) Density plots of \log_2 -transformed count per million RNA-seq data (Intensity) before (left) and after (right) the trimmed mean of M-values (TMM) normalization. All 114 samples in *in vitro* and *in planta* (6 hpi) conditions were plotted. This figure was adopted from (Nobori et al., 2018b).



Supplementary figure 3: Heatmap of *Pto* transcriptomes (relative expression; RE) in all samples analyzed in this study

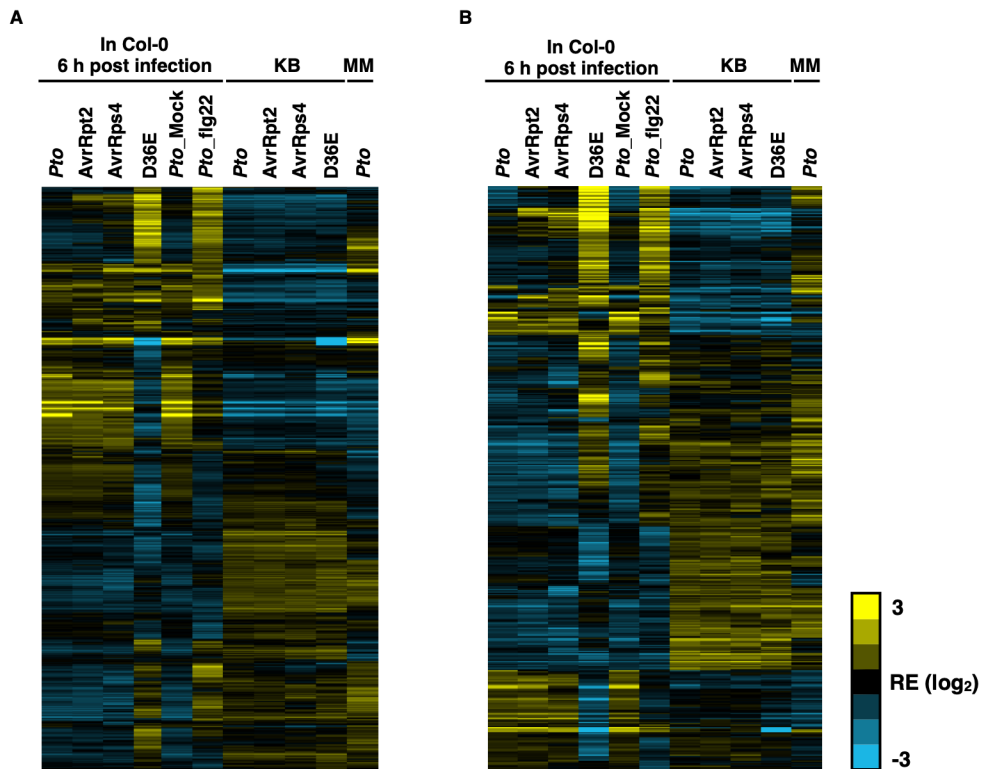
Hierarchical clustering was performed for both the rows (genes) and the columns (samples). The sample name consists of the name of bacterial strains preceded by the name of host genotypes, pretreatments to Col-0, or *in vitro* conditions (see Figure 4A for the acronyms and (Nobori et al., 2018b) for the mean expression values). This figure was adopted from (Nobori et al., 2018b).

6. Supplementary figures



Supplementary figure 4: *Pto* populations did not change at 6 h post infection

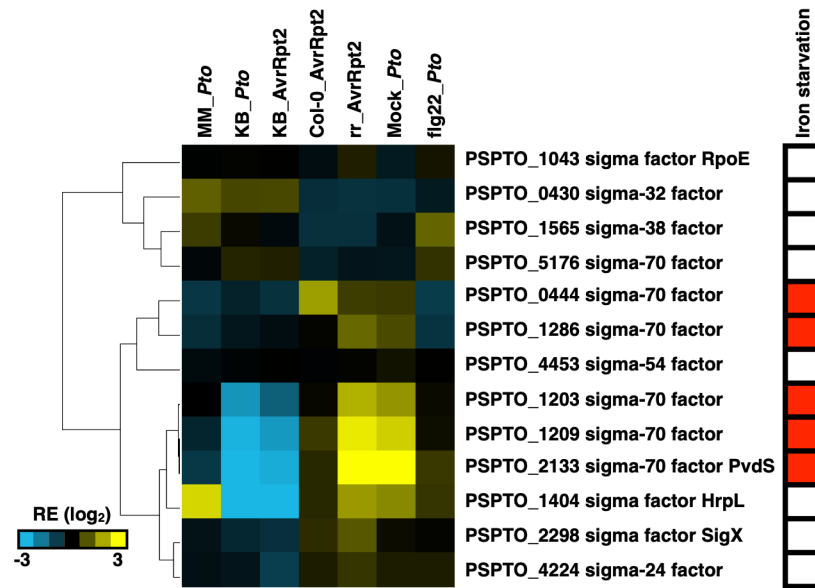
Growth assay of *Pto* or *Pto AvrRpt2* in Col-0 and *dde2 ein2 pad4 sid2 (deps)* plants at the indicated time points. Bacterial suspension ($OD_{600} = 0.5$) was syringe infiltrated into leaves. Mean \pm s.e.m was calculated by using mixed linear model (n= 24 biological replicates from two independent experiments). Different letters indicate statistically significant differences in each genotype (adjusted $P < 0.001$; the Benjamini-Hochberg method). This figure was adopted from (Nobori et al., 2018b).



Supplementary figure 5: Profiles of *Pto* transcriptome under various conditions

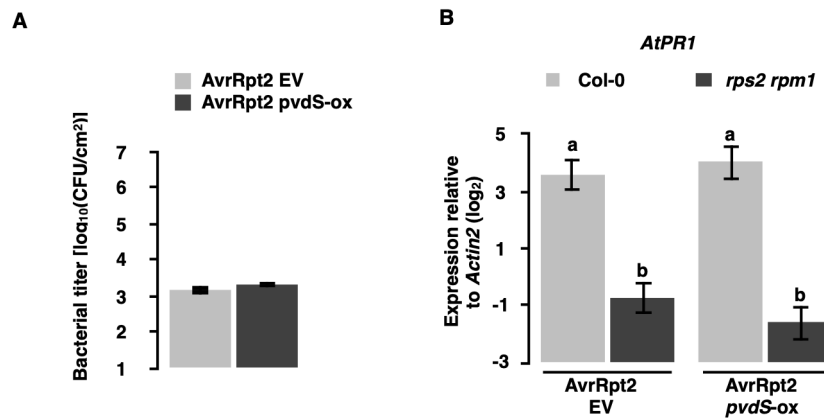
(A) Hierarchical clustering of the relative expression (RE) of 3344 genes detected in all of the samples.
 (B) Hierarchical clustering of the RE of genes annotated as “hypothetical protein” that were differentially regulated in at least one of the comparisons shown in Figure 5C. This figure was adopted from (Nobori et al., 2018b).

6. Supplementary figures



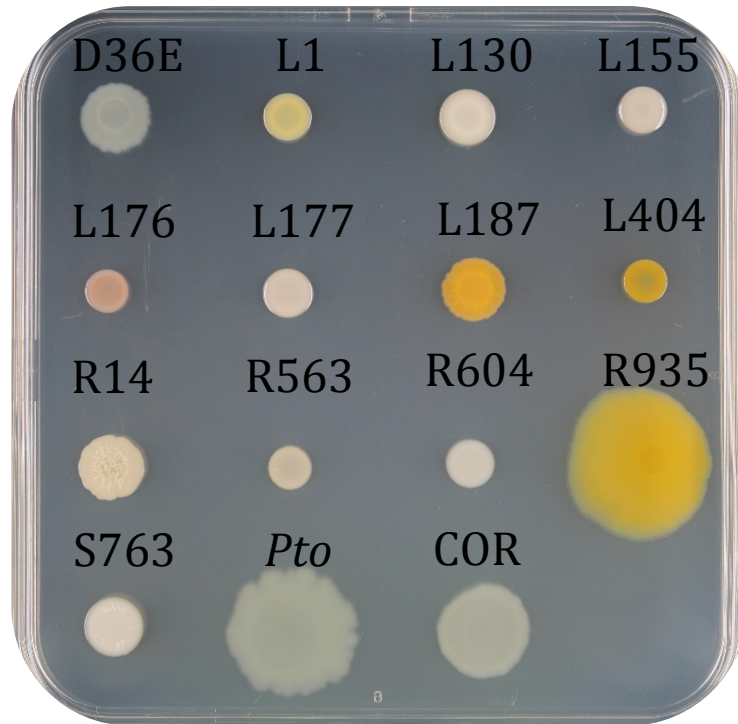
Supplementary figure 6: Hierarchical clustering of the relative expression (RE) of *Pto* sigma factors

The red marks show the iron starvation related sigma factors. MM, minimal medium; KB, King's B medium; *rr*, *rps2 rpm1*. This figure was adopted from (Nobori et al., 2018b).



Supplementary figure 7: Infection assay of *pvdS*-overexpressing *Pto*

(A) Growth assay of *Pto* AvrRpt2 (EV) and *Pto* AvrRpt2 *pvdS*-ox ($OD_{600} = 0.001$) in Col-0 and *rps2 rpm1* plants at 0 h post infection (hpi). (B) RT-qPCR analysis of *PR1* expression in Col-0 and *rps2 rpm1* plants infected with *Pto* AvrRpt2 (EV) or *Pto* AvrRpt2 *pvdS*-ox ($OD_{600} = 0.001$) at 24 hpi. Mean \pm s.e.m was calculated by using a mixed linear model (A: $n = 52$ biological replicates from six independent experiments, B: $n = 2$ biological replicates from two independent experiments). Different letters indicate statistically significant differences (adjusted $P < 0.05$; the Benjamini-Hochberg method). This figure was adopted from (Nobori et al., 2018b).

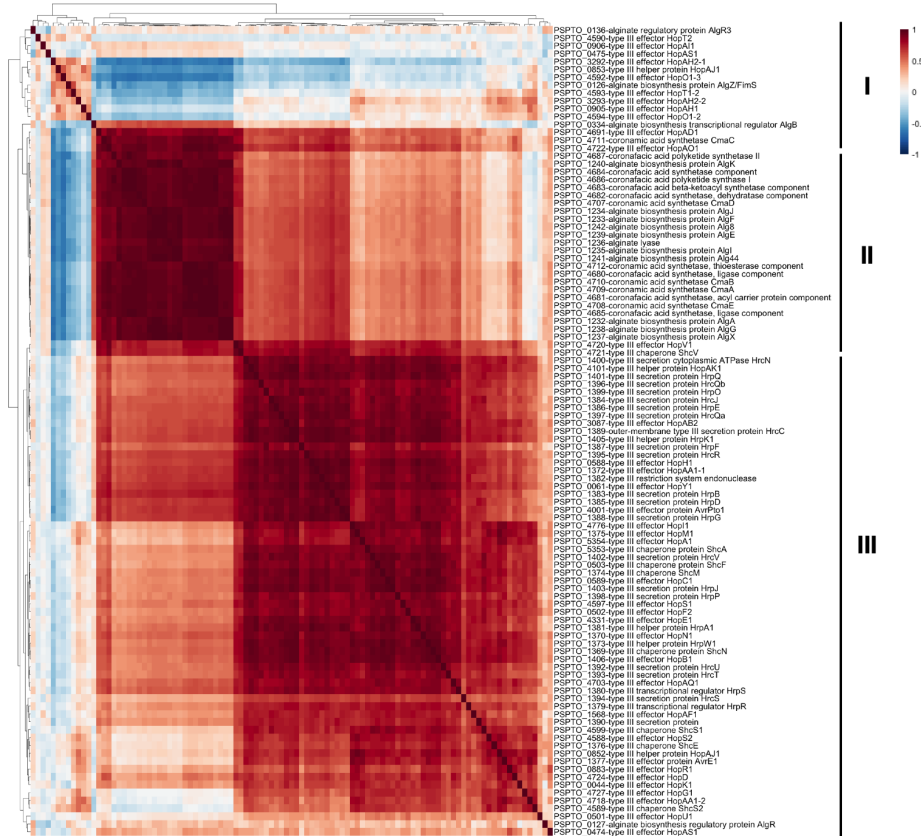


Supplementary figure 8: Colonies of bacterial strains

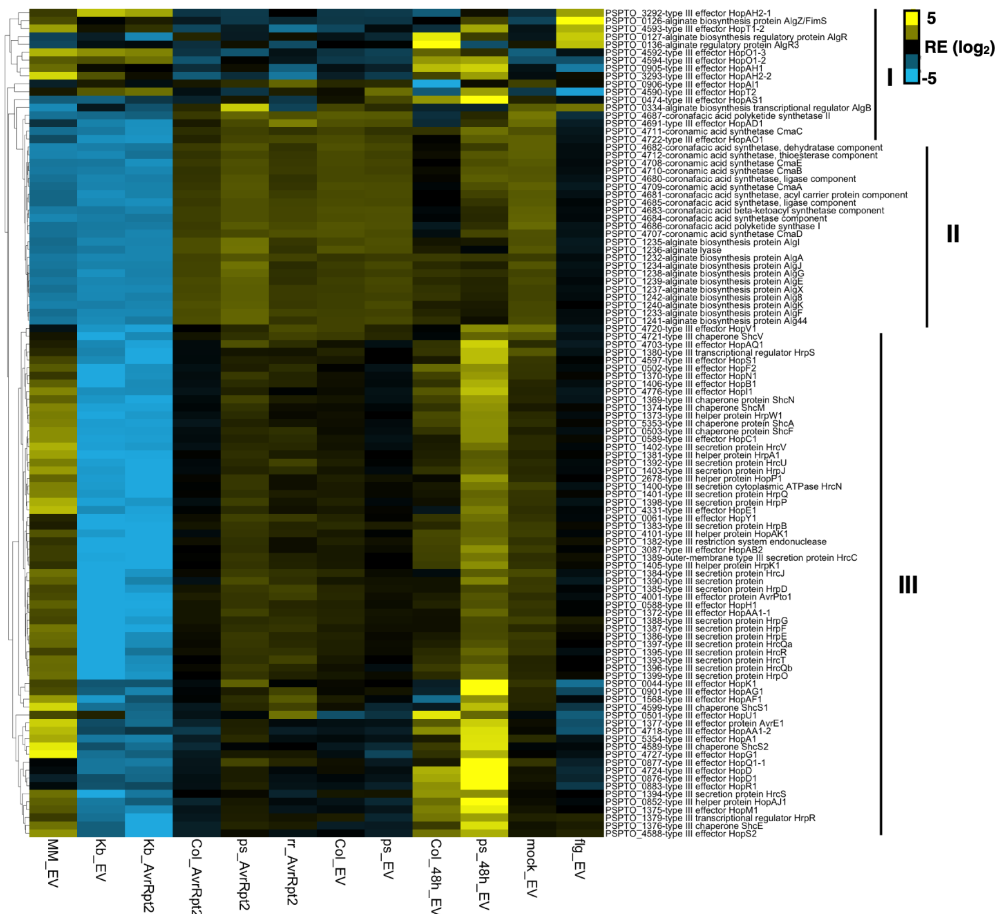
Bacterial suspensions were spotted on 50% TSB plate. The picture was taken three days after spotting bacterial suspensions on the plate. COR: coronatine deficient *Pto*. The other strains are listed in Figure 4A and Table 1.

6. Supplementary figures

A

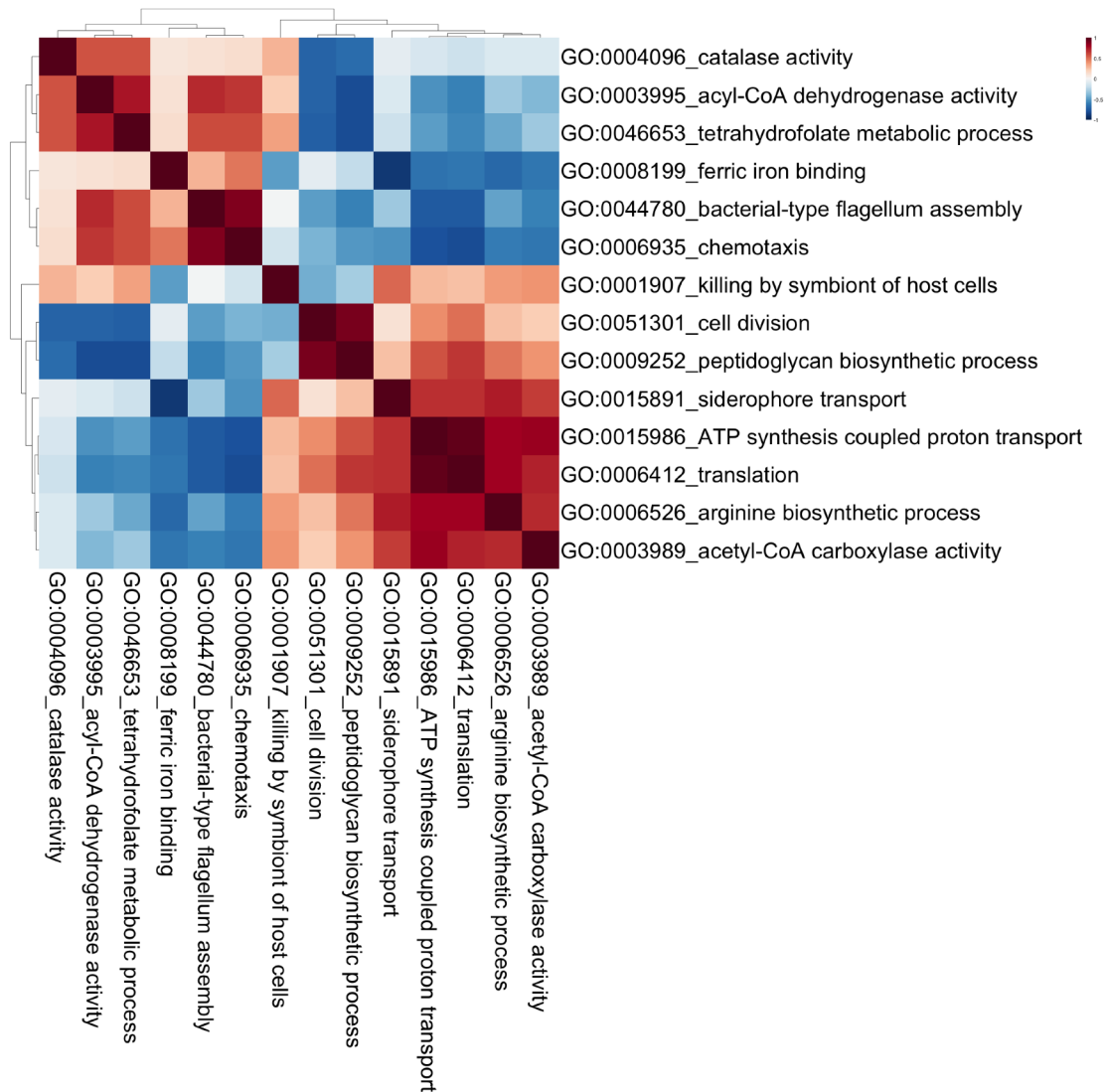


B



Supplementary figure 9: Expression of genes related to coronatine, alginate, and the type III secretion system

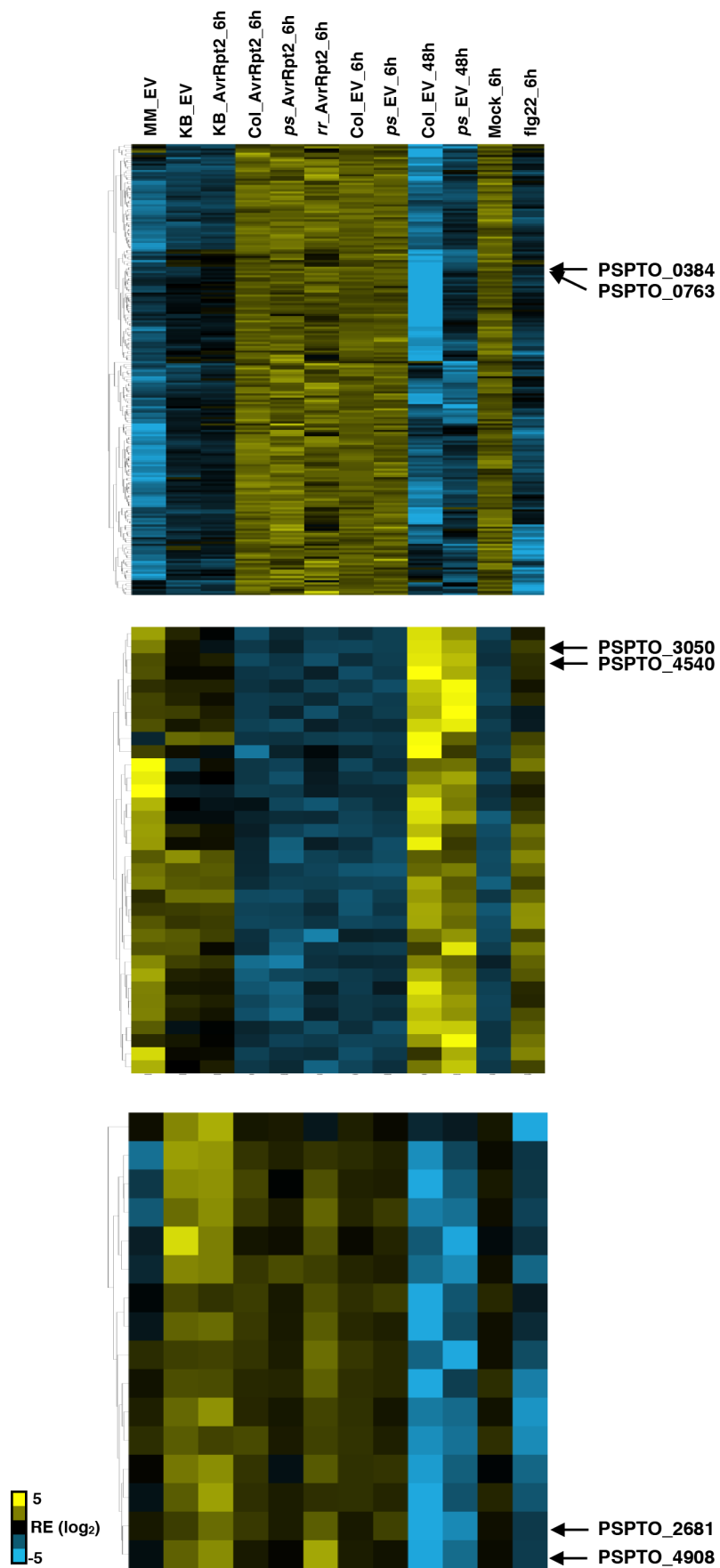
Correlation matrix (A) and hierarchical clustering (B) of expression of genes related to coronatine, alginate, and the type III secretion system (T3SS) under various conditions. Gene cluster I and III contain T3SS genes and cluster II contains genes related to coronatine and alginate. This figure was adopted from Nobori et al. (*in preparation*).



Supplementary figure 10: Gene ontologies showing negative correlation in expression

Correlation matrix of bacterial GO expression generated from 132 bacterial RNA-seq data (38 conditions). This figure was adopted from Nobori et al. (*in preparation*).

6. Supplementary figures



Supplementary figure 11: Co-expression patterns of genes in *Pto*

6. Supplementary figures

Hierarchical clustering of highly co-expressed genes including putative transcriptional regulators and their predicted targets (indicated by arrows). This figure was adopted from Nobori et al. (*in preparation*).

6. Supplementary figures

Supplementary table 1: List of samples used in this study for RNA-seq

Bacterial strain	Host genotype	Pretreatment	Time point	Number of replicates
<i>Pto</i>	Col-0	water (Mock)	6 hpi	5
<i>Pto</i>	Col-0	flg22	6 hpi	5
<i>Pto</i>	Col-0	chitin	6 hpi	3
<i>Pto</i>	Col-0	SA	6 hpi	3
<i>Pto</i>	Col-0	-	6 hpi	13
<i>Pto</i>	<i>pad4</i>	-	6 hpi	4
<i>Pto</i>	<i>sid2</i>	-	6 hpi	3
<i>Pto</i>	<i>pad4 sid2</i>	-	6 hpi	4
<i>Pto</i>	<i>npr1</i>	-	6 hpi	2
<i>Pto</i>	<i>dde2 ein2</i>	-	6 hpi	2
<i>Pto</i>	<i>dde2 ein2 pad4 sid2</i>	-	6 hpi	2
<i>Pto</i>	<i>sid2 pmr4</i>	-	6 hpi	2
<i>Pto</i>	<i>cyp79b2 cyp79b3</i>	-	6 hpi	2
<i>Pto</i>	<i>stp1 stp13</i>	-	6 hpi	2
<i>Pto</i> AvrRpt2	Col-0	-	6 hpi	16
<i>Pto</i> AvrRpt2	<i>pad4</i>	-	6 hpi	4
<i>Pto</i> AvrRpt2	<i>sid2</i>	-	6 hpi	3
<i>Pto</i> AvrRpt2	<i>pad4 sid2</i>	-	6 hpi	3
<i>Pto</i> AvrRpt2	<i>npr1</i>	-	6 hpi	3
<i>Pto</i> AvrRpt2	<i>dde2 ein2</i>	-	6 hpi	3
<i>Pto</i> AvrRpt2	<i>dde2 ein2 pad4 sid2</i>	-	6 hpi	3
<i>Pto</i> AvrRpt2	<i>sid2 pmr4</i>	-	6 hpi	2
<i>Pto</i> AvrRpt2	<i>cyp79b2 cyp79b3</i>	-	6 hpi	2
<i>Pto</i> AvrRpt2	<i>stp1 stp13</i>	-	6 hpi	2
<i>Pto</i> AvrRpt2	<i>rps2 rpm1</i>	-	6 hpi	2
<i>Pto</i> AvrRps4	Col-0	-	6 hpi	2
<i>Pto</i> D36E	Col-0	-	6 hpi	3
<i>Pto</i>	Col-0	-	48 hpi	3
<i>Pto</i>	<i>pad4</i>	-	48 hpi	3
<i>Pto</i>	<i>sid2</i>	-	48 hpi	3
<i>Pto</i>	<i>pad4 sid2</i>	-	48 hpi	3
<i>Pto</i> AvrRpt2	Col-0	-	48 hpi	3
<i>Pto</i> AvrRpt2	<i>pad4</i>	-	48 hpi	3
<i>Pto</i> AvrRpt2	<i>sid2</i>	-	48 hpi	3
<i>Pto</i> AvrRpt2	<i>pad4 sid2</i>	-	48 hpi	3
EK10	Col-0	-	6 hpi	2
EK47	Col-0	-	6 hpi	2
Leaf 1	Col-0	-	6 hpi	1
Leaf 155	Col-0	-	6 hpi	1
Leaf 176	Col-0	-	6 hpi	1
Leaf 187	Col-0	-	6 hpi	2

6. Supplementary figures

Leaf 404	Col-0	-	6 hpi	2
Bacterial strain	Growth medium	Pretreatment		Number of replicates
<i>Pto</i>	King's B medium	-		2
<i>Pto</i>	Hrp-inducible minimal medium	-		4
<i>Pto</i> AvrRpt2	King's B medium	-		3
<i>Pto</i> AvrRps4	King's B medium	-		2
<i>Pto</i> D36E	King's B medium	-		3
EK10	50% TSB	-		2
EK47	50% TSB	-		2
Leaf 1	50% TSB	-		2
Leaf 155	50% TSB	-		2
Leaf 176	50% TSB	-		2
Leaf 187	50% TSB	-		2
Leaf 404	50% TSB	-		2

Contributions

Most of the experiments and analyses described in this thesis were conducted by myself. Those that were conducted by and in corporation with other people were indicated below.

- Figure 3B: This method was established by the group of Prof. Dr. Sheng Yang He at the Michigan State University.
- Figure 7 C and D: These experiments were conducted with Dr. Yiming Wang at Max-Planck Institute for Plant Breeding Research (MPIPZ).
- Figure 8 F and G: Part of the data (*in planta* 6 hpi) was obtained by Dr. Jingni Wu at MPIPZ.
- Figure 16 and 17D: These data were generated by Dr. Yiming Wang at MPIPZ.
- Supplementary figure 8: The picture was taken by Mr. Yu Cao at MPIPZ.
- RNA sequencing and LC-MS analyses were supported by the Max-Planck Genome Centre and Protein Mass Spectrometry Service, respectively, at MPIPZ.

Acknowledgements

First and for most, I would like to thank my direct supervisor Dr. Kenichi Tsuda for providing with me complete intellectual freedom and opportunities to step up as an independent scientist. I also appreciate the member of my thesis advisory committee, Prof. Dr. Paul Schulze-Lefert, who is also the first examiner of my thesis committee, and Prof. Dr. Eric Kemen for beneficial discussions that drove my projects forward. I thank to Prof. Dr. Stanislav Kopriva Prof. Dr. Corné Pieterse, and Prof. Dr. Gunther Döhlemann for being the second examiner, third examiner, and the chair of my thesis committee, respectively. A special gratitude goes to the generous financial support from the Nakajima foundation throughout my PhD study.

The thesis projects involved many collaborators and colleagues: Dr. Sajjad Khani, Dr. Yiming Wang, Dr. Jingni Wu, Ms. Yayoi Tsuda, Mr. Yu Cao, Mr. Dieter Becker, Dr. Samuel Kroll, Mr. Paul Runge, Dr. Barbara Kracher, Dr. Bruno Huettel and people in the Max-Planck Genome Centre, Dr. Hirofumi Nakagami and his group, and Prof. Dr. Sheng Yang He (Michigan State University) and his group, among others. I am also grateful to gardeners, people in the media kitchen, and Dr. Stephan Wagner (the PhD office) who provided and maintained a perfect scientific environment. The success of the projects was not possible without their efforts. I thank Dr. Kathrin Wippel and Ms. Saskia Bauer for editing the Zusammenfassungin of the thesis.

The last four years at the MPIPZ were full of fun thanks to the lab members and friends in the institute. I was fortunate that I have been physically and mentally healthy throughout my PhD study. I owe this to the time I spent with you guys inside and outside the lab. And finally, I must express my very profound gratitude to my family members who have supported me along the way. Thank you.

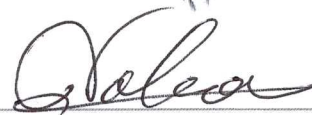
Erklärung

Ich versichere, dass ich die von mir vorgelegte Dissertation selbständig angefertigt, die benutzten Quellen und Hilfsmittel vollständig angegeben und die Stellen der Arbeit – einschließlich Tabellen, Karten und Abbildungen –, die anderen Werken im Wortlaut oder dem Sinn nach entnommen sind, in jedem Einzelfall als Entlehnung kenntlich gemacht habe; dass diese Dissertation noch keiner anderen Fakultät oder Universität zur Prüfung vorgelegen hat; dass sie – abgesehen von oben angegebenen Teilpublikationen – noch nicht veröffentlicht worden ist, sowie, dass ich eine solche Veröffentlichung vor Abschluss des Promotionsverfahrens nicht vornehmen werde.

Die Bestimmungen der Promotionsordnung sind mir bekannt. Die von mir vorgelegte Dissertation ist von Prof. Dr. Paul Schulze-Lefert betreut worden.

Ich versichere, dass ich alle Angaben wahrheitsgemäß nach bestem Wissen und Gewissen gemacht habe und verpflichte mich, jedmögliche, die obigen Angaben betreffenden Veränderungen, dem Dekanat unverzüglich mitzuteilen

Köln, 02.04.2019



Tatsuya Nobori